

A SMART GRID APPROACH TO SUSTAINABLE POWER SYSTEM INTEGRATION

A Dissertation

by

ABDULLAH ABDULAZIZ M ALMEHIZIA

Submitted to the Office of Graduate and Professional Studies of
Texas A&M University
in partial fulfillment of the requirements for the degree of

DOCTOR OF PHILOSOPHY

Chair of Committee, Mehrdad (Mark) Ehsani
Committee Members, Chanan Singh
Laszlo B. Kish
Won-Jong Kim
Head of Department, Miroslav Begovic

August 2018

Major Subject: Electrical Engineering

Copyright 2018 Abdullah Abdulaziz M Almehezia

ABSTRACT

Many factors can be identified for faster incorporation of renewable energy resources to displace the traditional fossil fuel energy sources. These factors are divided into three different aspects. First is the rapid decline of the cost of renewable energy sources and their associated components. The second factor can be attributed to the increasing pressure to transition from fossil-fuel energy sources which have detrimental environmental effects towards more sustainable energy source. A third aspect can be introduced in countries which are blessed with an enormous amount of fossil fuel resources, where the preservation of these limited natural resources is of paramount importance to the country that holds it. The dissertation includes the Kingdom of Saudi Arabia as the primary case study. However, the algorithm developed is applicable for other geographical locations which share similarities to the kingdom. The kingdom is considered to be one of the countries with an abundance of fossil-fuel reserves. The unique features of Saudi Arabia are primarily the availability of solar radiation and wind speed as well as high percentage of electrical loads which can be controlled such as energy-intensive desalination plants. This feature, in particular, provides a significant driver for renewables to penetrate the electricity generation mixture. With loads that are deferrable, the issue of renewable sources variability can be mitigated and reduced with an optimized operation strategy. Therefore, the research tends to define and model electrical loads by how susceptible they are to the time of service. The types of loads considered are summarized as non-deferrable such as typical electrical loads in which the demand must be satisfied instantly, semi-deferrable loads which they share the same features as the non-deferrable, however, a storage medium is available to store energy products for later usage. This category of loads is represented by a water desalination plant with a water tank storage. The final load model is the fully deferrable

load which is flexible in regarding time of service, and this type of load can be represented by an industrial production factory, such as a steel or aluminum plants. The concept of value storage is introduced, where energy can be stored in different forms which are quite different from a typical storage component (i.e., batteries).

The justification to start increasing the penetration of renewable sources into the existing grid in countries which have abundant fossil fuel might not be evident. However, the dissertation provides both economical as well as environmental justifications and incentives to approach more sustainable energy sources.

The economical and technical evaluation is referred to as the Generation Expansion Planning (GEP). This type of problem is associated with high complexity and non-linearity. Therefore, computational intelligence based optimization methods are used to resolve these issues. Heuristic optimization methodologies are utilized to solve the developed problem which provides a fixable approach to solve optimization problems.

DEDICATION

To my mother, my father and my family

ACKNOWLEDGMENTS

I would like to thank my advisor Dr. Mehrdad Ehsani, for his continuous help and support for without him this dissertation would not be possible. I would also like to extend my thanks and gratitude towards my Ph.D. dissertation committee Dr. Chanan Singh, Dr. Laszlo B. Kish and Dr. Won-Jong Kim for taking time and effort as well as providing their expert opinions.

Also many thanks to my family, colleagues and friends for their support and insightful comments throughout my Ph.D. studies in Texas A&M. I truly appreciated all the encouragement to pursue a higher level of education.

CONTRIBUTORS AND FUNDING SOURCES

Contributors

This work was supported by a dissertation committee consisting of Professor Chanan Singh and Laszlo B. Kish of the Department of Electrical and Computer Engineering and Professor Won-Jong Kim of the Department of Mechanical Engineering.

The majority of raw data used was provided by the Saudi Electricity Company (SEC) as well as the King Abdullah City for Atomic and Renewable Energy (KA-CARE). All other work conducted for the dissertation was completed by the student independently.

Funding Sources

Graduate study was supported by a scholarship from the government of Saudi Arabia represented by King Abdulaziz City For Science and Technology (KACST).

TABLE OF CONTENTS

	Page
ABSTRACT	ii
DEDICATION	iv
ACKNOWLEDGMENTS	v
CONTRIBUTORS AND FUNDING SOURCES	vi
TABLE OF CONTENTS	vii
LIST OF FIGURES	xi
LIST OF TABLES	xiv
1. INTRODUCTION AND LITERATURE REVIEW	1
1.1 Renewable Energy Technologies	1
1.1.1 Photovoltaic (PV)	1
1.1.2 Wind Turbine Generators (WTGs)	2
1.1.3 Other Alternative Sources	5
1.2 Energy Storage Technologies	7
1.2.1 Chemical	7
1.2.2 Thermal	8
1.2.3 Mechanical	9
1.2.4 Electrical	10
1.3 Current Status of Renewable Energy Implementation in Global Perspective	11
1.4 Challenges with Integration and High Penetration of Renewable Energy Sources	13
1.5 The Kingdom of Saudi Arabia and the Potential Towards Sustainable Energy	16
1.5.1 The Kingdom’s Energy Production and It’s Presence in the Global Energy Market	17
1.5.2 Structure of the Electricity Sector	18
1.5.3 The Water Industry and the Associated Desalination Technologies	23
1.5.4 Brief History of Renewable Energy Development in Saudi Arabia	28
1.5.5 Review of Previous Studies of Renewable Energy Utilization in the Kingdom	30

1.5.6	Potential and Challenges of Renewable Energy Incorporation and the Saudi Arabian Vision for 2030	34
1.6	The Smart Grid Concept	40
2.	ENERGY SOURCES MODELING	42
2.1	Sun and Surface Angles	42
2.2	Sun Position Tracking System	51
2.2.1	Fixed Axis	51
2.2.2	Single Axis	51
2.2.3	Two Axis	52
2.3	Solar Radiation Components	52
2.4	Solar Radiation on Tilted Surfaces	54
2.4.1	Isotropic Diffusion Model	56
2.4.2	HDKR Diffusion Model	56
2.4.3	Perez Diffusion Model	57
2.5	Solar Photovoltaic (PV)	58
2.5.1	Simple Efficiency Model	60
2.5.2	Temperature Adjusted Simple Efficiency Model	60
2.5.3	Standard Test Condition Power Model with Temperature Adjustment	62
2.5.4	Voltage-Current Model	62
2.6	Wind Turbine Generators (WTGs)	63
2.6.1	First Order Model	64
2.6.2	Third Order (Cubic) Model	65
2.6.3	Power Coefficient Model	65
2.7	Legacy Grid	65
3.	SYSTEM LOAD MODELING AND ANALYSIS	66
3.1	Conventional Electrical Load	66
3.2	Controllable Loads and The Concept of Value Storage	67
3.2.1	Direct Load Control	67
3.2.2	Indirect Load Control	67
3.3	Advanced Electricity Pricing	68
3.3.1	Time of Use Pricing (TOUP)	68
3.3.2	Real Time Pricing (RTP)	68
3.3.3	Critical Peak Pricing (CPP)	69
3.4	Demand Side Management	69
3.4.1	Techniques of DSM	70
3.4.2	Benefits of DSM	72
3.4.3	Challenges and Barriers of DSM Implementation	72
3.5	Water Desalination Plant Load Model	73
3.6	Industrial Facilities Load Model	74

4.	GENERATION EXPANSION PLANNING	77
4.1	Problem Statement	80
4.2	System Components Cost Breakdown and Financial Aspects	80
4.2.1	Financial Parameters	80
4.2.2	Renewable Energy System	80
4.2.3	Water Tank Storage	81
4.2.4	Desalination Plant Capacity Expansion	81
4.2.5	Grid	81
4.3	Design Objectives	82
4.3.1	Economical Criteria	82
4.3.2	Environmental Criteria	83
4.4	Uncertainty Handling	83
4.5	System Configurations	87
4.5.1	Desalination Plant Powered by Renewables	87
4.5.1.1	Design Constraints	87
4.5.1.2	System Operation Strategy	88
4.5.2	Desalination Plant Powered by Renewables and Legacy Grid	90
4.5.2.1	Design Constraints	91
4.5.2.2	System Operation Strategy	92
4.5.3	Conventional Load and Desalination Plant Powered by Renewables and Legacy Grid	93
4.5.3.1	Design Constraints	94
4.5.3.2	System Operation Strategy	96
4.5.4	Conventional Load, Desalination Plant and Industrial Factories Powered by Renewables and Legacy Grid	98
4.5.4.1	Design Constraints	98
4.5.4.2	System Operation Strategy	100
4.5.5	Conventional Load, Desalination Plant and Industrial Factories Powered by Renewables Coupled with Batteries and Legacy Grid	102
4.5.5.1	Design Constraints	103
4.5.5.2	System Operation Strategy	104
4.6	Inverters Sizing	105
4.7	Economical and Technical Analysis	108
4.8	Renewable Energy Sources Footprint	112
4.8.1	Solar Farm Physical Layout	112
4.8.2	Wind Farm Physical Layout	115
5.	IMPLEMENTED OPTIMIZATION TECHNIQUES	119
5.1	Optimization Methodologies	119
5.2	Constraint Handling	122
5.3	Genetic Algorithm (GA)	123

5.3.1	GA Working Principle	123
5.3.2	Fitness Function	124
5.3.3	Selection Operators	124
5.3.4	Crossover Operators	126
5.3.5	Mutation Operators	127
5.3.6	Non-Domination Sorting Genetic Algorithm (NSGA-II)	129
5.4	Mutation Based Particle Swarm Optimization (MBPSO)	130
5.4.1	Working Principle	130
5.4.2	Velocity Operator	131
5.4.3	Position Operator	131
5.4.4	Mutation Operator	131
5.4.5	Multi-Objective Particle Swarm Optimization (MOPSO)	132
5.5	Imperialist Competitive Algorithm (ICA)	133
5.5.1	Working Principle	133
5.5.2	Total Cost Operator	133
5.5.3	Assimilation Operator	134
5.5.4	Revolution Operator	134
5.5.5	Intra-Empire Competition Operator	134
5.5.6	Inter-Empire Competition Operator	134
6.	RESULTS AND SENSITIVITY ANALYSIS	141
6.1	Candidate Cities and Data Required	141
6.2	System Components Costs and Associated Technical Data	142
6.3	Test Cases for Different System Configurations	145
6.3.1	Desalination Plant Powered by Renewables	145
6.3.2	Desalination Plant Powered by Renewables and Legacy Grid	146
6.3.3	Conventional Load and Desalination Plant Powered by Renewables and Legacy Grid	147
6.3.4	Conventional Load, Desalination Plant and Industrial Factories Powered by Renewables and Legacy Grid	148
6.4	Sensitivity Studies	151
6.4.1	Oil Prices	151
6.4.2	System Components Cost	152
6.4.3	Solar Radiation and Wind Speed Variability	153
6.4.4	Water Load Percentage to Total Load	154
7.	CONCLUSIONS AND FUTURE WORK	156
7.1	Conclusions	156
7.2	Further Study	158
	REFERENCES	161

LIST OF FIGURES

FIGURE	Page
1.1 Oil exports	17
1.2 Distribution of generation capacities among producers	19
1.3 Organizational structure of the electricity sector in the Kingdom [22] . . .	19
1.4 Fuel types used for electricity generation	20
1.5 Map of generation units [23]	21
1.6 Map of transmission lines (380 kV) [23]	22
1.7 Distribution of consumption among SEC business sectors	22
1.8 Evolution of peak demand	23
1.9 Map of desalination plants [26]	24
1.10 Schematic diagram of MSF unit [29]	26
1.11 Schematic diagram of MED unit [29]	27
1.12 Schematic diagram of RO unit [29]	28
1.13 Schematic diagram of ED unit [29]	28
1.14 GHI distribution in Saudi Arabia [45]	36
1.15 DNI distribution in Saudi Arabia [45]	36
1.16 KACARE suggested energy mix in 2032	38
1.17 Justification for moving towards sustainable energy sources in GCC countries	40
2.1 Illustration of the celestial sphere and coordinates [62]	46
2.2 Surface and sun angles [63]	47
2.3 Beam, diffuse, and ground-reflected radiation on a tilted surface [63] . . .	55

2.4	Practical solar cell model	58
2.5	Current-voltage characteristics of a multi-crystalline silicon PV [1]	61
2.6	Ideal power curve of WTs [4]	64
3.1	Categories of DSM [95]	70
3.2	Techniques for implementing DSM [96]	71
4.1	Typical discretization of the probability distribution of the solar radiation and wind speed forecast error	85
4.2	System configuration of desalination plant powered by renewables	87
4.3	System configuration of desalination plant powered by renewables and legacy grid	90
4.4	System configuration of conventional load and desalination plant powered by renewables and legacy grid	94
4.5	System configuration of conventional load, desalination plant and industrial factories powered by renewables and legacy grid	98
4.6	System configuration of conventional load, desalination plant and industrial factories couple with BESS and powered by renewables and legacy grid	102
4.7	Solar farm physical layout	117
4.8	Wind farm physical layout	118
5.1	Classification of meta-heuristic algorithms [132]	120
5.2	Roulette-wheel selection scheme [137]	125
5.3	Genetic Algorithm (GA) flow chart	136
5.4	Non-dominated Sorting Genetic Algorithm (NSGA II) flow chart	137
5.5	Mutation based Particle Swarm Optimization (MPSO) flow chart	138
5.6	Multi-Objective Particle Swarm Optimization (MOPSO) flow chart	139
5.7	Imperialist Competitive Algorithm (ICA) flow chart	140

6.1	Performance of the optimization algorithms of system configuration one with the water storage tank	145
6.2	Performance of the optimization algorithms of system configuration two with the water storage tank	146
6.3	Performance of the optimization algorithms of system configuration three with the water storage tank	147
6.4	Performance of the optimization algorithms of system configuration four with the water storage tank	148
6.5	Performance of the optimization algorithms of system configuration four with the battery energy storage system	149
6.6	Pareto frontier of system configuration four with the water storage tank . .	149
6.7	Pareto frontier of system configuration four with the battery energy storage system	150
6.8	Variation of differential cost with global oil prices	152
6.9	Variation of differential cost with PVs and WTGs capital cost	152
6.10	Variation of differential cost with water storage and desalination expansion capital cost	153
6.11	Variation of differential cost with solar radiation and wind speed	154
6.12	Impact of water to total load percentage on the differential cost	155

LIST OF TABLES

TABLE	Page
1.1 Breakdown of total renewable power capacities in 2016	13
1.2 Breakdown of renewable power capacities by technology in major countries	13
6.1 Data of candidate city	141
6.2 Load data	141
6.3 GA parameters	141
6.4 MPSO parameters	142
6.5 ICA parameters	142
6.6 Cost parameters of the hybrid system	142
6.7 Desalination plant associated costs	142
6.8 Legacy grid associated costs	143
6.9 Technical and economical data	143
6.10 Technical parameters of the solar panel	143
6.11 Technical parameters of the wind turbine generator	143
6.12 Technical parameters of the inverters	144
6.13 Technical parameters of the battery energy storage system	144
6.14 Technical parameters of the legacy grid	144
6.15 Results of system configuration one with the water storage tank	145
6.16 Technical and economical metrics of system configuration one with the water storage tank	145
6.17 Results of system configuration two with the water storage tank	146

6.18	Technical and economical metrics of system configuration two with the water storage tank	146
6.19	Results of system configuration three with the water storage tank	147
6.20	Technical and economical metrics of system configuration three with the water storage tank	148
6.21	Results of system configuration four with the water storage tank	150
6.22	Technical and economical metrics of system configuration four with the water storage tank	150
6.23	Results of system configuration four with the battery energy storage system	151
6.24	Technical and economical metrics of system configuration four with the battery energy storage system	151

1. INTRODUCTION AND LITERATURE REVIEW

This chapter is intended for providing background information on the research presented in this dissertation. Renewable energy sources are described, and their different attributes are discussed. Followed by an overview of the current situation of renewable energy sources projects worldwide. Leading to the primary case study in this dissertation which is the Kingdom of Saudi Arabia. Different aspects of the of the kingdom are discussed in the energy and water sectors.

1.1 Renewable Energy Technologies

1.1.1 Photovoltaic (PV)

Photovoltaics directly convert solar radiation into electricity. The solar cell is made of a doped p-n junction. The doping process is to add impurities into the semiconductor crystal which is commonly a silicon crystal having four covalent bonds to the neighboring atoms. A majority of free negative charges region is referred to as n-region. It can be realized by having impurities with more electrons in the outer shell than the silicon crystal have. Most commonly used is phosphorus, since it has five outer electrons. On the other hand, a p-region with majority carries being holes can be achieved by doping the silicon crystal with boron atoms. Boron has three electrons in its outer shell, this will result in a lack of electron when binding with a silicon crystal which is equivalent to having an extra hole. An electric field is formed at the junction between the p-region and the n-region. This electric field is due to the difference in concentration between the two regions in which the electrons will diffuse into the p-region, and the hole will diffuse to the n-region [1].

The energy conversion that takes place in a photovoltaic solar panel consists mainly of two steps. First, the light absorbed by the panel will generate an electron-hole pair inside the solar cell. This pair will then be separated where the electrons will migrate to the

negative terminal and the hole towards the positive terminals [2].

Photovoltaic panels based on fabrication can be divided into three different types [3]:

- Mono-crystalline silicon cells (c-Si). Which is manufactured from a pure monocrystalline silicon. By using a single continuous silicon crystal lattice structure with almost no impurities. This type has higher efficiency, around 15%. The disadvantage, on the other hand, is that these cells have a complicated manufacturing process resulting in higher costs than other PV technologies.
- Multi-crystalline silicon cells (mc-Si). The production of multi-crystalline cells involves many grains of mono-crystalline silicon. Molten poly-crystalline silicon is cast into ingots, then cut into thin wafers and assembled into complete cells. This type of cells has an average efficiency of around 12%, yet it is cheaper to produce than mono-crystalline as the manufacturing process is much simpler.
- Amorphous silicon (a-Si). In this technology instead of the crystalline structure, amorphous silicon cells are composed of silicon atoms in a thin homogeneous layer. Light absorption is more efficient in amorphous silicon than crystalline silicon leading to thinner cells, referred to as thin film PVs. The main disadvantage of this technology is its relatively low efficiency which is around 6%. However, amorphous silicon can be deposited on a wide range of substrates, both rigid and flexible which is a great advantage.

1.1.2 Wind Turbine Generators (WTGs)

The Energy available in the wind is the kinetic energy of large masses of air moving over the earth's surface. This energy is harvested by the blades of the wind turbine which is then transformed into electrical form. The WTGs consists of the following components [4].

- Tower: The main function of the tower is to support the rotor and nacelle of a wind turbine at the required height. The most common types are the lattice tower, tubular steel tower, and guyed tower.
- Rotor: Which is the most important part of a wind turbine. The rotor converts the kinetic energy received from the wind stream into mechanical energy delivered to the shaft. The wind turbine rotor as a whole is comprised of blades, hub, shaft, bearings and other internals.
- High speed and low-speed shafts: These shafts are connecting elements from the rotor passing through the gearbox and ending at the generator.
- Gearbox: Are used to manipulate the speed according to the requirement of the generator.
- Generator: Smaller size wind turbines are usually equipped with DC generators of a few Watts to kiloWatts rated capacity. Larger systems use a single or three phase AC generators. Since large-scale wind generation plants are connected to the grid, the three-phase AC generators would be the appropriate option for turbines installed at such plants. The type of generators used in this condition can either be induction (asynchronous) generators or synchronous generators.
- Controllers and power regulation units: The wind turbines are designed to generate power as the wind speed crosses the cut-in designed speed. The power will continue to increase as the wind speed increases and settles at the rated power when the speed reaches the rated wind speed and beyond while still under the cut-out wind speed. Beyond the cut-out speed of the wind turbine, the safety systems will disconnect the turbine. Different methods are implemented to control and regulate the power output

from the turbines. These include pitch control, stall control, active stall control and yaw control.

- Safety systems: The wind turbine can be subjected to different events which could jeopardize it and lead to a catastrophic situation. For example, a failure could occur on the power transmission lines connected to the wind turbine, and the safety systems should recognize this issue and intervene. Also, safety breaks are utilized with this group of safety systems. These breaks are needed during periods of extremely high winds, much higher than the cut-out wind speed of the rotor, as such the wind turbines should be completely stopped for its safety.

Wind turbines can be classified by their axis of rotation into Horizontal Axis Wind Turbine (HAWT) and Vertical Axis Wind Turbine (VAWT). Most of the commercial wind turbines are HAWT. Horizontal axis machines have the advantages of low cut-in wind speed and easy furling. Also, they show relatively high power coefficient. On the other hand, the generator and gearbox of this type are mounted on the tower which makes its design more complicated and expensive. Furthermore, a yaw drive is needed to orient the turbine towards the wind direction. Horizontal axis wind turbines can have a single blade, two blades, three blades, and multi-blades. The single blade turbines have the advantage of being cheap as fewer blade materials are required. Also, the drag losses are minimum. However, a counterweight has to be placed opposite to the hub to balance the blade. Single bladed designs are not common due to problems in balancing and visual acceptability. Two bladed rotors share the same drawbacks but to a lesser extent. Most of the available commercial turbines have three blades [5].

The vertical axis wind turbine (VAWT) can receive wind from any direction, which can eliminate the complexity of yaw devices as compared HAWT. Another advantage is the simplicity and low cost of the tower as well as, low maintenance cost since that the

generator and gearbox can be housed at the ground level. For these systems, pitch control is not required when used for synchronous applications. The disadvantages of this type can be summarized as having a low tip-speed ratio, inability to self-start and control the power output or speed by pitching the rotor blades.

Some of the factors affecting the power produced by a WECS are:

- Strength of the wind spectra prevailing at the site and its availability to the turbine.
- Aerodynamic efficiency of the rotor in converting the power available in the wind to mechanical shaft power.
- Efficiencies in manipulating, transmitting and transforming power into the desired form. Therefore assessment of the performance of a WECS is a complex process.

1.1.3 Other Alternative Sources

It consists of mainly two components, the solar field and the power block. The solar field comprises of many arrays, and each array consists of mirrors that concentrate the sun's heat by reflecting it to a point or line receiver to produce heat at medium (400-550 °C) or high (600-1000 °C) temperatures. Then, this concentrated heat utilizes a heat transfer fluid (thermal oil, molten salt, water, air, hydrogen or helium) running through the receiver's tubes and deliver it to a conventional generator in the power block to produce electricity. The storage system can be integrated with CSP plants to store some of the energy in times of excess availability and release it to generate electricity in the cloudy days or when the sun sets. CSP plants can be hybridized with fossil fuel generators to make the plant produce electricity for 24 h which would improve the thermal efficiency and capacity factor and subsequently reduce the cost of the technology [6].

Four CSP technologies have been used worldwide, namely parabolic trough collector, solar tower power, Stirling/dish and linear Fresnel collector. The parabolic trough col-

lector and the linear Fresnel collector technologies concentrate the sun's heat along the focal length of the collector. Thus, they are referred to as line focus technologies. The Stirling/dish and the solar tower power technologies concentrate the sun's heat on a point at the tower or the center of the parabolic dish, and they are referred to as a point focus technology [6].

The line focus technologies produce heat at about 400-550 °C and generate steam at a moderate quality. On the other hand, point focus technologies produce heat at about 600-1000 °C, which is double the reached temperature at the line focus technique. As a result point, focus techniques are more efficient than line focus techniques. As it reduces the land usage, as well as, the effective cost per kWh of the plant. However, the line focus techniques have the advantage of being less expensive and technically less challenging than the point focus techniques [6].

Hydro-power or hydraulic power is the power derived from the force or energy of moving water. Even a slow stream of water or moderate sea swell can yield considerable amounts of energy as water is much denser than air. There are different categories of water power currently utilized or in development. These categories primarily include hydroelectricity, which is based on utilizing the gravitational force of falling or flowing water for generating electrical power and ocean energy, which mainly refers to the energy carried by ocean waves and tides [7].

The energy contained as heat inside the earth is referred to as geothermal energy. Geothermal heat pumps are highly efficient for heating and cooling. The technology relies on the fact that, at high depth, the temperature is relatively constant. Thus, the heat stored in the earth can be to a certain area during the winter, and transfer heat out of the area during the summer. Also, the technology can be used to generate electricity by using the heat to produce steam and drive a turbine [8]. Geothermal has the advantage of providing power without intermittence for 24-h a day where other sources of renewable

energy such as wind or solar have higher variability and uncertainty. The investment cost of such technology is relatively expensive. However, the operating costs are low, resulting in low energy costs for appropriate sites. With proven technology and abundant resources, the geothermal energy can contribute towards reducing the emission of greenhouse gases, especially in arid areas. It can be used to heat greenhouses and to provide fresh water [7].

1.2 Energy Storage Technologies

1.2.1 Chemical

One of the oldest electricity storage systems are the rechargeable batteries in which electrical energy is stored in the form of chemical energy. It is considered to be the most flexible, responsive for stand-alone generating systems and reliable as compared to other storage technologies. Batteries have the advantage of being modular and non-polluting, it can be placed near load centers or integrated with renewable energy sources [9]. Different types of battery storage are available which includes, lead-acid, nickel-cadmium, sodium-sulfur, vanadium redox as well as, lithium-ion batteries. Each type has its advantages and drawbacks which constitute its best application. Lead-acid batteries have a low energy density (30-50 Wh/kg), short cycle life (500-1000 cycles), failure of deep discharge and processing of lead. Its primary applications include an uninterruptible power supply (UPS), power quality and integration with intermittent renewable energy sources. Nickel-cadmium (NiCd) batteries have a relatively higher energy density than lead-acid batteries in the range of (50-75 Wh/kg). This type of batteries is considered to be reliable and requires less maintenance. However, the main disadvantage of this type of batteries includes relatively high cost and low cycle life in the range of (2000-2500). It also suffers from environmental issues as cadmium is a toxic heavy metal. Sodium-sulfur (NaS) batteries do not suffer from self-discharge and achieve efficiencies of 90% including heat losses. Flow batteries include vanadium redox, zinc bromide battery (ZnBr) and Polysulphide bromide

battery (PSB).

The main issues with integrating battery energy storage systems (BESS) are cost, number of cycles, reliability and the depth of discharge. Fuel cells and hydrogen storage are also considered as a chemical process energy storage [9].

Lithium batteries consist of two main types: Lithium-ion (Li-ion) and lithium-polymer cells. For lithium-ion batteries, self-discharge rate is very low and the lifetime is temperature dependent and can reach beyond 1500 cycles. Deep discharges also, affect the lifetime and can severely shorten it. Thus, unsuitable for use in backup applications as complete energy discharge is required. The high energy and power densities of lithium-ion batteries make it a very suitable technology for portable electronics. Some challenges for making large-scale Li-ion batteries is the high cost (>\$600/kWh) due to the need for special packaging and internal overcharge protection circuits [10].

The lifetime of lithium-polymer batteries is only about 600 cycles and has a much narrower temperature range as compared to Li-ion batteries. However, lithium-polymer batteries are lighter and safer with minimum self-inflammability [11].

1.2.2 Thermal

Thermal energy storage (TES) can be broadly divided based on the state of energy storage material into three categories, sensible, latent and chemical TES. The basic principle of a TES system is the same for all as energy is supplied to the TES and stored and at times of energy need it is discharged from the TES. Sensible TES stores the energy by changing the temperature of the storage medium. The storage density is considered to be low, and thus, a large volume is needed. This particular technology has the advantage of being reliable and available with low cost and enjoys a long lifespan. In latent TES, the thermal storage medium would change phase with the latent heat being higher than the sensible heat for a particular substance which will yield a smaller storage volume with

minimum temperature variation.

The chemical TES can be separated into two types namely, thermo-chemical reactions and sorption processes. The technology, in general, has a higher energy density and low heat losses. The main disadvantages are the high capital costs and the complexity of this type of technology.

Thermal energy storage is widely recognized as a means to integrate renewable energies into the electricity production mix on the generation and load side as an element for providing demand response. It has a significance utilization for solar thermal applications such as heating, hot water, cooling, air-conditioning and CSP plants as well [11].

1.2.3 Mechanical

The main and widely used mechanical energy storage technologies are the pumped hydro storage (PHS), compressed air energy storage (CAES) and flywheels. Pumped hydroelectric storage is considered to be a mature technology with high efficiency and large storage periods. The typical pumped hydro plant has two separate reservoirs, in which during times of low power demand, water is pumped from the lower reservoir to the upper reservoir. During hours of peak electricity demand, the water is discharged and flow into the lower reservoir as the potential energy of water is used to rotate hydro turbines that drive the coupled generators. The amount of energy depends on the available water discharged from the upper reservoir as well as, the difference in height between the two reservoirs. This type of storage technology requires large areas to accommodate the upper and lower reservoirs. The round trip efficiency of the pumped hydro plant varies in the range of (60-80%) [9].

The CAES utilizes off-peak electrical energy to compress air into an underground surface tank. During periods of high electricity demand, the compressed air is used for heating and combustion of fuels to run the turbine which drives a generator. Underground medium

for the storage of compressed air includes porous rock formation, salt or rock formation and natural gas fields which indicates that this type of energy storage requires a specific geographical location. The AC-AC round-trip efficiency of CAES varies in the range of (85-90%) [9].

Flywheels stores kinetic energy by spinning a disk about its axis. The amount of energy stored in the disk is directly proportional to the square of the wheel's speed and rotor's mass moment of inertia. At times where power is required, flywheel uses the rotor's inertia and converts stored kinetic energy into electricity. This technology is suitable for regenerative braking, voltage support, transportation, power quality and UPS applications. The round trip efficiency of flywheels depends on the winding and bearing losses, as well as, the cycling process, and it varies in the range of (80-85%) [9].

1.2.4 Electrical

Superconducting magnetic energy storage (SMES) and supercapacitors are the most common energy storage in this category. SMES, in general, comprises of three parts: a superconducting magnetic coil, a power conditioning equipment, and a refrigeration system. Excess off-peak AC power is converted into direct current and supplied to a superconducting magnetic coil. The magnetic field created is used to store the energy. The coils of SMES are kept at a superconductive temperature to meet the superconducting properties of the magnetic coil. This storage system has high efficiency in storing DC electric energy. The disadvantages of such techniques involve high system cost and environmental issues (strong magnetic field) which hinder the mass deployment of SMES as storage for renewable energy systems [9].

Supercapacitors have two layer plates for the effective separation of charges. One advantage of this technology is the long cyclic life. Supercapacitors are suited for high power as well as short duration discharge applications. Supercapacitors have higher energy

density as compared to batteries and conventional capacitors [9].

1.3 Current Status of Renewable Energy Implementation in Global Perspective

The adoption and integration of renewable energy resources are growing significantly as governments and policymakers are pushing for increased penetration of alternative energy sources to contribute towards the electricity generation mix. Renewable power generation technologies include solar photovoltaic, wind turbines, hydropower plants, biomass and geothermal plants as well as harvesting the energy from ocean waves, and tides. The key driver for incorporating these technologies are mainly, to reduce carbon emissions and the dependence on fossil fuels for energy production, improving power quality and reliability, it can potentially increase system efficiency and provide economic benefits.

Increased penetration of renewable energy sources into the grid is still a challenge, primarily because of their intermittency as they are considered to be non-dispatchable resources. Usually, an energy storage unit would be integrated with the renewable sources system, to avoid any shortages in power that might occur. Another approach is to consider hybridization of two or more renewable energy sources which have complementary characteristics on a daily or seasonal basis. The obvious example of this kind of hybridization is to utilize solar and wind resources. Different configurations of renewable sources can increase the efficiency and performance of the system. Coordination and control of the hybrid sources are of paramount importance to gain the full potential of them. Therefore, optimization techniques are heavily involved in feasibility studies where renewables and storage elements are to be incorporated [12].

Extensive research is conducted regarding renewable energy sources and their integration; these studies include system modeling and control as well as feasibility studies and adequacy. The generation expansion planning problem is well established in the literature.

Many papers and books have been published on this critical topic.

Renewable energy sources provided approximately 19.3% of the global energy consumption in 2015. Most of the additional renewable sources capacities were primarily in China and the developing countries. This growth contributed to the economy of these countries by enabling the employment of 9.8 million people in 2016, which translated to a 1.1% increase from 2015. Most installed capacities in 2016 were provided by solar PVs and biofuels-related industries, where the biofuels remained the primary renewable energy in the transportation sector.

Renewable power generation capacity peaked in 2016 with the implementation of estimated 161 GW of added capacity, which translates to nearly 9% increase compared to 2015, where 47% of the newly installed capacity was solar PVs, followed by wind turbines by 34% and 15.5% hydropower. The added capacity of renewable sources in 2016 surpassed all net capacity additions from all types of fossil fuel, as 62% of net additional power generation capacity were renewable. Electricity production from renewables was dominated by large utility companies in 2016, and the net renewable power capacity reached 2017 GW. The estimated share of renewable energy sources was 24.5% of the global electricity production in 2016, and 75.5% was provided by non-renewable energy sources.

The growth in renewable sources can be attributed to the continuous decline of components' costs and the rapid increase of power demand in some countries. The net investment cost in renewables including capacities more than 1 MW in 2016 was estimated to be \$241.6 Billion. Table I provide a detailed breakdown of total renewable power capacities in 2016.

China is considered the leading country in installed renewable power capacity with an estimated capacity of 564 GW followed by the United States with a capacity of 225 GW. Other major countries with significant renewable power capacities such as Germany,

India, Japan, and Italy have capacities of 104, 94, 73 and 52 GW respectively [13].

Table 1.1: Breakdown of total renewable power capacities in 2016

Technology	Capacity Power (GW)
Solar PV	303
Wind power	487
Concentrated solar thermal power	4.8
Hydropower	1096
Bio-power	112
Geothermal power	13.5

Table 1.2: Breakdown of renewable power capacities by technology in major countries

Technology	Power Capacity by Country					
	China	United States	Germany	Japan	India	Italy
Solar PV	77	41	41	43	9.1	19.3
Wind power	169	82	50	3.2	29	9.3
Concentrated solar thermal power	0	1.7	0	0	0.2	0
Hydro-power	305	80	5.6	23	47	18.5
Bio-power	12	16.8	7.6	4.1	8.3	4.1
Geothermal power	0	3.6	0	0.5	0	0.8

1.4 Challenges with Integration and High Penetration of Renewable Energy Sources

With all the advantages that renewable energy sources provide, it still suffers from unpredictability which can affect the reliability of power supply. Imposing a challenge for high renewable sources penetration into the electricity grid.

The variability and uncertainty of solar radiation and wind speed pose severe challenges for grid operators. Variability is defined as the continuous fluctuation of power generation based on the availability of primary fuel source (solar radiation, wind). Uncertainty is related to the magnitude and timing of the renewable generation output being less predictable than conventional power generation systems [14]. These issues have to be dealt with to maintain system balance. Thus, the system operators need to ensure sufficient resources are available to accommodate significant ramps either up or down in the wind and solar power generation to maintain system balance. The mismatch between renewable generation and load demand can be characterized as producing more power during low load demand in which curtailment or storage elements would be necessary. On the other hand, the opposite could happen which is experiencing low renewable power resource in times where high demand is required and in this situation storage elements would need to be brought up and also conventional generators would need to ramp up and sometimes beyond their maximum ramp capability which could cause severe damage. This issue is more attributed to wind power generation, as solar power is considered to be more coincide with the load especially in hot regions like Saudi Arabia [15]. Also since long-term accurate wind speed forecast is not yet possible, power production from the wind turbines can suffer from low or extremely high wind speeds which is a problematic situation for power dispatching.

The presence of renewable energy sources integrated with the legacy grid system would have some impacts on the conventional sources of energy. The conventional generators would be required to turn on and off more often, which will lower the efficiency and increase the stress on this equipment and increase wear and tear.

To mitigate these challenges is to improve the forecasting of solar radiation and wind speed which can reduce the uncertainty of the renewable sources power production. A better forecast can provide system operators with more informative information to efficiently

commit or de-commit generators to accommodate changes in wind and solar generation and prepare for severe events; it also can reduce the need for operating reserve which will eventually reduce the balancing costs of the system.

The Gulf Cooperation Council (GCC) region shares the same challenges previously mentioned, as well as additional challenges as it suffers from sandstorms, dust movement and accumulation which can have a detrimental effect on the solar panels. The Kingdom of Saudi Arabia, as well as other GCC countries, are considered to be lagging in renewable energy implementation, and the main reasons for this lag and can be attributed to many factors, which are summarized in the following [16]:

- Heavy energy price subsidies
- Lack of sufficient awareness among the decision makers.
- Higher investment costs.
- Fear of implications that could happen with implementing intermittent and uncertain renewable energy sources.
- Lack of incentives and clear regulations.
- Lack of studies exploiting the potential and benefits of renewable energy in the region as well as the lack of expertise.

It is reported in [16] a 10 mg/cm^2 of dust would reduce the panel's power output by 90%, and a 4 grams/m^2 of dust would reduce the power output by 40%. Rain cannot be relied on for cleaning and removing dust from the panels as it is very scarce in the GCC region. Thus, panel dust resistance coating as well as washing it with water is necessary, which will affect the operational cost of the plant [16].

1.5 The Kingdom of Saudi Arabia and the Potential Towards Sustainable Energy

The Kingdom of Saudi Arabia is a country located in the middle east, at the furthest part of southwestern Asia. According to the general authority for statistics in the kingdom, Saudi Arabia occupies about four-fifths of the Arab Peninsula, with a total area of around 2 million square kilometers and an estimated population of approximately 32 million people. There are 13 administrative regions in the kingdom. With the vast area size of the kingdom, a diverse topography is expected. The Tihama coastal plain along the Red Sea is 1100 km long and 60 km wide in the south, and it narrows north at the Aqaba Gulf. A chain of mountains called Sarawat is located to the east of Tihama coastal plain, and these mountains are highest at the south where they rise to 9000 feet and gradually fall to 3,000 feet in the north. From the east of these mountains, a Plateau called Najd Plateau extends to the Samman desert and Dahnaa Dunes in the east and southward to Dwaser valley. Najd Plateau also stretches northward to Najd plains, passing through Hail then connects with the Great Nefud Desert, until it reaches the borders of Iraq and Jordan. Twwaig, Al-Aridh, Aja and Salmah mountains are some of the mountains that can be found on the Plateau. In the southeastern region of the Kingdom lies the Empty quarter desert which has an estimated area of 640 thousand square kilometers and is parallel to Najd Plateau. The eastern coastal plain consisting mainly of large sand areas and Salinas stretches for about 610 km.

The diverse topographical features of the country affect the climate, where it is expected to vary from a region to another, with generally extreme hot weather in the summer season and cold weather in the winter season which is attributed to the subtropical high-pressure system. The central part of the country experience dry and hot summers and cold winters. Moderate climate is noticed in the west and southwestern parts of the country, and high temperature and humidity can be observed in the coastal regions. Significant rainfall

is expected in the southwestern mountains in the summer season where other significant parts of the country receive small amounts of rain mostly in spring and winter seasons [17].

1.5.1 The Kingdom's Energy Production and It's Presence in the Global Energy Market

The economy of Saudi Arabia is mainly dominated by the oil and gas industry. The estimations predict that the country possesses 16% of the world's proven petroleum reserves, and is considered as the largest petroleum exporter in the world which emphasis its rule in OPEC. The GDP for the year 2016 was estimated to be over 2.5 Trillion Saudi riyals which is equivalent to \$667 Billion, where oil exports shown in figure 1.1 accounted for 510.7 Billion Saudi riyals (\$136.2 Billion) [18]. The petroleum sector in the kingdom provides about 87% of the budget revenues, 90% of export earnings and has a 42% contribution to the GDP. However, the government of Saudi Arabia is aiming at lowering the enormous dependent on oil revenues and plans to diversify their economy which will also be beneficial in employing more Saudi citizens [19].

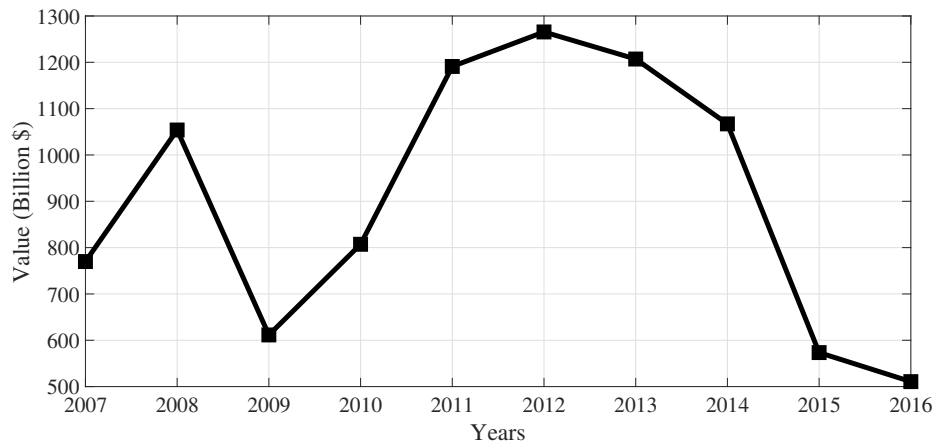


Figure 1.1: Oil exports

Saudi Aramco is a fully integrated chemical and global petroleum enterprise, an oil company, owned by the government of Saudi Arabia. The estimated amount of crude oil and condensate reserves are 260.8 Billion barrels and 298.7 trillion scf of gas reserves. In 2016 crude oil production was estimated to be 3828 million barrels and 2799 million barrels were exported. The liquid natural gas production for the same year is reported to be 497.5 million barrels. On average the company daily produced 10.5 million barrels of crude oil as well as 1.4 million barrels of liquid natural gas. Thus, the company is considered to be the world's largest crude oil exporter [20].

1.5.2 Structure of the Electricity Sector

The Saudi Electricity Company (SEC), is the primary provider of electrical energy in the kingdom with a total electric power capacity of 74.3 GW [21]. The company's responsibility includes generation, transmission, and distribution of electricity. While other entities contribute to the total electricity production, SEC is the dominant provider of electrical energy. Other entities which also provide electrical power include the Saline Water Conversion Corporation (SWCC), Hajar Electricity company, Jubail Water and Electricity company and others. The distribution of the total power capacity among the different producers is indicated in figure 1.2 .The total number of power plants is 81 distributed throughout the kingdom [22]. The current electricity structure of the kingdom is shown in figure1.3.

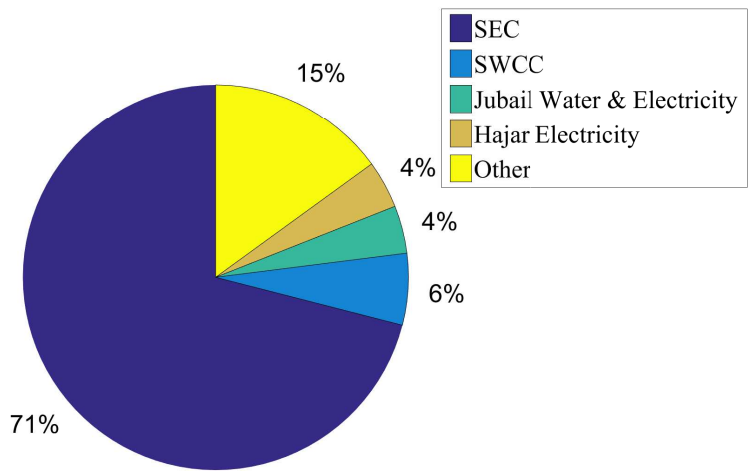


Figure 1.2: Distribution of generation capacities among producers

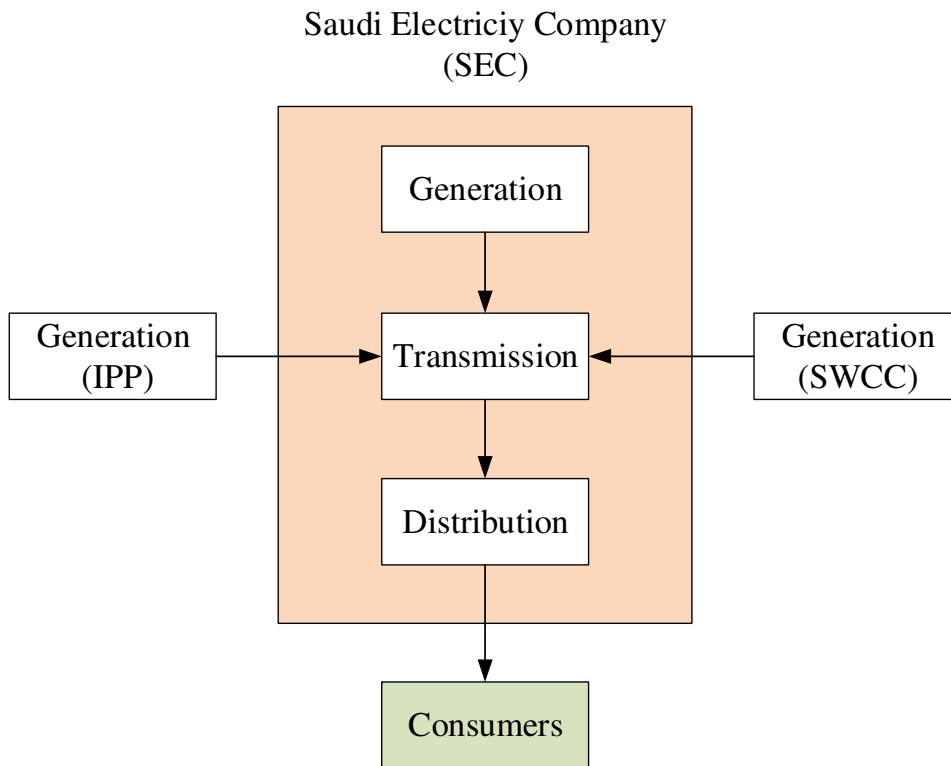


Figure 1.3: Organizational structure of the electricity sector in the Kingdom [22]

The electricity sector is divided into four geographical regions, central, eastern, western and southern. A 4737 MW of additional power capacity was installed by SEC in 2016 which represents a 9.4% increase over 2015 due to a rapid increase in electrical power demand [21]. The power generation is primarily based on conventional fossil fuel-fired generation, where the types of fuel were, 44% crude oil, 32% natural gas 13% heavy fuel oil and 11% diesel fuel which is demonstrated in figure 1.4. The unit cost of the electrical energy is subjected to many variables, the breakdown of this cost is as follows: 30% depreciation, 24% operational expenses, 17% purchased energy cost, 15% fuel costs and finally 14% capital expenses. The average unit cost of electricity in the kingdom is considered to be as one of lowest costs in the world in which the cost was 0.154 SR (\$0.041) per kWh. This low cost is possible due to substantial government subsidies to provide low fuel prices to electricity generation entities. Without these lower prices of fuel, the unit cost of electrical energy can reach up to 0.8 SR (\$0.21) per kWh [22]. The distribution of SEC power plants throughout the kingdom is shown in figure 1.5.

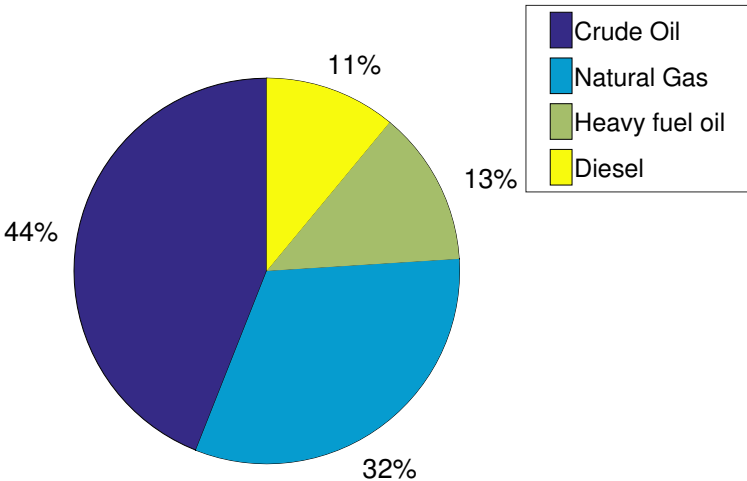


Figure 1.4: Fuel types used for electricity generation

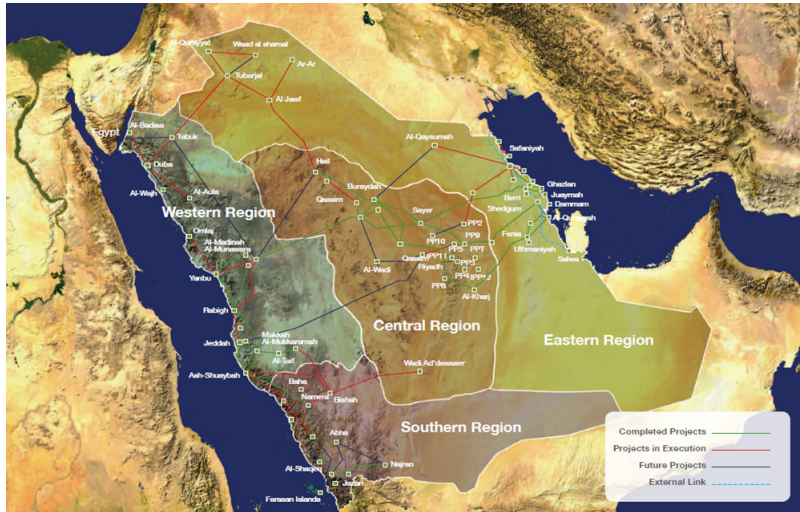


Figure 1.6: Map of transmission lines (380 kV). Reprinted from [23]

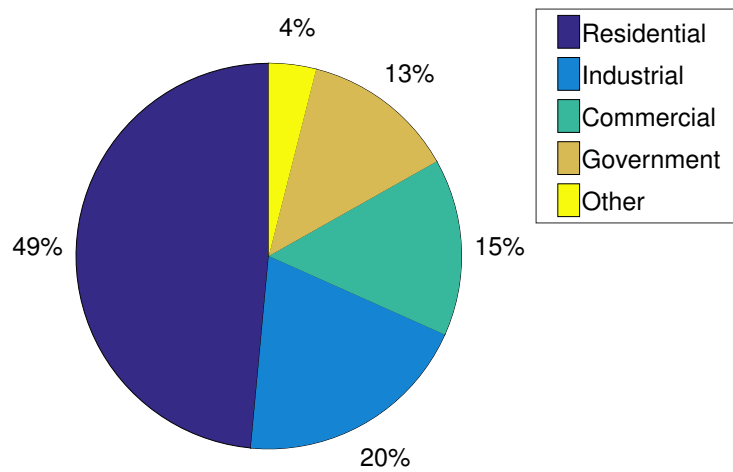


Figure 1.7: Distribution of consumption among SEC business sectors

The peak electricity demand in Saudi Arabia has risen over the last two decades, from 13069 MW in 1990 to 60828 MW in 2016 as can be seen in figure 1.8. The rapid increase in peak demand constitutes a burden on the generation power capacity. As each year SEC

is forced to increase its power capabilities to cope with the demand, such as in the years 1993, 2007, 2010 and 2015 where the power capacities had to be increased by an average of over 10% [24].

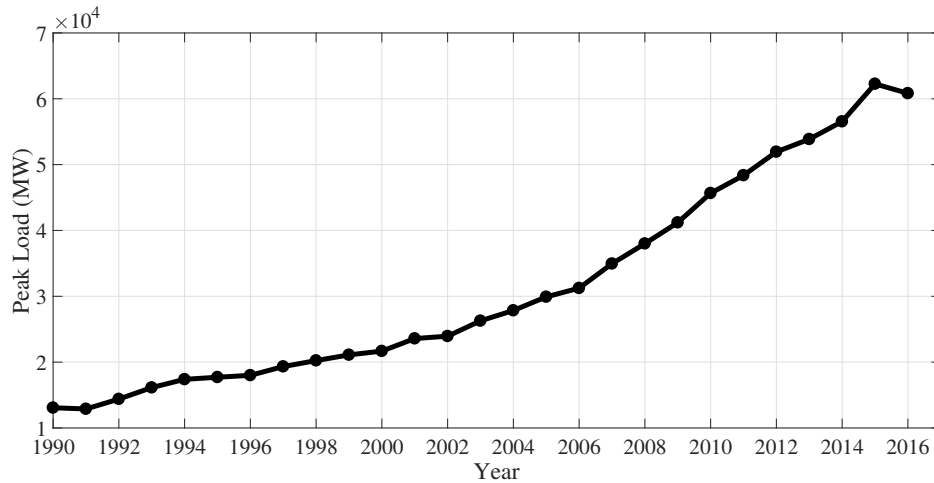


Figure 1.8: Evolution of peak demand

1.5.3 The Water Industry and the Associated Desalination Technologies

According to [25], the total number of desalination plants is 18426 plants worldwide. It is estimated that the average daily desalinated water is more than 86.8 million m³. There are 150 countries where water desalination technology is used, and more than 300 million people worldwide depend on desalinated water for their daily need [25].

Water resources in Saudi Arabia are scarce, and the demand for freshwater cannot be fulfilled from natural water resources only. Which led the kingdom to invest heavily in other solutions, primarily water desalination technologies. The Kingdom of Saudi Arabia holds the title for the largest producer of desalinated water, the reported amount of desalinated water production in 2014 was 1.1076 Billion m³, which is 10% increase from the

previous year of 2013. The Saline Water Conversion Corporation (SWCC) is a Saudi government corporation responsible for the planning and operation of the desalination plants as well as producing electrical power in along with SEC. A total of 28 operational desalination plant was reported in 2014, and the desalination plants are located at both coasts of the kingdom, the Red Sea in the west and the Arabian Gulf in the east. Around 557.5 million m³ of desalinated water was produced from the west coast plants which represent 50.3% of total desalinated water produced in 2014. Thus the east coast plants produced the remaining 49.7% which translates to 550.1 million m³ of desalinated water. The distribution of the desalination plants in the kingdom is shown in figure 1.9. Other entities also participate in the water desalination industry, since SWCC only produce 58% of the daily water load. Shuaibah Water and Electricity have a share of 14%, Jubail Water and Electricity has 13%, and the remaining 15% are from other different producers. The average daily production from all producers was estimated to be 6.22 million m³ [22].

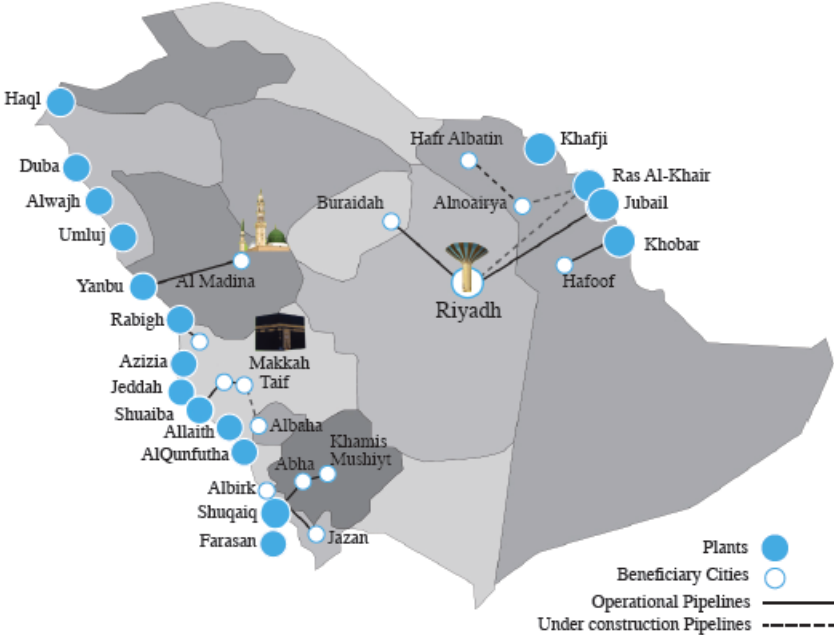


Figure 1.9: Map of desalination plants. Reprinted from [26]

The water desalination technology can be categorized into two fundamental processes; thermal also referred to as phase change and membrane processes. The thermal process mimics the natural water cycle of evaporation and condensation, in which in feed water is heated to boiling temperature. The pollutants in water including salt and minerals remain in the base water as they are heavy elements. The steam is then cooled and condensed which produces water with low salinity levels. Membrane or single phase processes, separate salts without the need for phase transition and it has the advantage of lower energy requirements as compared with the thermal processes. The thermal process plant includes Multi-Stage Flash (MSF) and Multiple Effect Distillation (MED), and the Reverse Osmosis (RO) plant is an example of a membrane process plant [27], [28].

The working principle of MSF (figure 1.10) is that in feed seawater undergo a successive set of stages at successively decreasing temperature and pressure. A vapor would generate from the seawater due to the sudden reduction in pressure as the seawater enters the evacuated chambers, and this process is repeated for multiple stages at a decreasing pressure. An external steam supply is required, and normally it operates at a temperature in the range of 100 °C. To avoid scaling, the maximum temperature is limited by the concentration of the salt, which limits the performance of this method. One of the solutions to this issue is to use bulk liquid boiling which alleviates the issue of scale formation on the heat transfer tubes.

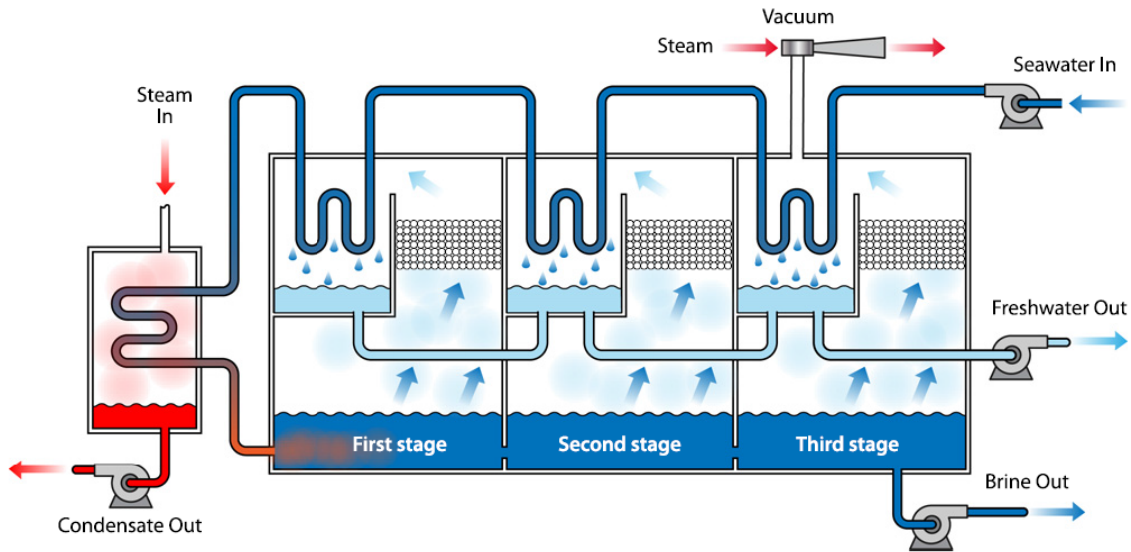


Figure 1.10: Schematic diagram of MSF unit. Reprinted with permission from [29]

As for the MED process (figure 1.11), it shares the same principle of successive stages of decreasing temperature and pressure. Generation of vapors is done due to the absorption of thermal energy by the seawater. In each stage/effect, the steam generated would be able to heat the salt solution of the next stage/effect as every stage is at a lower temperature and pressure from its previous stage. The process performance is proportional to the number of stages/effects. The process also utilizes an external steam supply but at a lower temperature of around 70 °C. The low temperature helps achieve low energy consumption, higher heat transfer coefficient as well as providing higher quality water and also reduces the pre-treatment requirements.

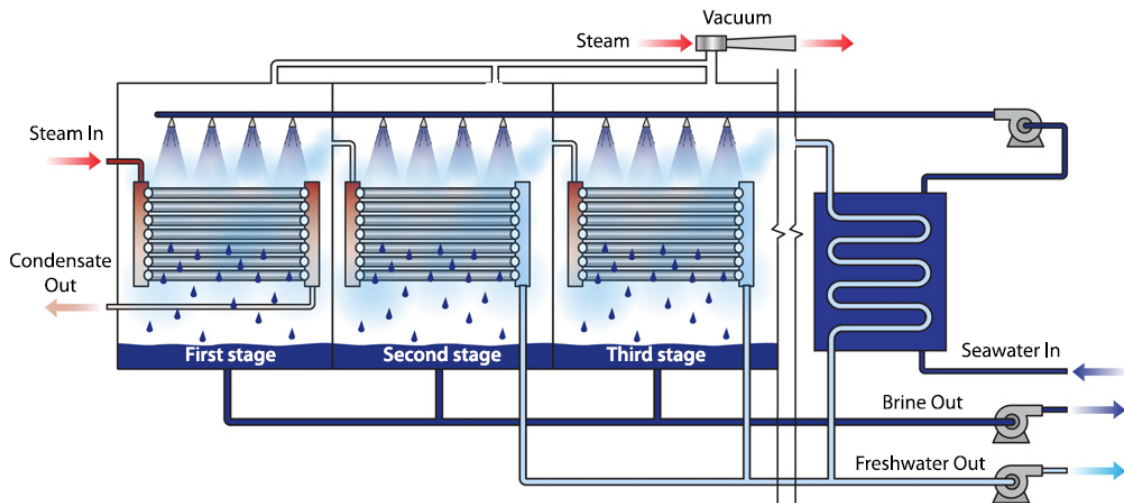


Figure 1.11: Schematic diagram of MED unit. Reprinted with permission from [29]

The membrane process, on the other hand, does not involve phase changes. As previously mentioned RO (figure 1.12) is one of the technologies that involves membranes. Another technology is the Electrodialysis (ED)/Electrodialysis Reversal (EDR) which is usually limited to brackish water, while RO is suitable for both brackish water and seawater. Both processes RO and ED require energy to overcome osmotic pressure between freshwater and saltwater. The fundamental principle of ED which is shown in figure 1.13 is to use electrical currents to attract salt through a selected membrane which would separate salt water from fresh water. The RO process uses high pressure to force seawater against membranes in which water molecules would be able to pass through the membranes and leave behind the salts as a briny concentrate [30].

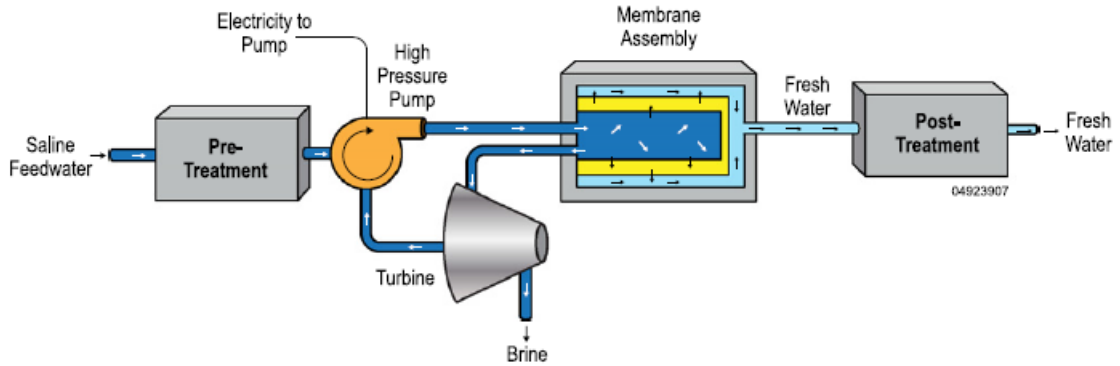


Figure 1.12: Schematic diagram of RO unit. Reprinted with permission from [29]

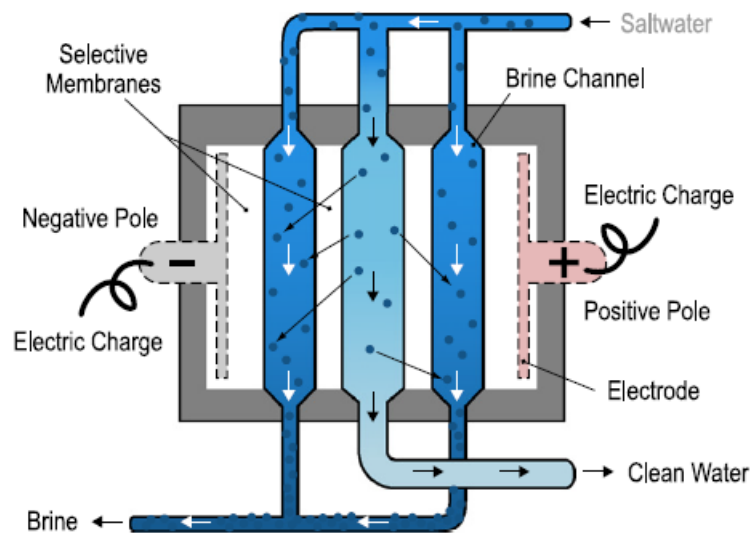


Figure 1.13: Schematic diagram of ED unit. Reprinted with permission from [29]

1.5.4 Brief History of Renewable Energy Development in Saudi Arabia

The application of renewable energy in Saudi Arabia has been growing since 1960, with the first solar PV installed at the airport of Madinah Al Munnawara city. Also, small-scale university projects were established in 1969. In 1977 King Abdulaziz City

for Science and Technology (KACST) initiated a significant research and development project for developing solar energy technologies. A joint program between Saudi Arabia and the United States of America was signed in 1977 called the Saudi Arabian-United States Program for Cooperation in the Field of Solar Energy Program (SOLERAS). The project addressed the technological and economic issues of solar energy [31]. One of several projects conducted by the program in 1980 involved supplying two villages namely Al-Jubaila and Al-Uyaina which were not connected to the main grid by solar energy and Saudi Arabia was the first country in the middle east at that time to research such an approach. The SOLERAS program concluded in 1997 [32].

German-Saudi Arabian Cooperative Program for Research, Development, and Demonstration of Solar Hydrogen Production as well as Utilization of Hydrogen as an Energy Carrier (HYSOLAR) was established in 1987 as a long-term project. The first phase of the project was intended to investigate hydrogen production technologies; this phase ended in 1991. The second phase was a continuation of phase one where the emphasis was on hydrogen utilization technologies [33].

Accurate measurements of solar radiation were very critical to be able to carry out different studies related to solar radiation. Leading to the initiation of the Saudi Atlas Project in 1994 which was a joint project between the Energy Research Institute (ERI) at KACST and the National Research Energy Laboratory (NREL). Twelve different cities were involved in the Atlas, Riyadh, Qassim, Al-Ahsa, Al-Jouf, Tabuk, Madinah, Jeddah, Qaisumah, Wadi Al Dawasir, Sharurah, Abha, and Jazan. All these stations were connected to a central data collection unit [34].

Wind speed measurements were also an interest, as Ansari et al. constructed in 1986 the Saudi Arabia Wind Energy Atlas utilizing hourly data collected from 20 different airports weather stations. The data of 12 years from 1970 to 1982 were used to describe diurnal and seasonal variations of wind speed as well as the wind direction [35].

More recently in 2010, the Kingdom has begun building the first solar-powered water desalination plant divided into three phases. Saudi Aramco has also participated in the renewable sector by developing a pilot project with a capacity of 10 MW in 2011, and a 20 MW solar power plant is planned to be constructed at King Abdullah University of Science and Technology (KAUST) [32].

1.5.5 Review of Previous Studies of Renewable Energy Utilization in the Kingdom

Although renewable energy implementation is not significant for the time being, many studies have been performed to assess the feasibility of implementing such technologies. An economical and technical assessment of a Building Integrated Photovoltaics (BIPV) in the GCC region was done by Sharples and Radhi [36]. The study emphasized the effect of high temperatures on the PV modules efficiency. The analysis revealed that as a result of high temperatures typically expected in the GCC region, the PV efficiency degraded by 4% to 6% which ultimately will reduce the PV power output. The study concluded that BIPV is not able to compete with the conventional power generation sources based on cost per unit energy. However, if other aspects were included such as environmental and social benefits, then BIPV could be a feasible solution. The benefits of BIPV are reduction in CO₂ emission as well as savings in capital costs since the expansion of power plants, transmission and distribution facilities can be deferred or even eliminated. Also, BIPV can be utilized to reduce peak demand which is usually provided by high-cost natural gas units, thus, providing more security to the economy as these fossil fuel resources are available for export at a much higher price.

Al-Hadhrami [37], evaluated the performance of a small power capacity wind turbines as an off-grid power provider for the town of Juaymah, east of the kingdom. The performance evaluation involved 24 WT, where 16 are Horizontal Axis Wind Turbine (HAWT), and the rest are Vertical Axis Wind Turbine (VAWT). The performance of different WTs

based on energy output was done by varying the hub height of the WT tower, which yielded a higher energy output as the height increases. However, the relation between hub height and energy produced is not linear as such careful consideration for the selection of hub height is necessary for economic and technical purposes. The study also concluded that HAWT are more efficient than VAWT for the same rated capacity, as HAWT has a lower cut-in and rated wind speeds.

An economical, as well as an environmental evaluation of a grid-connected 5 MW PV system, was done by Rehman, *et al.* [38]. The study involved determining the most suitable location for a PV power plant from 41 different cities throughout the kingdom. The study concluded that the city of Bisha located in the southwestern region of the kingdom was the best location. Given that Bisha had a high annual average solar radiation potential of a 2560 kWh/m², and an average sunshine duration of about 9.2 hours. Yielding the lowest cost for energy at about 0.2 \$/kWh. As for the environmental aspect of the study, it was shown that a potential of 8182 tons of greenhouse gases (GHG) can be avoided per year.

Solar thermal power (CSP) generation studies are briefly presented in the following section. In [39] Alnasser, investigated the performance and economic viability of a Parabolic Trough Collector (PTC) plant in the industrial city of Jubail, Saudi Arabia. The plant has a footprint of 0.86 km², with a 50 MW electrical generator. The study predicted a capacity factor of about 39% and an overall efficiency of 23%. The levelized cost of energy was three times higher than a conventional power plant at 0.107 \$/kWh. However, this cost can be lowered if environmental benefits and thermal storage were taken into consideration.

The effect of dust accumulation on PV panels was investigated in [40], as dust storms are quite frequent in the region. The study was done in the eastern part of the kingdom, and one of the significant results were, dust accumulation on PV panels for more than six months without cleaning can reduce the power output from the panel be more than

50%. Thus, a comprehensive cleaning process must be done on a regular basis as well as whenever a sandstorm strikes the panels. However, implementing sun trackers with the PV panels help reduce the dust accumulation and thus, increased the power output. A more comprehensive study on the impact of dust and mitigation approaches are reported in [41]. The authors reviewed many previous studies related to climate impacts on the performance of solar collectors in many different geographical locations. Every reviewed study in the kingdom agrees with the reduction of PV power output due to dust accumulation. The study also proposed mitigation approaches to minimize or even eliminate the effect of dust. The mitigation approach was divided into two main categories, preventive and restorative actions. The preventive actions include PV panel surface modification and coating. A more advanced preventive action would be to use electrostatic repulsion also referred to as dry cleaning, as water is not involved in this process. This method is desirable in areas where water availability is scarce such as Saudi Arabia. As for the restorative actions, it primarily includes water washing or cleaning the surface of PV panels using chemical solutions. Other restorative actions can be, airflow directed to the surface of the PV panel and also surface vibration.

A comparative study of different renewable energy sources configuration was done by El-Khashab and Al-Ghamedi [42] in the industrial city of Yanbu on the west coast of Saudi Arabia. The configurations were to have a PV alone system, a PV, and WT system and finally a hybrid PV, WT and Fuel Cell (FC) system. All these systems were assumed to be connected to the main grid to avoid storage requirements. The PV only system had the lowest cost per unit energy at 0.36 \$/kWh, which is still higher than conventional generation. An interesting justification is that all the components required for integrated renewable energy sources would be imported without local fabricated parts. The study also pointed out that the cost of inverters are quite high to neglect and thus, it should be included in any PV feasibility studies. Alternatively, to avoid the necessary use of inverters

in AC systems, the authors suggest that a DC bus system should be used to supply remote residential areas for most of the applications needed.

A hybrid diesel, solar and wind generation study was done by Elhadidy and Shaahid [43] in Dhahran city in Saudi Arabia to supply the local demand. The study concluded that the combination of wind turbines, solar panels, and battery storage could provide up to 77% of the total load energy. However, this study lacks a significant parameter which is a detailed analysis of initial and operating costs. Rehman, *et al.* [44], investigated the cost of energy production from Wind Energy Conversion Systems (WECSs), from 20 different locations covering the central, eastern and western regions of Saudi Arabia. Three different power ratings of WECSs were used, a 2500 kW, 1300 kW and a 600 kW. It was concluded that Yanbu, which is a city located in the west coast of Saudi Arabia, had the lowest cost per unit energy at 0.0234 \$/kWh, 0.0295 \$/kWh and 0.0438\$/kWh for the 2500 kW, 1300 kW and the 600 kW WECS respectively. While Najran, a city in the southwest region of Saudi Arabia had the highest cost of energy at 0.0706 \$/kWh, 0.0829 \$/kWh and 0.121 \$/kWh for the 2500 kW, 1300 kW and the 600 kW WECS respectively.

Al-Garni *et al.* [45], proposed a multi-criteria approach for evaluating renewable energy sources including, solar PV, solar thermal, wind, biomass, and geothermal energy sources. The criteria included economic, technical, socio-political and environmental aspects. The socio-political criteria included employment creation, social and political acceptance as well as the impact on human health and others. The decision-making approach was implemented by the use Analytical Hierarchy Process (AHP) which requires both qualitative and quantitative data. The hierarchy included defining the main goal, the criteria, and sub-criteria that would be used to identify the most suitable source. The last level of the hierarchy is the different renewable energy sources technologies to be investigated. The results of this study suggested that solar PV had the most potential followed by the solar thermal and wind power technologies, while biomass and geothermal energy

sources had the lowest potential as given by their overall performance index based on the criteria previously mentioned. However, this methodology required extensive qualitative data which can be difficult information to acquire.

The optimal interaction between supply and demand is considered to be one of the primary objectives to implement a smart grid framework successfully. Eltamaly, *et al.* [46], proposed a novel approach for optimal sizing of a hybrid renewable energy system while implementing load shifting techniques as the load is divided into high and low priority loads. The high priority loads represent electric demand that needed to be served immediately and cannot be differed. The low priority demand, on the other hand, is considered to be a deferrable electric demand which can be served based on renewable power availability. The hybrid system investigated consist of solar PV, wind power, diesel generators and battery storage system. The optimization problem was formulated as a multi-objective problem, which is to minimize the cost per unit energy and to maximize the reliability of the system by minimizing the Loss of Load Probability (LOLP) metric. The optimization technique used in this study was an iterative search algorithm where the PV area size and number of WT were varied in each step.

1.5.6 Potential and Challenges of Renewable Energy Incorporation and the Saudi Arabian Vision for 2030

Rapid growth in the electricity demand is expected to continue over the next decade in Saudi Arabia at a rate of 6% per year and anticipate the power demand to exceed 120 GW by 2032 [47]. This rapid growth will impose a significant burden on the country to be able to supply the demand. Thus, the kingdom is expected to invest in the range of 20-40 Billion Saudi riyals (\$5.3-\$10.67) Billion on expansion and upgrades of the electrical grid [48].

The continuous interest in renewable energy sources is attributed to their significant

advantages over conventional fossil fuel energy sources. They are considered to be a clean sustainable freely available source of energy. The detailed potential analysis of different renewable energy sources in Saudi Arabia is briefly described in the following.

The Kingdom of Saudi Arabia is blessed with abundant solar energy. By dedicating less than one 0.01% of the country's area for capturing solar energy, the entire energy need of the kingdom can be fulfilled. The average yearly solar radiation energy is 2200 kWh/m² [49]. An average daily radiation from 5.7 kWh/m²/day to 6.7 kWh/m²/day with relatively higher values inland than the coastal areas [49], which is greater than the global average of 1.36 kWh/m²/day [50]. These values represent the Global Horizontal Irradiance (GHI) shown in figure 1.14, which will be discussed in details in chapter 2. This solar radiation component is a major factor in PV operation as in general the higher this value is, the more energy is expected from the solar panels. These high values indicate that the PV technologies can have high performance throughout the kingdom, and extremely high-temperature regions should be avoided. Another solar radiation component is the Direct Normal Irradiance (DNI), this component is essential for Concentrated Solar Thermal (CSP) plants. The DNI annual daily average in the kingdom has more variability than the GHI, ranging from 4.4 kWh/m²/day to 7.3 kWh/m²/day, where the northwest regions of the country had the highest values and the clearest skies. The western region of the country recorded the highest annual daily average for DNI solar radiation component with values over 6.474 kWh/m²/day, which translates to 2400 kWh/m² average yearly. The eastern part of the country, on the other hand, had lower values, 5.51 kWh/m²/day annual daily average and 2000 kWh/m² annual average [49] A map showing the DNI distribution is given in figure 1.15.

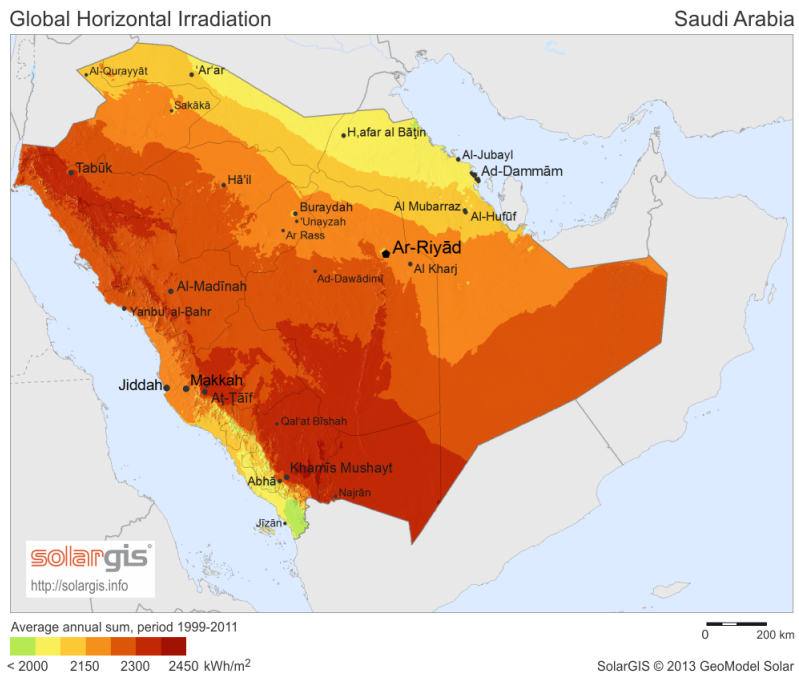


Figure 1.14: GHI distribution in Saudi Arabia. Reprinted with permission from [45]

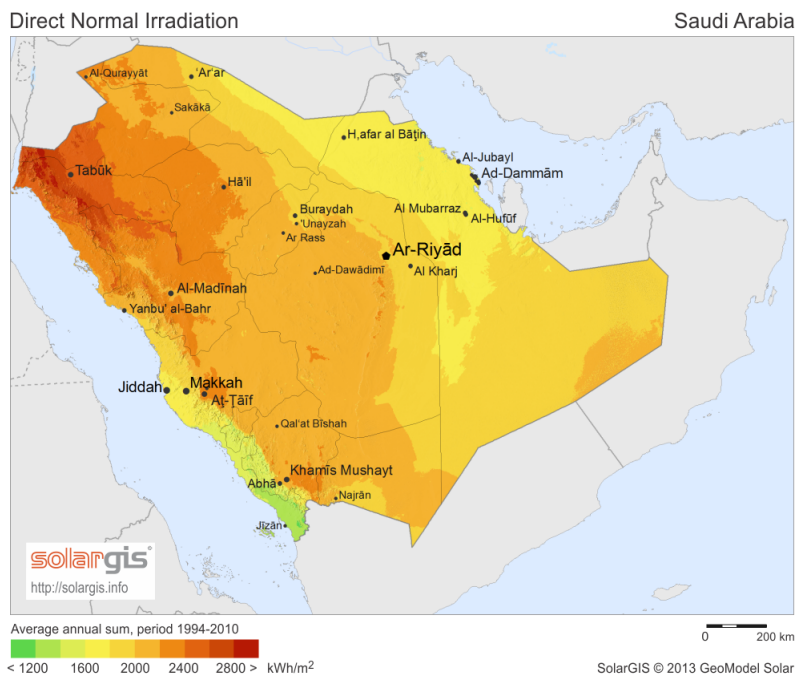


Figure 1.15: DNI distribution in Saudi Arabia. Reprinted with permission from [45]

The wind speed data recorded in the kingdom has a yearly average that varies from 3 to 4.5 m/s at a 10 m, with relatively higher speeds in the summer season (May to August) as compared to other months. This characteristic is considered as an advantage as the electrical load is usually higher in the summer than in any other season [51]. Al-Abbadi in [52], analyzed wind speed of five different sites in Saudi Arabia namely, Dhulum, Arar, Yanbu, Qassim, and Dhahran. These cities are scattered across the kingdom and represent different geographic and climate conditions. Seven years of wind data were used, and it indicated that both cities Dhulum, Arar had the highest annual average wind speed at 5.7 and 5.4 m/s. The wind speed frequency was found to be 60% and 47% for speeds higher than 5 m/s respectively which makes them candidates for stand-alone wind power system. Yanbu and Dhahran which are coastal cities had a lower annual average wind speed values of about 5 m/s. Thus, these two cities were identified as a potential for grid-connected wind power systems. The city of Qassim which is located in the central region of the country had the lowest annual average wind speed recorded among the other four cities. A study done by Radhwan [53] identified the high potential of wind power in the northern and coastal sites of Saudi Arabia, based on a study performed analyzing monthly average wind speeds of 20 different cities in the kingdom.

For the geothermal energy, the potential exists in Saudi Arabia, although, their availability is not abundant. A better approach could be to combine solar and geothermal power to provide electricity and water. As reported in [8], Saudi Arabia has ten hot springs in Jazan and Al Lith regions south of the country. The Study done in [8] concluded that a critical barrier for adopting geothermal energy is the lack of political support for this technology.

With the enormous renewable sources potential in the kingdom and the ever-increasing pressure on the country's hydrocarbon resources to meet the growing demand for energy, it is evident that renewable energy source would be exploited with an additional implicit

incentive of fuel savings which can potentially be exported to the global market [16].

The Kingdom of Saudi Arabia has already taken steps towards sustainable energy implementation, by establishing King Abdullah City for Atomic and Renewable Energy (KACARE) in 2010. Aiming at building alternative energy sources to penetrate the current electricity grid. A comprehensive evaluation study by KACARE concluded that hydrocarbon energy sources would remain a primary element of the energy mix in 2032, and suggests supporting it with nuclear, solar, wind, waste-to-energy, and geothermal as shown the figure 1.16 [47].

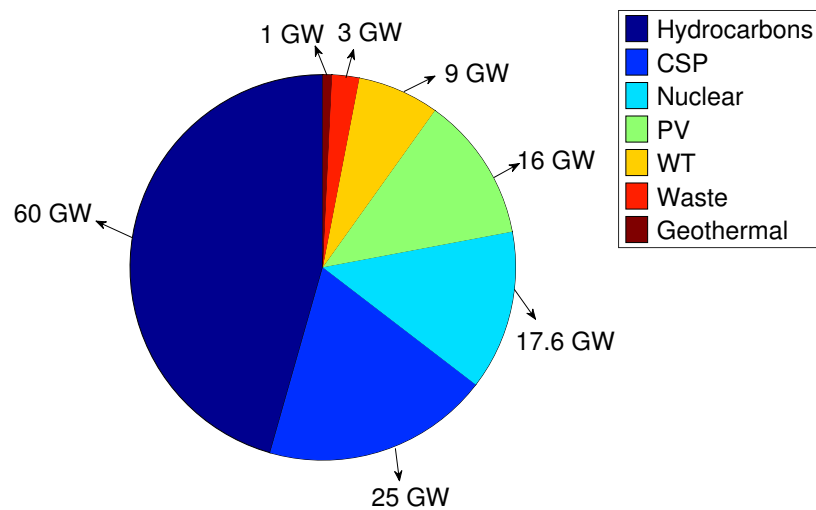


Figure 1.16: KACARE suggested energy mix in 2032

The Kingdom of Saudi Arabia represented by the Council of Economic and Development Affairs launched in 2016 its vision for 2030, which is a roadmap for the development of the whole country. It involves the transformation of different aspects of the kingdom, economically, socially and many other. The vision revolves around three many themes, a vibrant society, a thriving economy and an ambitious nation. Strategic objectives, targets,

commitments and performance indicators are established to be performed by the public, private, and nonprofit sectors [54]. A National Transformation Program (NTP) 2020 was also established across 24 government entities operating in the economic and development sectors, to track the progress of the immediate goals for 2020. One of the targeted ministries in the program that is of importance for this dissertation, is the Ministry of Energy, Industry, and Mineral Resources (MEIM). The NTP assigned ten strategic objectives to be fulfilled by MEIM. One of the objectives was to increase the efficiency of fuel used for electrical power generation. The Ministry of Environment, Water, and Agriculture (MEWA) was also assigned a strategic objective to optimize the use of renewable water resources for agricultural purposes. Also, KACARE has its share in the NTP with four key objectives. In which it needs to enable renewable energy to actively contribute to the national energy mix as well as enhance the competitiveness of energy sector, with a targeted renewable power capacity of 3.45 GW by 2020 which would represent a supply of 4% of total energy used. Other objectives related to KACARE include the localization of renewable energy technologies and also to localize the personnel working in the renewable energy sectors by having 7774 jobs related to the atomic and renewable energy sector and develop the necessary legislation to implement these technologies [55]. The justification for countries that are rich in fossil fuels can be demonstrated in the flowchart of figure 1.17.

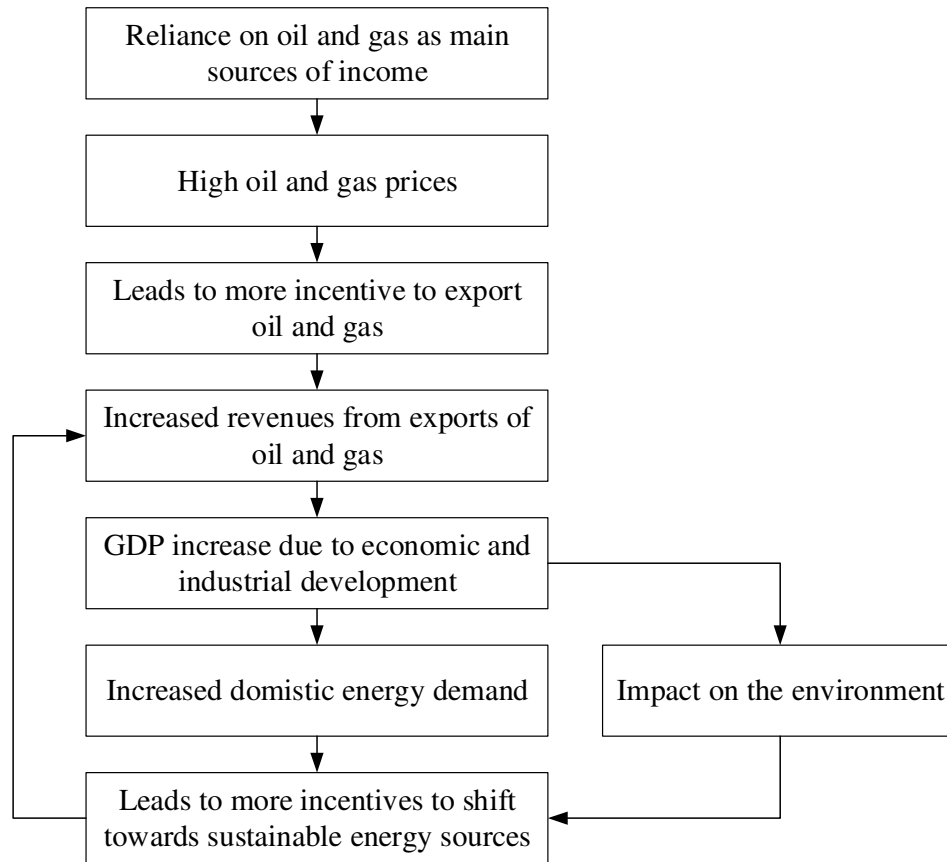


Figure 1.17: Justification for moving towards sustainable energy sources in GCC countries

1.6 The Smart Grid Concept

The conventional grid is designed to carry electrical power from large electricity generation utilities and deliver it to a large number of consumers. Smart Grid (SG) in contrast utilizes a bidirectional flow of electrical power and communication signals. It can help to deliver electric power more efficiently and also be able to respond and adapt to different system events (i.e., faults). Thus, the SG is an intelligent grid and can integrate activities from various grid users, such as generation utilities and their consumers to deliver an efficient, economical, reliable, and also sustainable electrical energy [56].

The Smart Grid provides a platform for maximizing specific features of an electrical

network including reliability, availability, efficiency, system security as well as economic performance.

The advantages gained from implementing an SG framework include the improvement of electrical power reliability and quality as well as the resilience to system disruption, it also provides a better accommodation for distributed energy sources including renewable sources. Reduction in fossil fuel power generation can be achieved as the SG can handle peak demand in a more efficient manner which would minimize the consumption of inefficient conventional generators [57].

Traditionally, the generation system would be planned to have a higher power capacity than the peak demand anticipated. A capacity margin of about 20% is considered to be sufficient to account for the load demand that varies on a daily and seasonally basis, and mostly uncontrollable. The average utilization factor of the generation system is below 55% which is considered a low percentage and opens up the realm of Demand-Side Management (DSM). Shifting load from peak to off-peak periods can potentially reduce the need for additional generating capacity and as such increase the plant utilization which will ultimately improve the overall system efficiency [58].

2. ENERGY SOURCES MODELING

2.1 Sun and Surface Angles

The first step towards calculating the power output of renewable sources is to model the available resources that reach the renewable energy technology in question. For the PV panels, the resource is the solar radiation that strikes the panel. Determining the sun's position as seen from the earth's surface is of paramount importance for accurately calculating solar radiations incident on a tilted surface which will ultimately impact the output power from the PV panels. Therefore, the solar coordinates must be addressed carefully to accurately predict the solar radiation that strikes the surface under consideration [59].

In the sun position algorithm, the effective time of the current time step is the midpoint of the time step for sun position calculations except for hours containing sunrise and sunset.

$$\begin{aligned} hr_{eff} &= hr - 1 \\ min &= 30 \end{aligned} \tag{2.1}$$

To account for leap years

$$k = \begin{cases} 1 & \text{if } \text{mod}(\text{year}, 4) = 0 \\ 0 & \text{if } \text{mod}(\text{year}, 4) = 1 \end{cases} \tag{2.2}$$

The total number of days in a year N is given as:

$$N = 365 + k \tag{2.3}$$

The current local hour is expressed in terms of universal time coordinated depending on the hour, minute and time zone of the selected location.

$$t_{utc} = hr_{eff} + \frac{min}{60} - tz \quad (2.4)$$

And it is forced to be within the range ($0 \leq t_{utc} \leq 24$)

$$t_{utc} = \begin{cases} t_{utc} + 24 & \text{if } t_{utc} < 0 \\ t_{utc} - 24 & \text{if } t_{utc} > 24 \end{cases} \quad (2.5)$$

The Julian day jd is used in the preliminary calculations of the ecliptic coordinates. The Julian day is also used to calculate the Greenwich mean sidereal time and subsequently the local mean sidereal time [60]. Here, $year$ and n are the simulation year and day number under consideration.

$$jd = 2432916.5 + 365(year - 1949) + \text{INT}\left(\frac{year - 1949}{4}\right) + n + \frac{t_{utc}}{24} \quad (2.6)$$

Following is the calculation of the difference in days between the current Julian date jd and the Julian date of January 1st of the year 2000.

$$\Delta jd = jd - 2451545 \quad (2.7)$$

The ecliptic coordinates of a location, define the photovoltaic array's position on the earth relative to the sun. The ecliptic coordinate variables are the mean longitude, mean anomaly, ecliptic longitude, and obliquity of the ecliptic. The ecliptic coordinates include the effect of the earth's inclination in the sun angle calculations which gives more accurate results than the equatorial coordinates [61].

$$ML = 280.46 + (0.9856474 \times \Delta jd) \quad (2.8)$$

$$ML^{corr} = ML - 360 \text{INT}\left(\frac{ML}{360}\right) \quad (2.9)$$

$$ML = \begin{cases} ML^{corr} & \text{if } ML^{corr} \geq 0 \\ ML^{corr} + 360 & \text{if } ML^{corr} < 0 \end{cases} \quad (2.10)$$

$$MA = 357.528 + (0.9856003 \times \Delta jd) \quad (2.11)$$

$$MA^{corr} = MA - 360 \text{INT}\left(\frac{MA}{360}\right) \quad (2.12)$$

$$MA = \begin{cases} \frac{\pi}{180} MA^{corr}, & \text{if } MA^{corr} \geq 0 \\ \frac{\pi}{180} (MA^{corr} + 360), & \text{if } MA^{corr} < 0 \end{cases} \quad (2.13)$$

$$EL = \left(ML + 1.915 \sin\left(MA \frac{180}{\pi}\right) + 0.02 \sin\left(2MA \frac{180}{\pi}\right) \right) \quad (2.14)$$

$$EL^{corr} = EL - 360 \text{INT}\left(\frac{EL}{360}\right) \quad (2.15)$$

$$EL = \begin{cases} \frac{\pi}{180} EL^{corr}, & \text{if } EL^{corr} \geq 0 \\ \frac{\pi}{180} (EL^{corr} + 360), & \text{if } EL^{corr} < 0 \end{cases} \quad (2.16)$$

$$Ob = 23.439 - 0.0000004 \times \Delta jd \quad (2.17)$$

$$Ob^{corr} = Ob - 360 \text{INT}\left(\frac{Ob}{360}\right) \quad (2.18)$$

$$Ob = \begin{cases} \frac{\pi}{180} Ob^{corr}, & \text{if } Ob^{corr} \geq 0 \\ \frac{\pi}{180} (Ob^{corr} + 360), & \text{if } Ob^{corr} < 0 \end{cases} \quad (2.19)$$

Where, ML is the mean longitude in degrees. MA , EL and Ob are the mean anomaly, ecliptic longitude and obliquity of ecliptic respectively in Radians.

The celestial coordinates including the right ascension RA and declination angle DA which are shown in figure 2.1 are given in radians as follows:

$$RA = \tan^{-1}(\cos(Ob) \tan(EL)) \quad (2.20)$$

$$RA = \begin{cases} RA + \pi, & \text{if } \cos(EL) < 0 \\ RA + 2\pi, & \text{if } \cos(Ob) \sin(EL) < 0 \end{cases} \quad (2.21)$$

$$DA = \sin^{-1}(\sin(Ob) \sin(EL)) \quad (2.22)$$

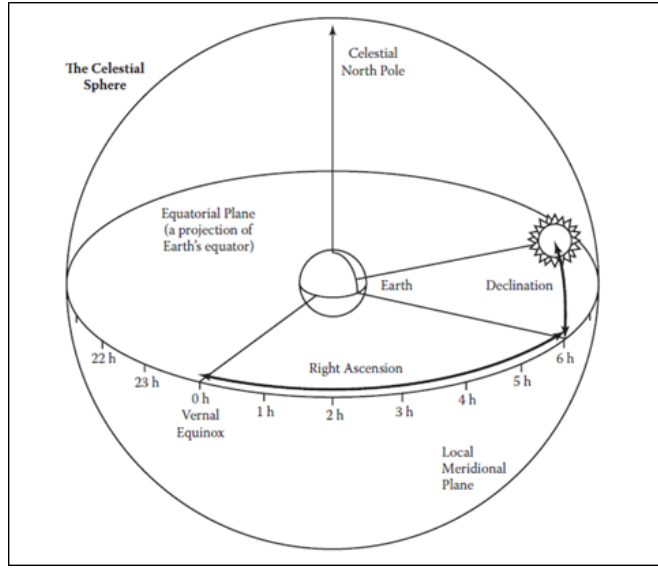


Figure 2.1: Illustration of the celestial sphere and coordinates. Reprinted with permission from [62]

The local coordinates are given by the Greenwich Mean Siderial Time $GMST$ and the Local Mean Siderial Time $LMST$ in hours which are required to calculate the hour angle HA in radians:

$$GMST = 6.697375 + (0.0657098242 \times \Delta jd) + t_{utc} \quad (2.23)$$

$$GMST^{corr} = \text{mod}(GMST, 24) \quad (2.24)$$

$$GMST = \begin{cases} GMST^{corr} + 24, & \text{if } GMST^{corr} < 0 \\ GMST^{corr}, & \text{Otherwise} \end{cases} \quad (2.25)$$

$$LMST = GMST + (lon/15) \quad (2.26)$$

$$LMST^{corr} = \text{mod}(LMST, 24) \quad (2.27)$$

$$LMST = \begin{cases} LMST^{corr} + 24, & \text{if } LMST^{corr} < 0 \\ LMST^{corr}, & \text{Otherwise} \end{cases} \quad (2.28)$$

$$ha = \left(15 \frac{\pi}{180}\right) LMST - RA \quad (2.29)$$

$$HA = \begin{cases} ha + 2\pi, & \text{if } ha < -\pi \\ ha - 2\pi, & \text{if } ha > \pi \\ ha & \text{Otherwise} \end{cases} \quad (2.30)$$

Now, that all the necessary angles have been found, the solar altitude θ_α , the sun's azimuth angle θ_γ and the zenith angle θ_Z can be easily calculated. The different angles are shown in figure 2.2.

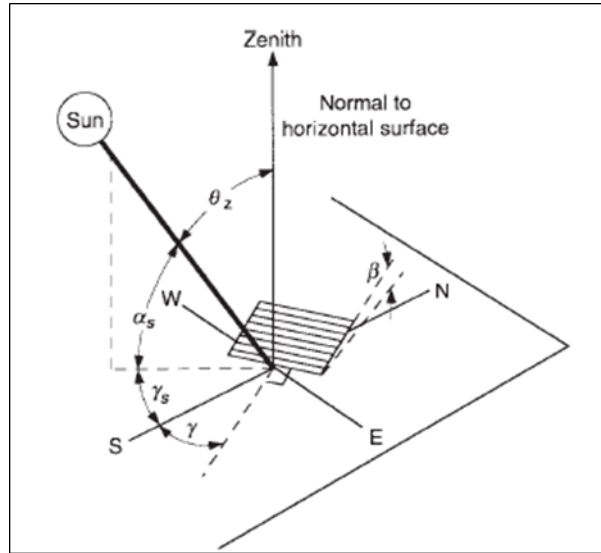


Figure 2.2: Surface and sun angles. Reprinted with permission from [63]

The notations used in figure 2.2 are different from the notations used in this dissertation. The description of the angles in the figure are: Zenith angle θ_Z , slope β , solar altitude

angle α_s , surface azimuth angle γ , and solar azimuth angle for a tilted surface γ_s .

$$\alpha = \left(\sin(DA) \sin\left(\frac{\pi}{180}lat\right) \right) + \left(\cos(DA) \cos\left(\frac{\pi}{180}lat\right) \cos(HA) \right) \quad (2.31)$$

$$\alpha_0 = \begin{cases} \sin^{-1}(\alpha), & \text{if } -1 \leq \alpha \leq 1 \\ \frac{\pi}{2}, & \text{if } \alpha > 1 \\ \frac{-\pi}{2}, & \text{if } \alpha < -1 \end{cases} \quad (2.32)$$

To account for refraction, the sun's altitude angle is corrected by initially converting the angle from Radians to degrees:

$$\alpha_{0d} = \frac{180}{\pi} \alpha_0 \quad (2.33)$$

The correction factor r is computed as shown below:

$$r = \begin{cases} 3.51561 \left(\frac{0.1549 + 0.0196\alpha_{0d} + 0.00002\alpha_{0d}^2}{1 + 0.505\alpha_{0d} + 0.0845\alpha_{0d}^2} \right), & \text{if } \alpha_{0d} > -0.56 \\ 0.56, & \text{if } \alpha_{0d} \leq -0.56 \end{cases} \quad (2.34)$$

Finally, the sun altitude angle corrected for refraction θ_α in Radians is calculated:

$$\theta_\alpha = \begin{cases} \frac{\pi}{2}, & \text{if } \alpha_{0d} + r > 90 \\ \frac{\pi}{2}(\alpha + r), & \text{if } \alpha_{0d} + r \leq 90 \end{cases} \quad (2.35)$$

$$a = \frac{\sin(\alpha_0) \sin\left(\frac{\pi}{180}lat\right) - \sin(DA)}{\cos(\alpha_0) \cos\left(\frac{\pi}{180}lat\right)} \quad (2.36)$$

$$\psi = \begin{cases} \cos^{-1}(a), & \text{if } -1 \leq a \leq 1 \\ \pi, & \text{if } \alpha_{0d} = 0 \text{ or } a < -1 \\ 0, & \text{if } a > 1 \end{cases} \quad (2.37)$$

The sun's azimuth angle θ_ψ in radians is given as follows:

$$\theta_\psi = \begin{cases} \psi, & \text{if } HA < -\pi \\ \pi - \psi, & \text{if } -\pi \leq HA \leq 0 \text{ or } HA \geq \pi \\ \pi + \psi, & \text{if } 0 < HA < \pi \end{cases} \quad (2.38)$$

The sun's zenith angle θ_Z in radians is the complement of the solar altitude angle given by:

$$\theta_Z = \frac{\pi}{2} - \theta_\alpha \quad (2.39)$$

With all these angles calculated, the angle at which the solar radiation strikes a PV panel is known as the angle of incidence θ_{AOI} in radians, and can be calculated by:

$$c = \sin(\theta_Z) \cos(\theta_\psi - \gamma_s) \sin(\beta_s) + \cos(\theta_Z) \cos(\beta_s) \quad (2.40)$$

$$\theta_{AOI} = \begin{cases} \pi, & \text{if } c < -1 \\ 0, & \text{if } c > 1 \\ \cos^{-1}(c), & \text{if } -1 \leq c \leq 1 \end{cases} \quad (2.41)$$

As previously mentioned, the midpoint of the time step is used to calculate all the aforementioned variables. However, this is not appropriate for time steps containing sunrise or sunset since the midpoint can be before the sun has risen or after the sun has set.

Therefore, an alternative method to the hour midpoint is used. First, the sunrise and sunset hours are calculated. Moreover, instead of using the midpoint of the hour, the end of the hour is used for the time step that contains sunrise. The beginning of the hour is used for the time step that contains sunset. This method ensures that when calculating the angles, the sun is always up.

The sunrise and sunset hour angles are given by the following equation:

$$har = -\tan\left(\frac{\pi}{180}lat\right)\tan(DA) \quad (2.42)$$

$$HAR = \begin{cases} 0, & \text{if } har \geq 1 \\ \pi, & \text{if } har \leq -1 \\ \cos^{-1}(har), & \text{if } -1 < har < 1 \end{cases} \quad (2.43)$$

To calculate the sunrise and sunset hours, the equation of time in hours EOT is needed

$$\tau = ML - \frac{RA}{15} \frac{180}{\pi} \quad (2.44)$$

$$EOT = \begin{cases} \tau, & \text{if } -0.33 \leq \tau \leq 0.33 \\ \tau + 24, & \text{if } \tau < -0.33 \\ \tau - 24, & \text{if } \tau > 0.33 \end{cases} \quad (2.45)$$

Now that all the required variables are computed, the sunrise and sunset hours t_{sr}, t_{ss} can be easily calculated.

$$t_{sr} = 12 - \frac{HAR}{15} \frac{180}{\pi} - \frac{lon}{15} + tz - EOT \quad (2.46)$$

$$t_{ss} = 12 + \frac{HAR}{15} \frac{180}{\pi} - \frac{lon}{15} + tz - EOT \quad (2.47)$$

2.2 Sun Position Tracking System

Solar collectors mainly PVs can be equipped with tracking systems. The main goal is to minimize the angle of incidence which will result in maximum incident radiation. The developed tool has three main tracking options, fixed axis, single and two axis tracking. Where β_0, β_s are the default and actual surface tilt angle in Radians. $\theta_{\psi_0}, \theta_{\psi_s}$ are the surface default and actual azimuth angle in Radians.

2.2.1 Fixed Axis

Here the PV panel is fixed at a certain tilt and azimuth angles. Thus, no tracking of the sun is done with this method which leads to lowest expected solar radiation capture.

$$\begin{aligned} \beta_s &= \beta_0 \\ \theta_{\psi_s} &= \theta_{\psi_0} \end{aligned} \quad (2.48)$$

2.2.2 Single Axis

This option provides a tracking mechanism for the panels to track the sun azimuth angle typically from east to west, which allows for a better solar radiation reception.

$$\begin{aligned} \beta_s &= \beta_0 \\ \theta_{\psi_s} &= \theta_{\psi} \end{aligned} \quad (2.49)$$

2.2.3 Two Axis

With this option a complete vertical and horizontal movement of the panels is allowed. This method provides the best solar radiation reception.

$$\begin{aligned}\beta_s &= \theta_Z \\ \theta_{\psi_s} &= \theta_\psi\end{aligned}\tag{2.50}$$

2.3 Solar Radiation Components

The solar radiation components are usually divided into three components namely, the Global Horizontal Irradiance (GHI), the Direct Normal Irradiance (DNI) and the Diffused Horizontal Irradiance respectively (DHI). Typically the solar radiation components are available before conducting a study to determine the amount of solar radiation incident on a tilted surface. It is obviously better to have all three components measured and available. However, that might not be the case, and thus a proceeding step must be done before the simulation step to determine the values of the missing data. It should be noted that by measuring two of the components, the third component can be calculated as in the formula below [62]:

$$G_g = G_b \cos(\theta_Z) + G_d\tag{2.51}$$

Where, G_g , G_b , G_d are the GHI, DNI, and DHI respectively in W/m^2 .

The ideal situation is to have all these values measured at an hourly time step resolution. However, some locations might lack the availability of hourly data for one of the solar radiation components, and thus the missing component would have to be calculated using equation (2.51).

If only G_g component is known which is sometimes the case, a clearness index is used to derive the other two components. An hourly clearness index k_T is defined as follows

[64], [61]:

$$k_T = \frac{G_g}{G_0} \quad (2.52)$$

The extraterrestrial radiation is defined as the solar radiation imposed above the earth's surface. on average the extraterrestrial radiation has a value of 1367W/m². This parameter is crucial in calculating the amount of energy that is received by earth's surface [62].

$$G'_{ext} = 1367 \left(1 + 0.033 \cos \left(\frac{\pi}{180} \frac{360n}{365} \right) \right) \quad (2.53)$$

$$G_0 = \begin{cases} G'_{ext} \cos(\theta_Z), & \text{if } 0 < \theta_Z \leq \frac{\pi}{2} \\ G'_{ext}, & \text{if } \theta_Z = 0 \\ 0, & \text{if } \theta_Z < 0 \text{ or } \theta_Z > \frac{\pi}{2} \end{cases} \quad (2.54)$$

From the clearness index the hourly values of the diffused component can be obtained by either using the Erbs *et al.*, correlations or the Orgill and Hollands correlations. The Erbs *et al.*, correlations are expressed as follows [64]:

$$\frac{G_d}{G_g} = \begin{cases} 1.0 - 0.09k_T & \text{for } k_T \leq 0.22 \\ 0.9511 - 0.1604k_T + 4.388k_T^2 - 16.638k_T^3 \\ + 12.336k_T^4 & \text{for } 0.22 < k_T \leq 0.8 \\ 0.165 & \text{for } k_T > 0.8 \end{cases}$$

Similarly, the Orgill and Hollands correlations can be formulated as follows [59]:

$$\frac{G_d}{G_g} = \begin{cases} 1.0 - 0.249k_T & \text{for } 0 \leq k_T < 0.35 \\ 1.557 - 1.84k_T & \text{for } 0.35 \leq k_T < 0.75 \\ 0.177 & \text{for } k_T > 0.75 \end{cases}$$

Both correlations produce similar results. From these correlations, it is assumed that the value of G_g is known (measured) and from it, G_d can be calculated. Furthermore, by using equation (2.51), the value of G_b can be obtained and thus, all the components of the solar radiation are available.

2.4 Solar Radiation on Tilted Surfaces

It would be relatively expensive to have a measured solar radiation data for every possible tilt angle. Thus the need for models to predict the amount of solar radiation collected on a tilted surface is needed. Many models have been developed to convert typical horizontal measured solar radiation into their equivalent tilted counterparts [65].

The direct solar beam radiation G_b^T , as well as the reflected solar radiation G_r^T for a tilted surface, can be easily calculated in W/m^2 by the following equations [63]:

$$G_b^T = G_b \cos \theta_{AOI} \quad (2.55)$$

$$G_r^T = \rho G_g \frac{1 - \cos \beta}{2} \quad (2.56)$$

The total incident solar irradiance striking a tilted surface can be expressed as:

$$G^T = G_b^T + G_r^T + G_{d,iso}^T + G_{d,cs}^T + G_{d,hb}^T \quad (2.57)$$

Where, G^T is the total solar irradiance on the tilted surface in W/m^2 . $G_{d,iso}^T$, $G_{d,cs}^T$ and $G_{d,hb}^T$ are the isotropic, the circumsolar and the horizon brightening components of the diffused solar irradiance on the tilted surface given in W/m^2 .

The challenging part is to estimate the tilted irradiance from the horizontal diffused solar component. Therefore, the need for accurate models to predict the diffused radiation on a tilted surface is of most importance. The sky diffuse models can be categorized into two main models, namely isotropic and anisotropic models. The isotropic model assumes that the diffuse radiation is uniform throughout the skydome. On the other hand, the anisotropic models take into account additional components. Namely, the circumsolar and horizon brightening components. The sky diffuse models are discussed in the following subsections [66], [63], [67]. The different components of solar radiation are illustrated in figure 2.3.

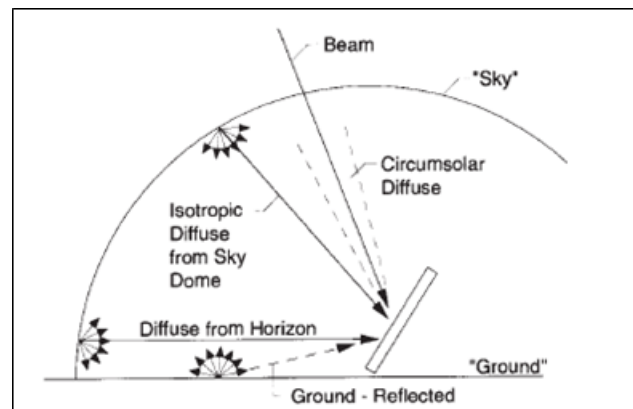


Figure 2.3: Beam, diffuse, and ground-reflected radiation on a tilted surface. Reprinted with permission from [63]

2.4.1 Isotropic Diffusion Model

This model was developed by Liu and Jordan (1963). And it assumes that the diffused component of the solar radiation only contain the isotropic part, and neglect the effect of both the circumsolar and the horizon brightening parts [3], [63], [59].

$$G_{d,iso}^T = G_d \frac{1 + \cos(\beta)}{2} \quad (2.58)$$

$$G_{d,cs}^T = 0 \quad (2.59)$$

$$G_{d,hb}^T = 0 \quad (2.60)$$

2.4.2 HDKR Diffusion Model

This model is the combination of two models. The first model was developed by Hay and Davies (1981), and they assumed that the diffused radiation have in addition to the isotropic component a circumsolar component and has the same direction as the beam radiation. The horizon brightening component was ignored. The second model is the Reindl *et al.*, model, where the horizon brightening factor was taken into consideration along with the isotropic and the circumsolar factors [3], [63], [68].

$$R_b = \frac{\cos(\theta_{AOI})}{\cos(\theta_z)} \quad (2.61)$$

$$A_i = \frac{G_b \cos(\theta_z)}{G_0} \quad (2.62)$$

$$M_f = \sqrt{\frac{G_b \cos(\theta_z)}{G_g}} \quad (2.63)$$

$$C_f = \sin^3 \frac{\beta}{2} \quad (2.64)$$

$$G_{d,iso}^T = G_d(1 - A_i) \frac{1 + \cos(\beta)}{2} \quad (2.65)$$

$$G_{d,cs}^T = G_d A_i R_b \quad (2.66)$$

$$G_{d,hb}^T = G_{d_{T,iso}} M_f C_f \quad (2.67)$$

Where, R_b is the ratio of incident beam to horizontal beam irradiance. A_i is the anisotropy index for the forward scattering circumsolar diffuse irradiance. M_f is the modulating factor for horizontal brightening correction. C_f is a correction factor used for the horizon brightening component.

2.4.3 Perez Diffusion Model

The Perez model is considered to be a more complicated and a detailed model than the aforementioned models. where the circumsolar and horizon brightness components are dealt with in a more detailed fashion. The main difference between the Perez model to that of the HDKR model is that the Perez model adopts empirical coefficients based on large number of measurements over wide range of sky conditions as well as locations [59], [63], [69].

$$a = \max(0, \cos \theta_{AOI}) \quad (2.68)$$

$$b = \max(\cos 85^\circ, \cos \theta_Z) \quad (2.69)$$

$$\epsilon = \frac{\frac{G_d + G_b}{G_d} + 5.535 \times 10^{-6} \theta_Z^3}{1 + 5.535 \times 10^{-6} \theta_Z^3} \quad (2.70)$$

$$m = \frac{1}{\cos \theta_Z} \quad (2.71)$$

$$\Delta = m \frac{G_d}{1367} \quad (2.72)$$

$$F_1 = \max \left[0, (f_{11} + f_{12} \Delta + \frac{\pi \theta_Z}{180} f_{13}) \right] \quad (2.73)$$

$$F_2 = \left(f_{21} + f_{22} \Delta + \frac{\pi \theta_Z}{180} f_{23} \right) \quad (2.74)$$

$$G_{d,iso}^T = G_d (1 - F_1) \frac{1 + \cos \beta}{2} \quad (2.75)$$

$$G_{d,cs}^T = G_d F_1 \frac{a}{b} \quad (2.76)$$

$$G_{d,hb}^T = G_d F_2 \sin \beta \quad (2.77)$$

Where, a and b are terms that account for the angles of incidence of the cone of the circumsolar radiation on the tilted and horizontal surfaces. ϵ is unit less clearness parameter. m is the absolute optical air mass, Δ is a unitless sky brightness parameter. f is the Perez sky diffuse irradiance model coefficients which can be found in [69]. F_1 and F_2 are the circumsolar and horizon brightness coefficients.

2.5 Solar Photovoltaic (PV)

Various methods for modeling the solar cell behavior when exposed to sun light are available in the literature. These models range from being simplistic for quick and easy estimation of output power, to very detailed and complicated models to accurately estimate the amount of energy produced by a given PV panel. The basic solar cell circuit is shown in figure 2.4 [70]:

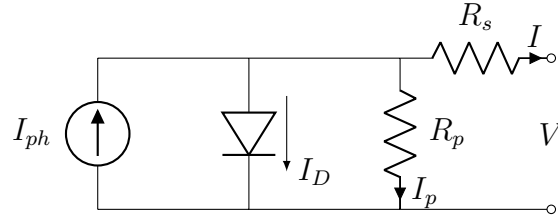


Figure 2.4: Practical solar cell model

$$I = I_{ph} - I_D - I_p \quad (2.78)$$

$$I_D = I_0 \left[\exp \left(\frac{q(V + IR_s)}{kT_c} \right) - 1 \right] \quad (2.79)$$

$$I_p = \frac{V + IR_s}{R_p} \quad (2.80)$$

Where, k is the Boltzmann's gas constant (1.381×10^{23} J/K). T_c is the absolute temperature of the cell (K). q is the electronic charge (1.602×10^{-19} J/V). V is the voltage imposed across the cell (V), I_0 is the dark saturation current, which depends strongly on the temperature (A). R_p and R_s are the parallel and series resistances respectively (Ω). These equations can be simplified by taking the following considerations. Firstly, the shunt resistance is considered to be much greater than the load resistance. Secondly, the series resistance is much smaller than the load resistance, which implies that less power is dissipated within the solar cell itself. Therefore, these two resistances can be ignored without losing much of the accuracy of the model, and the net current is given as [3], [63]:

$$I = I_0 \left[\exp \left(\frac{qV}{kT_c} \right) - 1 \right] \quad (2.81)$$

The standard practice with PV panels related studies is to provide values for the short-circuit current, the open circuit voltage, the maximum current, voltage, and power, as well as other parameters at stranded radiation and temperature, often referred to as the Standard Test Conditions (STC). It is thus helpful to develop models that can predict the PV current, voltage and ultimately the power output using these standardize values.

If the resistances are to be taking into consideration, the parallel resistance R_p is considered to be independent of temperature. However, it behaves inversely proportional to the solar radiation as:

$$R_p = R_p^{ref} \frac{G^{ref}}{G} \quad (2.82)$$

As for the series resistance R_s it is assumed to be independent from both solar radiation and temperature, and thus:

$$R_s = R_s^{ref} \quad (2.83)$$

The cell temperature can be expressed as follows [71]:

$$T_C = T_A + \left(\frac{NOCT - 20}{800} \right) G^T \quad (2.84)$$

Where, R_p^{ref} and R_s^{ref} are the parallel and series resistances at a certain cell temperature and solar radiation (Ω). G^{ref} is the solar radiation at testing most often referred to as (STC) (W/m^2). $NOCT$ is the Nominal Operating Cell Temperature which is the temperature of a cell operating at open circuit condition with an ambient temperature of 20°C , air mass of 1.5, an irradiance of $800 \text{ W}/\text{m}^2$ and a wind speed less than $1\text{m}/\text{s}$. This value is typically available with the solar panel data sheet. T_C and T_A are the solar cell and ambient temperatures at the location ($^\circ\text{C}$). Typical I-V curves for a particular solar cell is shown in figure 2.5. The primary goal in determining the behavior of a solar cell is to ultimately predict the amount of power that a particular solar cell able to produce under certain operating conditions mainly, solar radiation and temperature.

2.5.1 Simple Efficiency Model

The simple efficiency model is considered to be one of the simplest models in determining the DC power output of a solar panel P_{DC} [72], [73]. Where A and η_{pv} are the surface area in (m^2) and efficiency of the PV panel respectively.

$$P_{DC} = G^T A \eta_{pv} \quad (2.85)$$

2.5.2 Temperature Adjusted Simple Efficiency Model

The previous model neglects the effect of temperature on the solar cell and considers the efficiency of the cell to be constant over all ranges of temperature, thus in [61] this

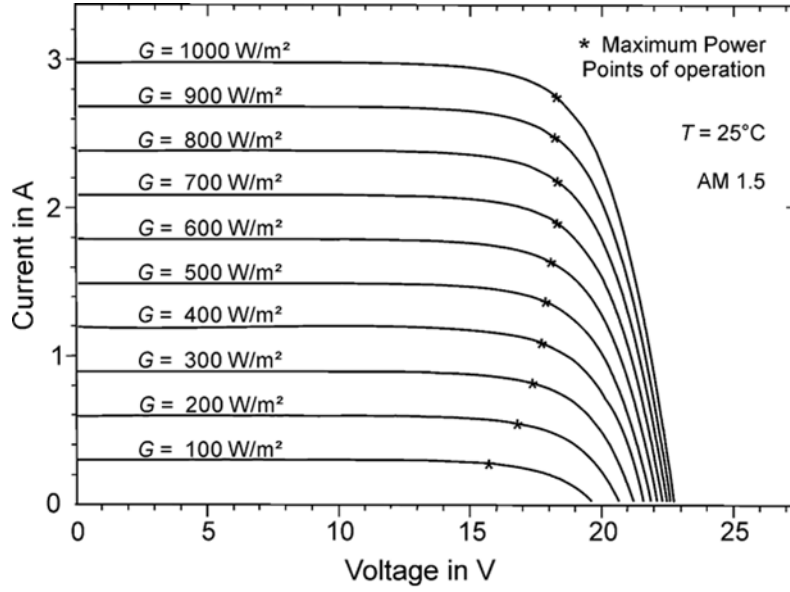


Figure 2.5: Current-voltage characteristics of a multi-crystalline silicon PV. Reprinted with permission from [1]

model is improved and can be rewritten as:

$$P_{DC} = G^T \eta_{mpp} A [1 + \alpha_{P_{mpp}} (T_C - T_C^{ref})] \quad (2.86)$$

Where, $\alpha_{P_{mpp}}$ is the maximum power point temperature coefficient ($\%/^\circ\text{C}$), A is the surface area in (m^2). η_{mpp} is the solar panel efficiency which is dependent on the temperature and can be calculated as [61]:

$$\eta_{mpp} = \frac{I_{mpp} V_{mpp}}{AG^T} + \alpha_{\eta_{mpp}} (T_C - T_C^{ref}) \quad (2.87)$$

$\alpha_{\eta_{mpp}}$ is the efficiency's maximum power point temperature coefficient ($\%/^\circ\text{C}$) This variable can be found by the following approximation [61]:

$$\alpha_{\eta_{mpp}} \approx \eta_{mpp}^{ref} \frac{\alpha_{V_{oc}}}{V_{mpp}} \quad (2.88)$$

Here, $\alpha_{V_{oc}}$ is the open circuit voltage temperature coefficient ($\%/^{\circ}\text{C}$), V_{mpp} is the voltage at maximum power point (V).

2.5.3 Standard Test Condition Power Model with Temperature Adjustment

Another slightly different approach would help avoid the need for calculating the panel's efficiency and thus reducing the number of variables needed, which can be found in [74–76]. The equation is given below:

$$P_{DC} = P_{mpp}^{ref} d_{pv} \left(\frac{G^T}{G^{ref}} \right) \left[1 + \alpha_{P_{mpp}} (T_C - T_C^{ref}) \right] \quad (2.89)$$

Here, d_{pv} is the PV derating factor ($\%$), P_{mpp}^{ref} is the maximum power at referenced operating conditions (W), $\alpha_{P_{mpp}}$ is the maximum power temperature coefficient ($\%/^{\circ}\text{C}$).

2.5.4 Voltage-Current Model

Lastly, a model which is commonly found in the literature is calculating the cell current and voltage separately. The current I_i in which i determines whether it is the short circuit or maximum power point current is almost linearly proportional to the incident solar radiation, and it increases slightly with temperature. The terminal voltage V_j in which j determines whether it is open circuit or maximum power point voltage, on the other hand, increases logarithmically with increasing solar radiation. However, the cell temperature is inversely proportional to the terminal voltage. The following equations relate these two operating conditions with a standardized value of the current and voltage [77]. This method can be found in [78–81] in which the equations are shown below:

$$I_{i=sc,mpp} = I_i^{ref} \frac{G^T}{G^{ref}} [1 + \alpha_{I_i} (T_C - T_C^{ref})] \quad (2.90)$$

$$V_{j=oc,mpp} = V_j^{ref} [1 + \alpha_{V_j} (T_C - T_C^{ref})] \quad (2.91)$$

$$FF = \frac{V_{mpp} I_{mpp}}{V_{oc} I_{sc}} \quad (2.92)$$

$$P_{mpp} = V_{oc} I_{sc} FF \quad (2.93)$$

Where, α_{I_i} is either the short circuit or maximum power point current temperature coefficient depending on the current to be calculated ($\%/^{\circ}\text{C}$). α_{V_j} is either the open circuit or maximum power point voltage temperature coefficient depending on the voltage to be calculated ($\%/^{\circ}\text{C}$). FF is the fill factor of the solar cell.

2.6 Wind Turbine Generators (WTGs)

The wind speed measurement at a certain location v is usually on a different height than the WT tower and thus, a wind speed adjustment to consider the height difference must be made before calculating the output power of the WTG [73].

$$v = v^{ref} \left(\frac{h^{hub}}{h^{ref}} \right)^{\sigma} \quad (2.94)$$

Here, v^{ref} is the wind speed in (m/s) at the referenced height h^{ref} (m). v is the wind speed in (m/s) at the hub height h^{hub} of the WT in (m).

The power output of a WTG P_{wt} can be determined from its power curve (figure ??), which is a plot of the output power against the wind speed. The WTG power curve is divided into three distinct sections. The first section involves wind speed up to the cut-in wind speed v_{ci} of the WTG. The WTG is designed to generate power at the cut-in speed and beyond. The section between the cut-in and rated wind speed v_r of the power curve can be modeled as a linear or a cubic relation which is both described below. As the wind speeds approach the rated WTG speed the power output will be fixed at the rated value P_{wt}^{rated} . Beyond the cut-out wind speed, v_{co} the WTG is shut down for safety reasons.

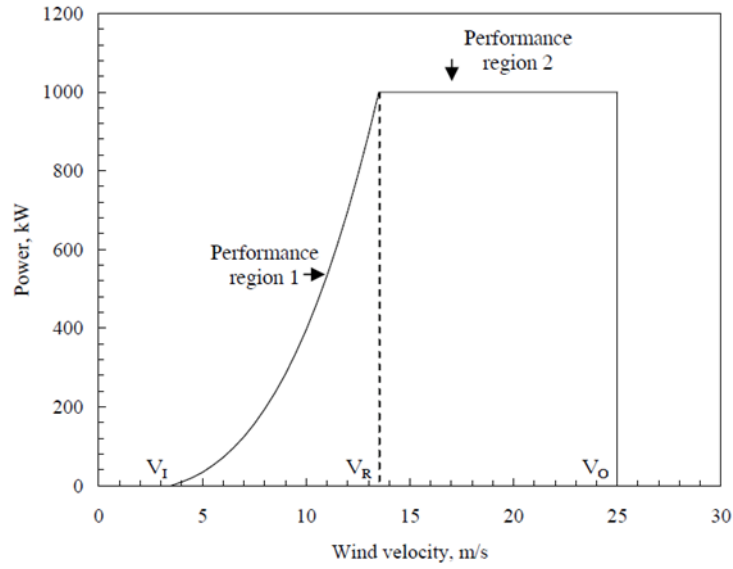


Figure 2.6: Ideal power curve of WTs. Reprinted with permission from [4]

2.6.1 First Order Model

In this model the section of the power curve for wind speeds between the cut-in and the rated speed is expressed as a linear relation [82]. η_{conv} is the efficiency of the converters.

$$P_{wt} = \begin{cases} P_{wt}^{rated} \left(\frac{v-v_{ci}}{v_r-v_{ci}} \right) \eta_{conv}, & \text{if } v_{ci} < v < v_r \\ P_{wt}^{rated} \eta_{conv}, & \text{if } v_r \leq v \leq v_{co} \\ 0, & \text{otherwise.} \end{cases}$$

2.6.2 Third Order (Cubic) Model

This model follows the previous one, however, the section of the power curve for wind speeds between the cut-in and the rated speed is expressed as a cubic function [4].

$$P_{wt} = \begin{cases} P_{wt}^{rated} \left(\frac{v^3 - v_{ci}^3}{v_r^3 - v_{ci}^3} \right) \eta_{conv}, & \text{if } v_{ci} < v < v_r \\ P_{wt}^{rated} \eta_{conv}, & \text{if } v_r \leq v \leq v_{co} \\ 0, & \text{otherwise.} \end{cases}$$

2.6.3 Power Coefficient Model

In this model the air temperature and density are used to calculate the power output from a WTG [5], [4].

$$T_k = T_a + 273.15$$

$$\rho = \frac{353.049}{T_k e^{(-0.0342 \frac{h_{hub}}{T_k})}} \quad (2.95)$$

$$P_{wt} = \frac{1}{2} \rho C_p A_{swt} v^3 \eta_{gb} \eta_{gen} \eta_{conv} \quad (2.96)$$

The temperature T_k used is in Kelvin. ρ is the air density measured in (kg/m³). C_p is the turbine power coefficient. The gearbox, generator and converter efficiencies are given by η_{gb} , η_{gen} and η_{conv} respectively. A_{swt} is the swept area of the WT (m²).

2.7 Legacy Grid

The system grid is assumed to have full capacity to supply the demand. The main idea is to penetrate this legacy grid with renewable energy sources that will have a positive impact regarding minimization of the costs and hazardous emissions. Thus, the grid would be used as a buffer at times of low renewable resource availability.

3. SYSTEM LOAD MODELING AND ANALYSIS

Typical power system planning studies model the electric load (demand) as a constant power within a specified time interval usually an hour. Therefore, the load curve can be constructed by scanning the chronological hourly data points of the demand. Alternative models exist as reported in [83]. An important metric for characterizing electric demand is the load factor (LF) [84]:

$$LF = \frac{P_{avg}}{P_{peak}}, \quad 0 < LF \leq 1 \quad (3.1)$$

A higher value of LF is desirable by the utilizes, as if the consumer's peak demand P_{peak} equals the average demand P_{avg} , the LF would be one which means that the utility companies would not experience any variation in the load and the cost of energy would be minimum. However, this is a hypothetical situation, and it cannot be realized in practice, as the load demand is variable by nature. A low LF is a sign of inefficient operation as the cost of energy will be higher. In general the higher the LF, the lower the variation in load demand and vice versa [85].

3.1 Conventional Electrical Load

The conventional load refers to the demand that needs to be supplied immediately, as it cannot be deferred or controlled. Thus, this type of load is considered to have priority when the power is dispatched from the generators. The demand data points are presented as a chronological hourly data of active power in MW, by which the load profile will be constructed. This type of load is referred to as the *primary* load in this dissertation [83].

3.2 Controllable Loads and The Concept of Value Storage

Controllable loads are defined as loads which their demand can be deferred to a later time interval given that a total amount of energy has to be supplied by the end of a pre-defined period. Thus, power balance constraint is no longer an issue as the operator is not bonded to specific power demand. This flexibility in demand would be beneficial to accommodate substantial penetration of renewable energy sources as it virtually eliminates the variability and intermittency issues related to renewable sources as mentioned in chapter one. The definition of controllable load is also stretched in this dissertation to account for power demand which can be stored as discussed in the following section.

3.2.1 Direct Load Control

This method is considered to be one of the most efficient and popular ways to implement DSM. It is based on an agreement between the utility company and the customers to remotely turn off a customer's electrical equipment (e.g., lighting, refrigerators, air conditioner, water heater) on short notice. This program is offered to low consumption customers (i.e., residential and small commercial customers) [86], [87].

3.2.2 Indirect Load Control

An alternative to DLC is smart pricing, where the price of electricity varies at different hours of the day. The users are encouraged based on a price signal to individually and voluntarily manage their loads by reducing their consumption at peak hours and shift their load from the high-price hours to the low-price hours. Different types of pricing schemes are available such as critical-peak pricing (CPP), time-of-use pricing (TOUP) and real-time pricing (RTP) [87].

3.3 Advanced Electricity Pricing

3.3.1 Time of Use Pricing (TOUP)

Electricity usage for a particular area usually peaks around the same time every day. A time-of-use (TOU) price schedule is considered to be the simplest method for discouraging the use of electricity during peak hours. Time of Use (TOU) is a pricing scheme, which provides different electricity prices associated with different periods. Electricity is least expensive when loads are low and most expensive during peak times. The rates specified by TOU reflect the underlying average cost of electric power production and delivery during each time intervals [88], [86]. Customers who participate in a TOUP program may adjust their loads manually or use an automated energy management systems. The pricing may vary seasonally. However, it is typically set far in advance. TOUP is beneficial for solar PV, which produces power during the daytime when the price is usually high. [89]. This pricing scheme is widely implemented because it needs least enabling technologies [90]

3.3.2 Real Time Pricing (RTP)

The current deregulated electricity market is based on a real-time system of supply and demand, where the price of electricity changes continuously over time [91]. Real-time pricing (RTP) (sometimes called dynamic pricing) involves adjusting price profile forecasting at different time intervals throughout the day. It reflects the changes in the wholesale price of electricity [86]. This pricing model encourages consumers of electricity to reduce their demand at peak hours and shift their demand from high priced periods to low-priced periods. The price profiles usually cover the next few hours or days and are updated continuously. This pricing scheme requires customers to have smart loads or an automated energy management system to adjust the demand based on the dynamical price signals. The RTP signals provide a better approach to the production costs of electrical

power. RTP is considered to be a good model to use for renewable energy sources since the output of these resources often does not follow a predictable pattern [89].

3.3.3 Critical Peak Pricing (CPP)

Critical peak pricing (CPP) is a hybrid design of the TOU and RTP models [92]. The basic rate structure is TOU. However, the regular peak rate is replaced by a higher CPP under predefined conditions [92]. Thus, the CPP is a dynamic pricing program in which utilities allocates high electricity prices during a restricted number of days or hours in case of contingencies or high market prices which will help in reducing the peak load [86]. This price signal would notify the customers to reduce their loads and receive compensation later on. This pricing model helps to balance the cost and risk between the customers and the producers [93]. CPP customers can adjust loads manually or by an automated energy management systems [89].

3.4 Demand Side Management

DSM is regarded as a function of the SG framework, and it is defined as a set of measures that can be carried out to improve the energy system on the load side. It intends to manipulate the electricity demand from the consumers which will result in a more smooth load profile [94]. DSM includes many aspects so that it could be implemented, for example, improving energy efficiency is considered as one aspect of DSM implementation. Also, economic incentives that encourage electricity consumers to alter their energy consumption is another application of DSM. It also can be applied as sophisticated real-time control of distributed energy resources. In general, DSM comprises of all possible actions that can be done on the load side, from simple replacement of incandescent light bulbs with more efficient fluorescent lights to implementation of complicated dynamic load management systems [95]. DSM can be categorized based on timing and the level of impact on process quality into the following:

- Energy Efficiency (EE).
- Time of Use (TOU).
- Demand Response (DR).
- Spinning Reserve (SR).

Figure 3.1 provides a visual demonstration of the different DSM categories based on their application timing.

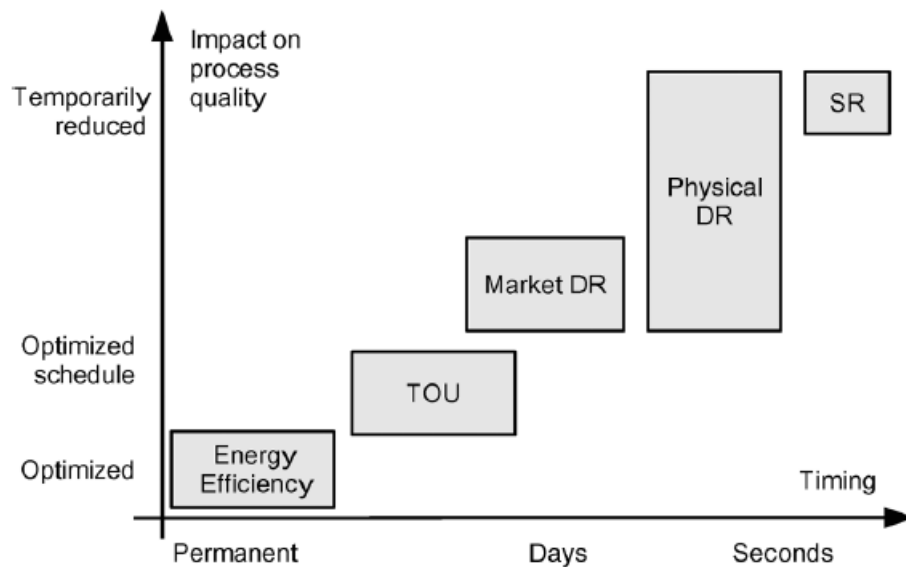


Figure 3.1: Categories of DSM. Reprinted with permission from [95]

3.4.1 Techniques of DSM

The techniques that can be used to realize DSM is shown in figure 3.2. Load shifting is the process of shifting time independent loads from peak hours to off-peak hours. Some applications of this technique include storage space heating and water heating as well

which can be used instead of the conventional electric water heater. It is considered to be the most effective technique for load management and commonly used in distribution networks. Valley filling aims to reduce the difference between the peak and valley load demands which would result in a more smoothed load curve, and thus, fewer peak units would be needed. Peak clipping as the name suggests is concerned with the reduction of the peak demand by directly controlling the load demand which can lower the operating cost of the generation units. Strategic conservation is focused on optimizing the load profile by implementing demand reduction methods at the consumer's end. Strategic load growth deals with more considerable demand than usually handled by valley filling by optimizing the daily response. It can involve increased market share of loads which can be served by non-conventional energy sources and energy storage, as well as balancing the growing load demand with the construction of the infrastructure needed to serve the load. Flexible load shape concept takes into account the load shape forecast including all DSM techniques incorporated then consumers with flexible load are identified who are willing during high demand periods to let their load be controlled by the utilities and in return they would receive a compensation [94], [96].

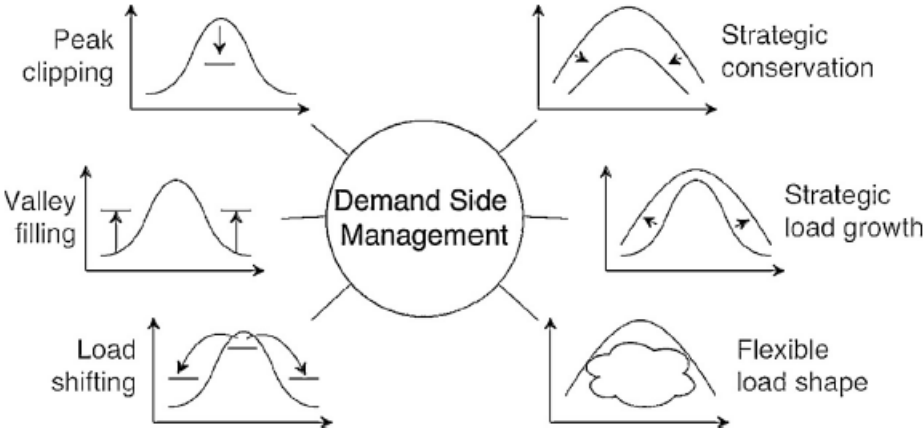


Figure 3.2: Techniques for implementing DSM. Reprinted with permission from [96]

3.4.2 Benefits of DSM

The conventional power system is designed as a unidirectional and top-down oriented system. It can be divided into the following main components, generation, transmission, distribution, and load. Generation units are connected and fed to the grid to supply the load. A balance between generation and demand has to be met at all times. The introduction of intermittent renewable energy source can jeopardize this balance. Thus, an intelligent control system is crucial. Despite increased efficiencies of electric devices, the issue of steadily increasing consumption every year can be problematic regarding grid capacity and ability to supply electrical power safely and securely. DSM could potentially be the answer for stretching the grid capabilities as the load can be utilized as an additional degree of freedom for system operators. It also promotes utilization of distributed generation (DG) as local load demand can be supplied by local generators and avoid long-distance transmission of power. DSM provides a less expensive option to intelligently influence the load, rather than building new power generation systems or expanding the transmission and distribution networks. One of the exciting programs of DSM is the Virtual Storage Power Plants (VSPP), where a special case of it is to utilize specific loads to act as virtual storage by shifting their demand. Aggregating many loads with such characteristics can alleviate pressure from the power system network [95].

3.4.3 Challenges and Barriers of DSM Implementation

Advanced metering, communications, control systems and information technologies are mostly absent from electrical systems. To support the successful implementation of DSM in system operation, significant deployment of sensors and advanced measurement units, as well as control systems, will be required. Also, a complex energy metering and trading functions will be required requiring a massive deployment of information and communication systems to control the generators, loads and all other network elements.

Therefore, a comprehensive analysis of the costs and benefits of building necessary infrastructure is needed. Leading to difficulties in finding a suitable representation and quantification of the benefits of DSM programs

Another barrier to the adoption of DSM is the increased operational complexity of the power system operation. However, these issues can be overlooked given that flexibility is a valuable tool to have for dealing with the uncertainty in the system. Also, the reduction in costs provided by DSM technologies can make DSM implementation significantly more competitive. The development of trial and pilot programs can help to increase confidence in the use of DSM technologies.

Building a successful business case for DSM implementation is also a challenge. Since the benefits associated with DSM techniques affect different participants of the electrical system which presents a complexity challenge as each entity within the electric network is trying to optimize its operation where no generating companies or transmission or distribution network operators are interested in trying to maximize the overall system by trading off the benefits between them. Thus, an appropriate regulatory body is essential to optimize the benefits of DSM within a deregulated environment [58].

3.5 Water Desalination Plant Load Model

In chapter one, water desalination methodology and technologies were explained and discussed. The specific energy consumption per unit volume is used to model the desalination plants as electrical power demand. As reported in many studies, a one unit volume of desalinated water would require a certain amount of electrical energy. This electrical energy is to be the electrical demand used to construct the load profile for the desalination plant. Desalination plants are usually built with an onsite storage tank, this tank can be utilized to store water in times where the renewable sources production is higher than the demand, and the water stored can then be used in times where the renewable sources are

not able to provide enough power. Therefore, the storage tank acts as a buffer which constitutes the concept of *value storage*, where instead of storing electrical energy, the value of that energy is stored in a different form.

$$E_{desal,e} = \kappa E_{desal,w} \quad (3.2)$$

$$P_{desal,e} = \frac{\kappa}{\Delta t} P_{desal,w} \quad (3.3)$$

Where, $E_{desal,w}$ is the volume of desalinated water (m^3), $E_{desal,e}$ is the electrical energy required to produce $E_{desal,w}$ (MWh). $P_{desal,w}$ is the water demand in (m^3/h) and $P_{desal,e}$ is the corresponding power demand in (MW). This transformation is done by the specific energy requirement κ which is represented in (kWh/m^3).

3.6 Industrial Facilities Load Model

Industrial factories are also considered as a load which can utilize the value storage concept. Different factories have various processes, and the industrial facilities of interest in this dissertation are facilities which produce materialized products, such as steel or aluminum plants, petrochemical plants and many other. These facilities usually include a storage warehouse within the premise of the plant to store their products. This storage facility can be used to realize the concept of value storage. The assumption made with industrial facilities is that it has a range of minimum and maximum power demand which translates to highest and lowest product production. A distinction is made between water desalination plants and industrial facilities that in the latter the electricity demand is provided as an energy demand of a longer time interval than an hour. In other words, The system operator can construct the appropriate load profile under the condition that a certain amount of electrical energy will be supplied within a pre-defined period and range of power supply. With this approach, the hinges of renewable energy sources unpredictability

and intermittency can be alleviated as the system operator is no longer required to supply a specific demand at every hour. Instead, the system operator will serve the industrial facility demand based on the availability of resources (i.e., solar radiation and wind speed). Thus, this type of load is referred to here as a *generation following* load.

$$E_{fact,e} = \delta E_{fact,ton} \quad (3.4)$$

Here, $E_{fact,ton}$ in (Tons) is the amount of products in tons that represent the demand. The electrical counter part is the electrical energy needed to produce $E_{fact,ton}$ which is $E_{fact,e}$ given in (MWh). This conversion is done in a similar manner as the desalination plant by utilizing a specific energy factor δ in (kWh/ton).

The total energy required for a year $E_{fact,e}^{year}$ is uniformly divided within 12 months $E_{fact,e}^{month}$. As such the system operator is required to severe the same amount of energy each month taking into consideration that different months of the year have different number of days. \mathcal{H} is the set of number of hours in each month and $P_{fact,e}$ in (MW) is the factroy electrical power demand.

$$E_{fact,e}^{month} = \frac{E_{fact,e}^{year}}{12}, \quad \sum_{h=1}^{H \in \mathcal{H}} P_{fact,e}(h) = E_{fact,e}^{month} \quad (3.5)$$

The scheduling process to construct the load profile for the industrial load is formulated as a least squares optimization problem following the approach in [97].

$$\begin{aligned} & \underset{P_{fact,e}}{\text{minimize}} && \frac{1}{2} \left\| \left(P_{fact,e}^{day} - P_{re}^{day} \right) \right\|_2^2 \\ & \text{subject to} && P_{fact,e}^{min} \leq P_{fact,e}^{day} \leq P_{fact,e}^{max} \\ & && -P_{fact,e}^{dn} \leq \Delta P_{fact,e}^{day} \leq P_{fact,e}^{up} \\ & && \sum P_{fact,e}^{day} = E_{fact,e}^{day} \end{aligned}$$

$$\mathbf{P}_{re}^{day} = \mathbf{P}_{pv}^{day} x_{pv} + \mathbf{P}_{wt}^{day} x_{wt} \quad (3.6)$$

Where \mathbf{P}_{re}^{day} and $\mathbf{P}_{fact,e}^{day}$ are the daily vectors of renewable power output and factory power demand respectively (MW). $\mathbf{P}_{fact,e}^{min}$ and $\mathbf{P}_{fact,e}^{max}$ are the minimum and maximum factory power limits (MW). $\mathbf{P}_{fact,e}^{dn}$ and $\mathbf{P}_{fact,e}^{up}$ are the factory ramp down and up rates (MW/h).

$$\mathbf{P}_{fact,e} = \left[\mathbf{P}_{fact,e}^{day(1)} \quad \dots \quad \mathbf{P}_{fact,e}^{day(365)} \right]^T \quad (3.7)$$

The primary objective is to construct a load profile for the factory which ideally follows the renewable power output. The constraints imposed are to account for the process of the industrial plant. The first constraint is related to the range of power supply that the plant can withstand to stay online. The second constraint is to account for the process that can only tolerate a specific amount of ramps each hour. The third constraint ensures the daily energy required is satisfied.

Now that the factory load is expressed in electrical terms it can be aggregated with the conventional load as the following equation:

$$\mathbf{P}_{L,e} = \mathbf{P}_{con} + \mathbf{P}_{fact,e} \quad (3.8)$$

4. GENERATION EXPANSION PLANNING

The generation expansion planning (GEP) problem, is related to identifying which energy resource should be used and how much from a portfolio of available energy sources (i.e fossil fuel generation, renewable energy sources) to serve the load at the lowest cost possible. In some cases maximum reliability as well as minimum environmental impact are taken into consideration and a trade-off between these objectives will have to be done as they are conflicting in nature [84]. The GEP problem is a constrained nonlinear problem with discrete variables [98]. A complete enumeration solution is needed to find the optimal plan, which is not possible in a real world GEP problem as the computational requirements to solve such problem is enormous. The uncertainty associated with the input data, such as the electricity demand and renewable sources forecast, economic and technical parameters of generating units all add to the difficulty of the GEP problem [99].

y	Set of labels which include $\{pv, wt, bat, inv\}$
$C_y^{o\&m}$	Yearly operation and maintenance cost per unit (\$/unit-yr)
S_y	Salvage value per unit (\$/unit)
C_y^{cap}, C_y^{rep}	Present worth of the capital and replacement costs (\$/unit)
$C_y^{o\&m}$	Present worth of the operation and maintenance cost (\$/unit)
S_y	Present worth of the salvage value cost (\$/unit)
C_y	Total present worth of all cost components (\$/unit)
N_y, N_y^{rem}	Component life, component remaining life at end of project (Years)

nr_y	Number of component replacements
i, f	Interest and inflation rates (%)
N_p, n	Project life time and index year (Years)
X	Vector of decision variables
c_{oil}, π_{oil}	Production cost and global price of a barrel of oil (\$)
$c_g^{fuel,(-,+)}$	Yearly grid fuel cost/profit per unit energy (\$/Wh-yr)
$c_g^{o\&m}$	Yearly operation and maintenance cost of the grid per unit energy (\$/Wh-yr)
$C_g^{fuel,(-,+)}$	Present worth of grid fuel cost and opportunity cost per unit energy (\$/Wh)
$C_g^{o\&m}$	Present worth of operation and maintenance cost of the grid per unit energy (\$/Wh)
λ_g^-	Total present worth of all grid cost components (\$/Wh)
λ_g^+	Total present worth of displaced barrel of oil (\$/Wh)
HC_{oil}	Heat content in a barrel of oil (mmBTU/bbl)
HR_{oil}	Heat rate of an oil based generator (BTU/kWh)
E_{bbl}	Equivalent energy from a barrel of oil (MWh)
$Cost_{hyd}$	Total present worth of the hybrid systems (\$)
E_{eq}^ω	Equivalent energy displaced from conventional generators in scenario ω (MWh)
$P_{pv}^\omega, P_{wt}^\omega$	PV and WTG power output in scenario ω (MW)
$E_{tk,lvl}^\omega, P_{tk}^\omega$	Water tank level and flow in scenario ω (m ³ , m ³ /h)

SOC_{bat}^{min}	Minimum allowable state of charge (kWh)
$SOC_{bat}^{\omega}, P_{bat}^{\omega}$	State of charge and battery power flow in scenario ω (kWh, kW)
$E_{bat,eff}^{\omega}$	Effective battery capacity available for delivery in scenario ω (kWh)
η_{bat}	Battery round trip efficiency (%)
$P_g^{\omega}, P_{dump}^{\omega}$	Grid and dumped power in scenario ω (MW)
$P_{L,e}$	Aggregated electrical demand (MW)
$\omega, \Omega, N_{\Omega}$	Scenario index, scenario set and number of scenarios
x_{pv}, x_{wt}	Number of PVs and WTGs (Units)
x_{tk}, x_d	Water tank size and desalination plant capacity (m ³ , m ³ /h)
x_{bat}	Battery storage size (kWh)
e, w	Electric and water notations
P_g^{dn}, P_g^{up}	Grid down and up ramp rates (MW)
ϕ	Grid emission factor (Tons CO ₂ /MWh)
Ξ	Output variable from the MCS (i.e., differential system cost)
$E(\Xi)$	Expected value of Ξ
$\sigma[E(\Xi)]$	Standard deviation of $E[\Xi]$
Δt	Simulation time step (1 Hour)

4.1 Problem Statement

The key driver for this dissertation is to penetrate the existing electricity grid with renewable energy sources which would displace conventional fossil fuel generation in an oil exporting country.

4.2 System Components Cost Breakdown and Financial Aspects

4.2.1 Financial Parameters

The economic model involves the cost functions of each component considered in the optimization problem. The cost functions include capital cost, operation, and maintenance cost, replacement cost and salvage value of the equipment at the end of the project life. A linear depreciation model of the components is assumed for the salvage value which means that the value of the component (PV, WTG, BESS, Inverters) decrease at a constant rate.

Interest and inflation rates are also critical parameters for long-term planning studies. The economic model is set up for one-year simulations giving all costs are represented in present worth.

4.2.2 Renewable Energy System

The cost functions associated with the hybrid sustainable system including PVs, WTGs, BESS, and inverters are given by the following equations [73]

$$C_y^{o\&m} = c_y^{o\&m} \sum_{n=1}^{N_p} \left(\frac{1+f}{1+i} \right)^n \quad (4.1)$$

$$C_y^{rep} = c_y^{rep} \sum_{r=1}^{nr_y} \left(\frac{1+f}{1+i} \right)^{rN_y} \quad (4.2)$$

$$S_y = s_y \left(\frac{1+f}{1+i} \right)^{N_p}, \quad s_y = c_y^{rep} \left(\frac{N_y^{rem}}{N_y} \right) \quad (4.3)$$

$$N_y^{rem} = N_y - (N_p - nr_y N_y), \quad nr_y = \text{INT}\left(\frac{N_p}{N_y}\right) \quad (4.4)$$

$$C_y = C_y^{cap} + C_y^{o\&m} + C_y^{rep} - S_y \quad (4.5)$$

4.2.3 Water Tank Storage

For The water tank storage, only the capital cost is included

$$C_{tk} = C_{tk}^{cap} \quad (4.6)$$

4.2.4 Desalination Plant Capacity Expansion

The costs included for the capacity expansion of the the desalination plant only have a capital cost component similar to the water storage tank.

$$C_d = C_d^{cap} \quad (4.7)$$

4.2.5 Grid

The Legacy grid has two cost components, fuel cost as well as operation and maintenance cost.

$$C_g^{o\&m} = c_g^{o\&m} \sum_{n=1}^{N_p} \left(\frac{1+f}{1+i}\right)^n \quad (4.8)$$

$$c_g^{fuel,-} = \frac{c_{oil}}{E_{bbl}}, \quad c_g^{fuel,+} = \frac{(\pi_{oil} - c_{oil})}{E_{bbl}}, \quad E_{bbl} = \frac{HC_{oil}}{HR_{oil}} \times 1000 \quad (4.9)$$

$$C_g^{fuel,(-,+)} = c_g^{fuel,(-,+)} \sum_{n=1}^{N_p} \left(\frac{1+f}{1+i}\right)^n \quad (4.10)$$

$$\lambda_g^- = C_g^{fuel,-} + C_g^{o\&m} \quad (4.11)$$

$$\lambda_g^+ = C_g^{fuel,+} \quad (4.12)$$

4.3 Design Objectives

4.3.1 Economical Criteria

For the sake of simplicity the hybrid system costs are added together as $Cost_{hyd}$. The hybrid system in this dissertation refers to either the combined system of PVs, WTGs, water storage tank and the desalination capacity, or the PVs, WTGs, BESS system.

$$Cost_{hyd} = C_{pv}x_{pv} + C_{wt}x_{wt} + C_{tk}x_{tk} + C_d x_d \quad (4.13)$$

The system cost as an objective function to be minimized will differ in formulation based on the underlying assumption of the availability of fossil fuel in the selected location. Whether the location under consideration is a net importer or exporter of oil. A unified cost function is given as a differential system cost, which is the difference between the total system cost and the profit gained from displacing grid supply.

$$\Delta Cost = Cost_{hyd} + \frac{1}{N_{\Omega}} \sum_{\omega \in \Omega} (\lambda_g^- \sum_{t=1}^T P_g^{\omega}(t) - \lambda_g^+ E_{eq}^{\omega}) \quad (4.14)$$

This cost function is suitable for solving generation expansion planning problem for both a net exporter or a net importer with some modification. The function as it is shown above can be directly used for a net exporter location. As for a problem considering a net importer country, a clear distinction from the net exporter case is that the cost and price of a barrel of oil and will be the same and thus, the grid cost factor (λ_g^+) will be zero. Since that the country in question is an importer of fossil fuels, the cost for production and

displacement will be the same. This translates to the following equation:

$$\pi_{oil} = c_{oil}, \quad \lambda_g^+ = 0 \quad (4.15)$$

$$Cost = Cost_{hyd} + \lambda_g^- \frac{1}{N_\Omega} \sum_{\omega \in \Omega} \sum_{t=1}^T P_g^\omega(t) \quad (4.16)$$

Equation (4.16) is the traditional cost objective function that is commonly found in the literature. Therefore, equation (4.14) represents a general case of the cost objective function which can be adjusted for a specific planning problem whether the location in question is considered to be a net exporter or a net importer of oil or any fossil fuel in general.

4.3.2 Environmental Criteria

Emissions of conventional generators as a secondary objective is to minimize the CO₂ emissions from such generators.

$$Emissions = \frac{1}{N_\Omega} \sum_{\omega \in \Omega} \sum_{t=1}^T \phi P_g^\omega(t) \quad (4.17)$$

4.4 Uncertainty Handling

Different types of uncertainties are associated with the GEP problem involving renewable energy sources. The main sources of uncertainties are described in the following [100]:

- **System costs:** This includes the fuel costs of the fossil fuel generators. Also the construction, operation and maintenance costs of power plants. These also have an impact on the price of electricity to the consumers.
- **Socio-political:** Which involves the regulatory bodies responsible for the electricity network operation as well as the government's policy in this industry.

- Electrical load: The electrical load growth in a specific region is related to many different aspects which include, population and economic growth, implementation of DSM programs and energy efficiency components.
- Resource and electrical component availability: The uncertainty of renewable resources (i.e., solar radiation, wind speed) is considered as one of the most important barriers for very high penetration of renewables to the existing grid. Since that renewable resources forecasting and prediction are much more difficult than the fuel availability of a typical thermal generator. Also, the component availability due to forced outages is an important aspect to consider as a source of uncertainty for any GEP problem for conventional and sustainable energy sources.

Several techniques are commonly used to address the uncertainties in a GEP problem. Scenario and sensitivity analysis as well as, probabilistic analysis are some of the most common ways to deal with uncertainties. Scenario analysis generates a broad range of potential futures, referred to as scenarios or realizations. Each scenario has a different forecast for critical uncertain variables. An expansion plan for each scenario is then generated. A clear example of this technique is to produce some scenarios varying specific variables at once which represent different possible futures and generating an expansion plan for each one. Sensitivity analysis, on the other hand, varies each key variable separately to distinguish some of the critical variables for the expansion problem. The scenario and sensitivity analysis suffer from the lack of any information about the flexibility and robustness of the generated plans. Probabilistic approaches have been developed to overcome these issues. By assigning probabilities to the occurrence of the uncertain variables by which an expansion plan can be established taking into consideration the probabilities of these uncertainties. An example of a probabilistic approach is the stochastic programming in which an optimal expansion plan is produced based on the best weighted average

objective function value over all scenarios.

The solar radiation and wind speed forecast errors $\varepsilon_{insolation}, \varepsilon_{wind}$ are modeled as a random variable following a normal distribution (figure 4.1) as follows [101–103]:

$$\varepsilon_{insolation} \sim N(0, 2) \quad (4.18)$$

$$\varepsilon_{wind} \sim N(0, 2) \quad (4.19)$$

$$G^{T,new} = G^T + \varepsilon_{insolation} \quad (4.20)$$

$$v^{new} = v + \varepsilon_{wind} \quad (4.21)$$

The vectors of the forecast error of both the solar radiation and wind speed are the input to the Monte Carlo Simulation (MCS). Many samples are generated to capture the stochastic distribution of the objective in question (i.e., differential cost, emissions). The stopping criterion for the MCS is by utilizing a Coefficient of Variation ε (COV) as follows:

$$\frac{\sigma[E(\Xi)]}{E(\Xi)} \leq \varepsilon \quad (4.22)$$

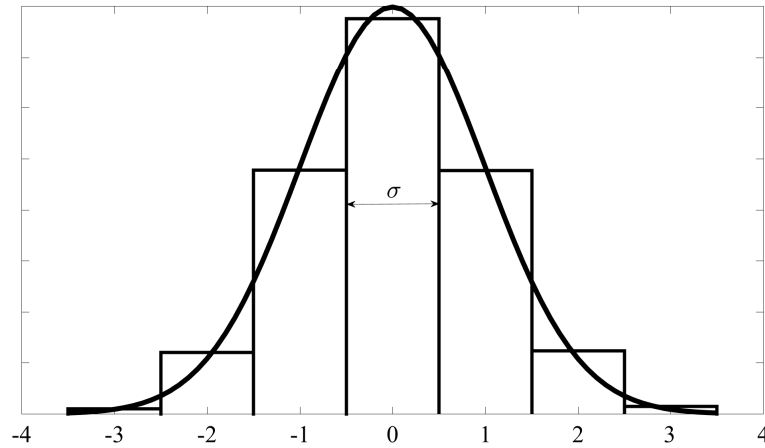


Figure 4.1: Typical discretization of the probability distribution of the solar radiation and wind speed forecast error

Failure of battery banks are included in the system configuration which utilize a Battery Energy Storage System (BESS). The failure is represented by a Forced Outage Rate (FOR) [104].

$$status_{bat} = \begin{cases} 1, & \text{if } rand \geq FOR \\ 0, & \text{if } rand < FOR \end{cases} \quad (4.23)$$

Where, $rand$ is a uniformly distributed random number. The $status_{bat}$ indicates that if the random number generated is higher than the (FOR), then the battery is available. However, if the random number generated is lower than the (FOR), then this represents a battery failure.

4.5 System Configurations

4.5.1 Desalination Plant Powered by Renewables

The first system configuration considered in this dissertation is shown in figure 4.2. Where only renewable energy sources are considered in the supply side. The load considered is a desalination plant coupled with water storage.

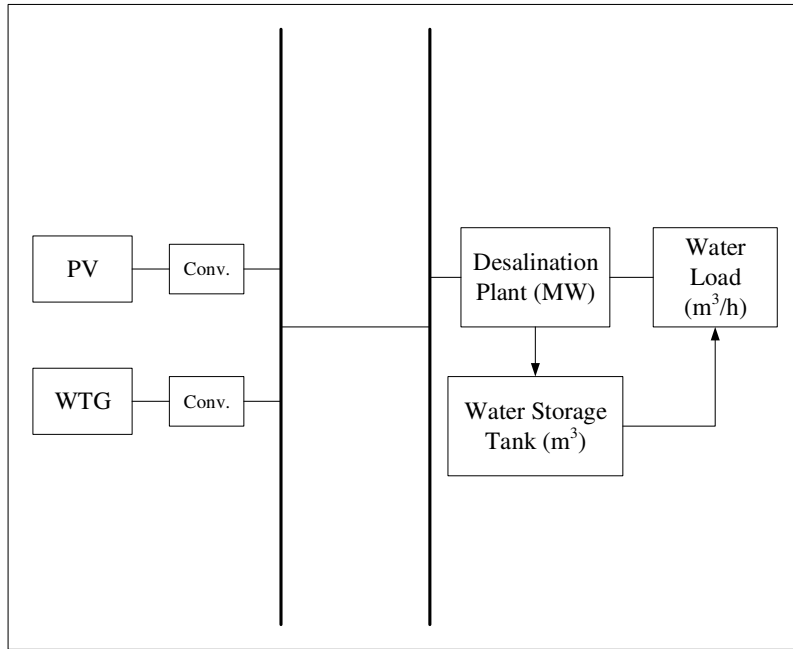


Figure 4.2: System configuration of desalination plant powered by renewables

4.5.1.1 Design Constraints

- Load balance: For any time instant t the total supply must be sufficient to handle the required demand.

$$P_{pv}^{\omega}(t)x_{pv} + P_{wt}^{\omega}(t)x_{wt} + \frac{\kappa}{\Delta t}P_{ik}^{\omega}(t) = P_{desal,e}(t) + P_{dump}^{\omega}(t), \quad \forall t, \forall \omega \quad (4.24)$$

- Water tank capacity and flow bounds: At any time instance, the total amount of stored water should not exceed the water tank capacity, which is mathematically represented in (4.25). The inequality constraint (4.26) states that the water inflow into the tank should do not exceed the desalination capability as well as the capacity of the storage tank. The water outflow from the tank should do not exceed the capacity of the water tank or the water load which is represented by (4.27).

$$0 \leq E_{tk,lvl}^\omega(t) \leq x_{tk}, \quad \forall t, \forall \omega \quad (4.25)$$

$$0 \leq P_{tk,in}^\omega(t) \leq \min(x_d, x_{tk}/\Delta t), \quad \forall t, \forall \omega \quad (4.26)$$

$$0 \leq P_{tk,out}^\omega(t) \leq \min(P_{desal,w}(t), E_{tk,lvl}^\omega(t)/\Delta t), \quad \forall t, \forall \omega \quad (4.27)$$

- Decision variables bounds and type: All the decision variables included in the optimization would be restricted to a specific range, this is referred to as the search space. Also all variables are discrete (integers).

$$\begin{aligned} x_{pv}^{min} &\leq x_{pv} \leq x_{pv}^{max}, & x_{pv} &\in \text{Integers} \\ x_{wt}^{min} &\leq x_{wt} \leq x_{wt}^{max}, & x_{wt} &\in \text{Integers} \\ x_{tk}^{min} &\leq x_{tk} \leq x_{tk}^{max}, & x_{tk} &\in \text{Integers} \\ x_d^{min} &\leq x_d \leq x_d^{max}, & x_d &\in \text{Integers} \end{aligned} \quad (4.28)$$

4.5.1.2 System Operation Strategy

The generated power from the renewable sources has the priority to serve the loads. Any excess power after serving all instantaneous demand is diverted towards the desalina-

tion plant to be stored as desalinated water.

$$\Delta P_{re}(t) = P_{pv}(t)x_{pv} + P_{wt}(t)x_{wt} - P_{desal,e}(t) \quad (4.29)$$

$$P_{tk}(t) = \begin{cases} P_{tk,in}(t) & \text{if } \Delta P_{re}(t) > 0; \text{ (Excess)} \\ P_{tk,out}(t) & \text{if } \Delta P_{re}(t) < 0; \text{ (Shortage)} \end{cases}$$

- If $\Delta P_{re}(t) > 0$, this indicates a power excess and its diverted to the water storage subject to constraints (4.25) and (4.26).

$$P_{tk,in}(t) = \frac{\Delta P_{re}(t)}{\kappa/\Delta t} \quad (4.30)$$

- If $\Delta P_{re}(t) < 0$ and $E_{tk,lvl}(t) \geq \frac{|\Delta P_{re}(t)|\Delta t}{\kappa}$, this represents a power shortage from the renewable sources to supply the load. However, the water storage can supply the whole deficit.

$$P_{tk,out}(t) = \frac{|\Delta P_{re}(t)|}{\kappa/\Delta t} \quad (4.31)$$

- If $\Delta P_{re}(t) < 0$ and $E_{tk,lvl}(t) < \frac{|\Delta P_{re}(t)|\Delta t}{\kappa}$, the same situation as the previous one. However, the water storage is not able to supply the whole deficit, and as such a loss of load will occur. This situation is not acceptable and the algorithm will consider it as a non feasible solution and discard it.

$$P_{tk,out}(t) = \frac{E_{tk,lvl}}{\Delta t} \quad (4.32)$$

The level of available water in the water storage for the next time step is:

$$E_{tk,lvl}(t+1) = \begin{cases} E_{tk,lvl}(t) + P_{tk}(t)\Delta t & \text{if } \Delta P_{re}(t) > 0; \\ E_{tk,lvl}(t) - P_{tk}(t)\Delta t & \text{if } \Delta P_{re}(t) < 0; \end{cases} \quad (4.33)$$

4.5.2 Desalination Plant Powered by Renewables and Legacy Grid

The second system configuration considered in this dissertation is shown in figure 4.2. Where the renewable energy sources are penetrating an existing legacy grid in the supply side. The load considered is similar to the previous configuration with a desalination plant coupled with water storage.

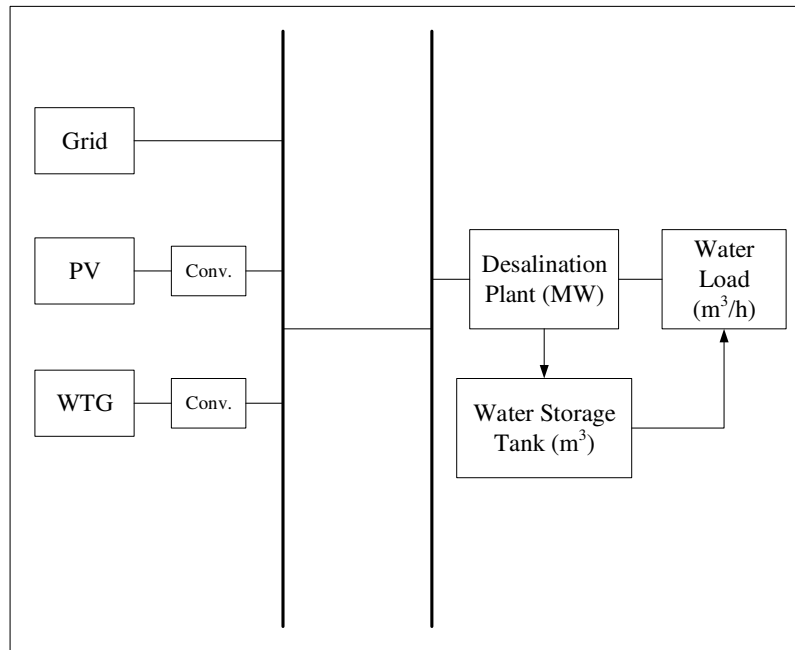


Figure 4.3: System configuration of desalination plant powered by renewables and legacy grid

4.5.2.1 Design Constraints

- Load balance: For any time instant t the total supply must be sufficient to handle the required demand.

$$P_{pv}^{\omega}(t)x_{pv} + P_{wt}^{\omega}(t)x_{wt} + \frac{\kappa}{\Delta t}P_{tk}^{\omega}(t) + P_g^{\omega}(t) = P_{desal,e}(t) + P_{dump}^{\omega}(t), \quad \forall t, \forall \omega \quad (4.34)$$

- Water tank capacity and flow bounds: At any time instance, the total amount of stored water should not exceed the water tank capacity, which is mathematically represented in (4.35). The inequality constraint (4.36) states that the water inflow into the tank should do not exceed the desalination capability as well as the capacity of the storage tank. The water outflow from the tank should do not exceed the capacity of the water tank or the water load which is represented by (4.37).

$$0 \leq E_{tk,lv}^{\omega}(t) \leq x_{tk}, \quad \forall t, \forall \omega \quad (4.35)$$

$$0 \leq P_{tk,in}^{\omega}(t) \leq \min(x_d, x_{tk}/\Delta t), \quad \forall t, \forall \omega \quad (4.36)$$

$$0 \leq P_{tk,out}^{\omega}(t) \leq \min(P_{desal,w}(t), E_{tk,lv}^{\omega}(t)/\Delta t), \quad \forall t, \forall \omega \quad (4.37)$$

- Legacy grid power and ramp bounds: The amount of power provided by the grid should be within a specified range and should not exceed the ramp rates.

$$P_g^{min} \leq P_g^{\omega}(t) \leq P_g^{max}, \quad \forall t, \forall \omega \quad (4.38)$$

$$-P_g^{dn} \leq \Delta P_g^{\omega}(t) \leq P_g^{up}, \quad \forall t, \forall \omega \quad (4.39)$$

- Decision variables bounds and type: All the decision variables included in the op-

timization would be restricted to a specific range, this is referred to as the search space. Also all variables are discrete (integers).

$$\begin{aligned}
x_{pv}^{min} &\leq x_{pv} \leq x_{pv}^{max}, & x_{pv} &\in \text{Integers} \\
x_{wt}^{min} &\leq x_{wt} \leq x_{wt}^{max}, & x_{wt} &\in \text{Integers} \\
x_{tk}^{min} &\leq x_{tk} \leq x_{tk}^{max}, & x_{tk} &\in \text{Integers} \\
x_d^{min} &\leq x_d \leq x_d^{max}, & x_d &\in \text{Integers}
\end{aligned} \tag{4.40}$$

4.5.2.2 System Operation Strategy

The generated power from the renewable sources has the priority to serve the loads. Any excess power after serving all instantaneous demand is diverted towards the desalination plant to be stored as desalinated water.

$$\Delta P_{re}(t) = P_{pv}(t)x_{pv} + P_{wt}(t)x_{wt} - P_{desal,e}(t) \tag{4.41}$$

$$P_{tk}(t) = \begin{cases} P_{tk,in}(t) & \text{if } \Delta P_{re}(t) > 0; \text{ (Excess)} \\ P_{tk,out}(t) & \text{if } \Delta P_{re}(t) < 0; \text{ (Shortage)} \end{cases}$$

- If $\Delta P_{re}(t) > 0$, this indicates a power excess and its diverted to the water storage subject to constraints (4.35) and (4.36).

$$P_{tk,in}(t) = \frac{\Delta P_{re}(t)}{\kappa/\Delta t} \tag{4.42}$$

- If $\Delta P_{re}(t) < 0$ and $E_{tk,lvl}(t) \geq \frac{|\Delta P_{re}(t)|\Delta t}{\kappa}$, this represents a power shortage from the renewable sources. However, the water storage can supply the whole deficit.

$$P_{tk,out}(t) = \frac{|\Delta P_{re}(t)|}{\kappa/\Delta t} \tag{4.43}$$

- If $\Delta P_{re}(t) < 0$ and $E_{tk}(t) < \frac{|\Delta P_{re}(t)|\Delta t}{\kappa}$, the same situation as the previous one. However, the water storage is not able to supply the whole deficit and as such the grid is required to supply some of the water load.

$$P_{tk,out}(t) = \frac{E_{tk,lvl}}{\Delta t} \quad (4.44)$$

$$P_g(t) = |\Delta P_{re}(t)| - \frac{\kappa}{\Delta t} P_{tk,out} \quad (4.45)$$

The level of available water in the water storage for the next time step is:

$$E_{tk,lvl}(t+1) = \begin{cases} E_{tk,lvl}(t) + P_{tk}(t)\Delta t & \text{if } \Delta P_{re}(t) > 0; \\ E_{tk,lvl}(t) - P_{tk}(t)\Delta t & \text{if } \Delta P_{re}(t) < 0; \end{cases} \quad (4.46)$$

4.5.3 Conventional Load and Desalination Plant Powered by Renewables and Legacy Grid

The third system configuration considered in this dissertation is shown in figure 4.4. Where the renewable energy sources are penetrating an existing legacy grid in the supply side. The load side in addition to desalination plant has a conventional (residential) load.

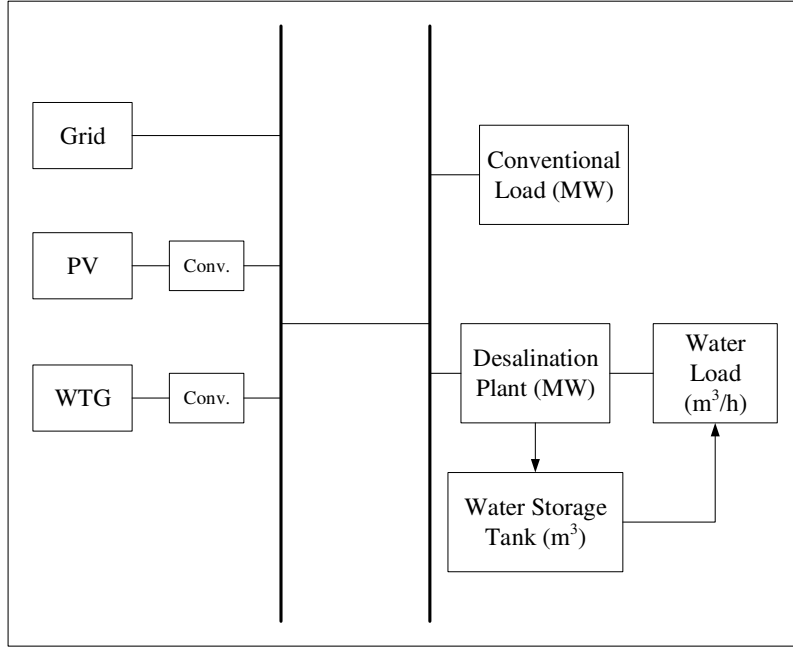


Figure 4.4: System configuration of conventional load and desalination plant powered by renewables and legacy grid

4.5.3.1 Design Constraints

- Load balance: For any time instant t the total supply must be sufficient to handle the required demand.

$$P_{L,e} = P_{con} \quad (4.47)$$

$$P_{pv}^{\omega}(t)x_{pv} + P_{wt}^{\omega}(t)x_{wt} + \frac{\kappa}{\Delta t}P_{tk}^{\omega}(t) + P_g^{\omega}(t) = P_{L,e}(t) + P_{desal,e}(t) + P_{dump}^{\omega}(t), \quad \forall t, \forall \omega \quad (4.48)$$

- Water tank capacity and flow bounds: At any time instance, the total amount of stored water should not exceed the water tank capacity, which is mathematically represented in (4.49). The inequality constraint (4.50) states that the water inflow into the tank should do not exceed the desalination capability as well as the capacity of the storage tank. The water outflow from the tank should do not exceed the

capacity of the water tank or the water load which is represented by (4.51).

$$0 \leq E_{tk,lvl}^\omega(t) \leq x_{tk}, \quad \forall t, \forall \omega \quad (4.49)$$

$$0 \leq P_{tk,in}^\omega(t) \leq \min(x_d, x_{tk}/\Delta t), \quad \forall t, \forall \omega \quad (4.50)$$

$$0 \leq P_{tk,out}^\omega(t) \leq \min(P_{desal,w}(t), E_{tk,lvl}(t)/\Delta t), \quad \forall t, \forall \omega \quad (4.51)$$

- Legacy grid power and ramp bounds: The amount of power provided by the grid should be within a specified range and should not exceed the ramp rates.

$$P_g^{min} \leq P_g^\omega(t) \leq P_g^{max}, \quad \forall t, \forall \omega \quad (4.52)$$

$$-P_g^{dn} \leq \Delta P_g^\omega(t) \leq P_g^{up}, \quad \forall t, \forall \omega \quad (4.53)$$

- Decision variables bounds and type: All the decision variables included in the optimization would be restricted to a specific range, this is referred to as the search space. Also all variables are discrete (integers). All decision variable are integers and restricted to a specific range.

$$\begin{aligned} x_{pv}^{min} &\leq x_{pv} \leq x_{pv}^{max}, & x_{pv} &\in \text{Integers} \\ x_{wt}^{min} &\leq x_{wt} \leq x_{wt}^{max}, & x_{wt} &\in \text{Integers} \\ x_{tk}^{min} &\leq x_{tk} \leq x_{tk}^{max}, & x_{tk} &\in \text{Integers} \\ x_d^{min} &\leq x_d \leq x_d^{max}, & x_d &\in \text{Integers} \end{aligned} \quad (4.54)$$

4.5.3.2 System Operation Strategy

The generated power from the renewable sources has the priority to serve the loads. Any excess power after serving all instantaneous demand is diverted towards the desalination plant to be stored as desalinated water.

$$\Delta P_{re}^1(t) = P_{pv}(t)x_{pv} + P_{wt}(t)x_{wt} - P_{L,e}(t) \quad (4.55)$$

$$\Delta P_{re}^2(t) = \Delta P_{re}^1(t) - P_{desal,e}(t) \quad (4.56)$$

$$P_{tk}(t) = \begin{cases} P_{tk,in}(t) & \text{if } \Delta P_{re}^2(t) > 0; \text{ (Excess)} \\ P_{tk,out}(t) & \text{if } \Delta P_{re}^1(t) < 0; \text{ (Shortage)} \end{cases}$$

- If $\Delta P_{re}^1(t) > 0$ and $\Delta P_{re}^2(t) > 0$, this indicates a power excess and its diverted to the water storage subject to constraints (4.49) and (4.50).

$$P_{tk,in}(t) = \frac{\Delta P_{re}^2(t)}{\kappa} \quad (4.57)$$

- If $\Delta P_{re}^1(t) > 0$, $\Delta P_{re}^2(t) < 0$ and $E_{tk,lvl}(t) \geq \frac{|\Delta P_{re}^2(t)|\Delta t}{\kappa}$, this indicates a power shortage and all the energy available from the renewable sources are directed towards serving the conventional load and any excess along with the available water in the storage tank will supply the water load.

$$P_{tk,out}(t) = \frac{|\Delta P_{re}^2(t)|}{\kappa/\Delta t} \quad (4.58)$$

- If $\Delta P_{re}^1(t) > 0$, $\Delta P_{re}^2(t) < 0$ and $E_{tk,lvl}(t) < \frac{|\Delta P_{re}^2(t)|\Delta t}{\kappa}$, this is the same situation as the previous one. However, the hybrid system (PV-WTG-Tank) by its own can

not fully supply the total demand. Thus, the grid is required to supply the deficit.

$$P_{tk,out}(t) = \frac{E_{tk,lvl}(t)}{\Delta t} \quad (4.59)$$

$$P_g(t) = |\Delta P_{re}^2(t)| - \frac{\kappa}{\Delta t} P_{tk,out}(t) \quad (4.60)$$

- If $\Delta P_{re}^1(t) < 0$ and $E_{tk,lvl}(t) \geq P_{desal,w}(t)\Delta t$, this represents a power shortage from the renewable sources to supply the conventional load. Thus, the grid will have to supply the deficit. The water load can be supplied completely by the water storage.

$$P_{tk,out}(t) = P_{desal,w}(t) \quad (4.61)$$

$$P_g(t) = |\Delta P_{re}^1(t)| \quad (4.62)$$

- If $\Delta P_{re}^1(t) < 0$ and $E_{tk,lvl}(t) < P_{desal,w}(t)\Delta t$, the same situation as the previous one. However, the grid is required to supply some of the water and conventional load.

$$P_{tk,out}(t) = \frac{E_{tk,lvl}(t)}{\Delta t} \quad (4.63)$$

$$P_g(t) = |\Delta P_{re}^1(t)| + \frac{\kappa}{\Delta t} (P_{desal,w}(t) - P_{tk,out}(t)) \quad (4.64)$$

The level of available water in the water storage for the next time step is:

$$E_{tk,lvl}(t+1) = \begin{cases} E_{tk,lvl}(t) + P_{tk}(t)\Delta t & \text{if } \Delta P_{re}^2(t) > 0; \\ E_{tk,lvl}(t) - P_{tk}(t)\Delta t & \text{if } \Delta P_{re}^1(t) < 0; \end{cases} \quad (4.65)$$

4.5.4 Conventional Load, Desalination Plant and Industrial Factories Powered by Renewables and Legacy Grid

The fourth system configuration considered in this dissertation is shown in figure 4.5. Where the renewable energy sources are penetrating an existing legacy grid in the supply side. The load side in addition to desalination plant and a conventional (residential) load has also an industrial load represented by an aluminum factory.

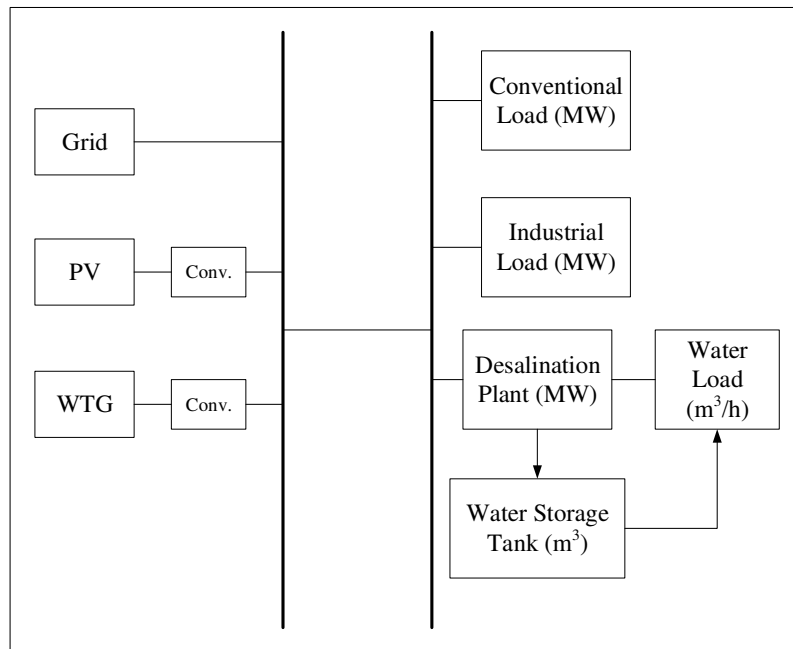


Figure 4.5: System configuration of conventional load, desalination plant and industrial factories powered by renewables and legacy grid

4.5.4.1 Design Constraints

- Load balance: For any time instant t the total supply must be sufficient to handle the required demand.

$$P_{L,e} = P_{con} + P_{fact,e} \quad (4.66)$$

$$P_{pv}^{\omega}(t)x_{pv} + P_{wt}^{\omega}(t)x_{wt} + \frac{\kappa}{\Delta t}P_{tk}^{\omega}(t) + P_g^{\omega}(t) = P_{L,e}(t) + P_{desal,e}(t) + P_{dump}^{\omega}(t), \quad \forall t, \forall \omega \quad (4.67)$$

- **Water tank capacity and flow bounds:** At any time instance, the total amount of stored water should not exceed the water tank capacity, which is mathematically represented in (4.68). The inequality constraint (4.69) states that the water inflow into the tank should do not exceed the desalination capability as well as the capacity of the storage tank. The water outflow from the tank should do not exceed the capacity of the water tank or the water load which is represented by (4.70).

$$0 \leq E_{tk,lvl}^{\omega}(t) \leq x_{tk}, \quad \forall t, \forall \omega \quad (4.68)$$

$$0 \leq P_{tk,in}^{\omega}(t) \leq \min(x_d, x_{tk}/\Delta t), \quad \forall t, \forall \omega \quad (4.69)$$

$$0 \leq P_{tk,out}^{\omega}(t) \leq \min(P_{desal,w}(t), E_{tk,lvl}(t)/\Delta t), \quad \forall t, \forall \omega \quad (4.70)$$

- **Legacy grid power and ramp bounds:** The amount of power provided by the grid should be within a specified range and should not exceed the ramp rates.

$$P_g^{min} \leq P_g^{\omega}(t) \leq P_g^{max}, \quad \forall t, \forall \omega \quad (4.71)$$

$$-P_g^{dn} \leq \Delta P_g^{\omega}(t) \leq P_g^{up}, \quad \forall t, \forall \omega \quad (4.72)$$

- **Decision variables bounds and type:** All the decision variables included in the optimization would be restricted to a specific range, this is referred to as the search

space. Also all variables are discrete (integers).

$$\begin{aligned}
x_{pv}^{min} &\leq x_{pv} \leq x_{pv}^{max}, & x_{pv} &\in \text{Integers} \\
x_{wt}^{min} &\leq x_{wt} \leq x_{wt}^{max}, & x_{wt} &\in \text{Integers} \\
x_{tk}^{min} &\leq x_{tk} \leq x_{tk}^{max}, & x_{tk} &\in \text{Integers} \\
x_d^{min} &\leq x_d \leq x_d^{max}, & x_d &\in \text{Integers}
\end{aligned} \tag{4.73}$$

4.5.4.2 System Operation Strategy

The generated power from the renewable sources has the priority to serve the loads. Any excess power after serving all instantaneous demand is diverted towards the desalination plant to be stored as desalinated water.

$$\Delta P_{re}^1(t) = P_{pv}(t)x_{pv} + P_{wt}(t)x_{wt} - P_{L,e}(t) \tag{4.74}$$

$$\Delta P_{re}^2(t) = \Delta P_{re}^1(t) - P_{desal,e}(t) \tag{4.75}$$

$$P_{tk}(t) = \begin{cases} P_{tk,in}(t) & \text{if } \Delta P_{re}^2(t) > 0; \text{ (Excess)} \\ P_{tk,out}(t) & \text{if } \Delta P_{re}^1(t) < 0; \text{ (Shortage)} \end{cases}$$

- If $\Delta P_{re}^1(t) > 0$ and $\Delta P_{re}^2(t) > 0$, this indicates a power excess and its diverted to the water storage subject to constraints (4.68) and (4.69).

$$P_{tk,in}(t) = \frac{\Delta P_{re}^2(t)}{\kappa/\Delta t} \tag{4.76}$$

- If $\Delta P_{re}^1(t) > 0$, $\Delta P_{re}^2(t) < 0$ and $E_{tk,lvl}(t) \geq \frac{|\Delta P_{re}^2(t)|\Delta t}{\kappa}$, this indicates a power shortage and all the energy available from the renewable sources are directed towards serving the aggregated load and any excess along with the available water in

the storage will supply the water load.

$$P_{tk,out}(t) = \frac{|\Delta P_{re}^2(t)|}{\kappa/\Delta t} \quad (4.77)$$

- If $\Delta P_{re}^1(t) > 0$, $\Delta P_{re}^2(t) < 0$ and $E_{tk,lvl}(t) < \frac{|\Delta P_{re}^2(t)|\Delta t}{\kappa}$, this is the same situation as the previous one. However, the hybrid system (PV-WTG-Tank) by its own can not fully supply the total demand. Thus, the grid is required to supply the deficit.

$$P_{tk,out}(t) = \frac{E_{tk,lvl}(t)}{\Delta t} \quad (4.78)$$

$$P_g(t) = |\Delta P_{re}^2(t)| - \frac{\kappa}{\Delta t} P_{tk,out}(t) \quad (4.79)$$

- If $\Delta P_{re}^1(t) < 0$ and $E_{tk,lvl}(t) \geq P_{desal,w}(t)\Delta t$, this represents a power shortage from the renewable sources to supply the aggregated load. Thus, the grid will have to supply the deficit. The water load can be supplied completely by the water storage.

$$P_{tk,out}(t) = P_{desal,w}(t) \quad (4.80)$$

$$P_g(t) = |\Delta P_{re}^1(t)| \quad (4.81)$$

- If $\Delta P_{re}^1(t) < 0$ and $E_{tk,lvl}(t) < P_{desal,w}(t)\Delta t$, the same situation as the previous one. However, the grid is required to supply some of the water and aggregated load.

$$P_{tk,out}(t) = \frac{E_{tk,lvl}(t)}{\Delta t} \quad (4.82)$$

$$P_g(t) = |\Delta P_{re}^1(t)| + \frac{\kappa}{\Delta t} (P_{desal,w}(t) - P_{tk,out}(t)) \quad (4.83)$$

The level of available water in the water storage for the next time step is:

$$E_{tk,lvl}(t+1) = \begin{cases} E_{tk,lvl}(t) + P_{tk}(t)\Delta t & \text{if } \Delta P_{re}^2(t) > 0; \\ E_{tk,lvl}(t) - P_{tk}(t)\Delta t & \text{if } \Delta P_{re}^1(t) < 0; \end{cases} \quad (4.84)$$

4.5.5 Conventional Load, Desalination Plant and Industrial Factories Powered by Renewables Coupled with Batteries and Legacy Grid

This is the same configuration as the previous one. However to study the effect of different storage mediums, the water tank was replaced with a Battery Energy Storage System (BESS). This configuration is shown in figure 4.6.

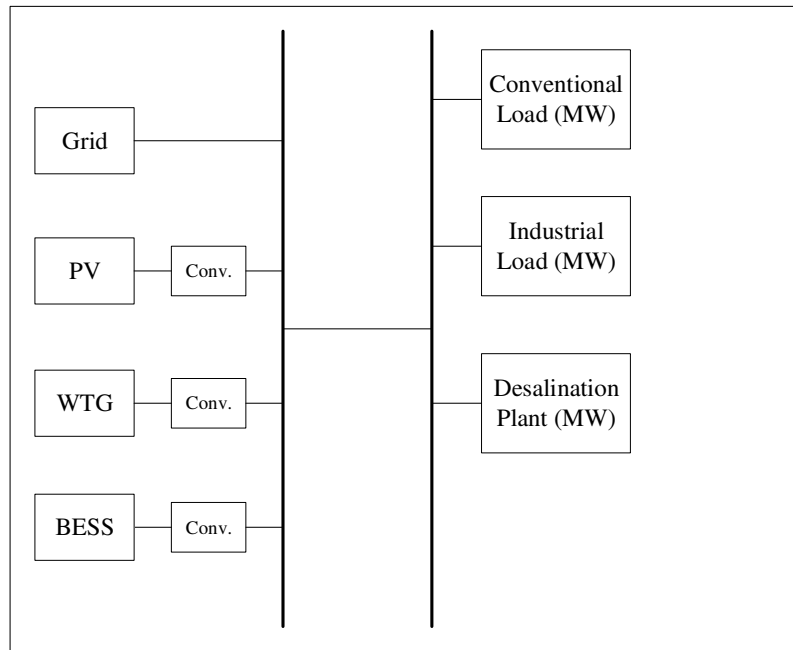


Figure 4.6: System configuration of conventional load, desalination plant and industrial factories couple with BESS and powered by renewables and legacy grid

4.5.5.1 Design Constraints

- Load balance: For any time instant t the total supply must be sufficient to handle the required demand.

$$\mathbf{P}_{L,e} = \mathbf{P}_{con} + \mathbf{P}_{desal,e} + \mathbf{P}_{fact,e} \quad (4.85)$$

$$P_{pv}^\omega(t)x_{pv} + P_{wt}^\omega(t)x_{wt} + P_{bat}^\omega(t) + P_g^\omega(t) = P_{L,e}(t) + P_{dump}^\omega(t), \quad \forall t, \forall \omega \quad (4.86)$$

- Battery energy storage system capacity and flow bounds: At any time instance, the total amount of stored energy should not exceed the batteries' capacity and should not as well reduce to below the minimum state of charge given by the maximum allowable Depth of Discharge (DOD), which is mathematically represented in (4.87). The inequality constraint (4.88) states that the power flow from or to the battery should do not exceed the batteries' capacity.

$$SOC_{bat}^{min} \leq SOC_{bat}^\omega(t) \leq x_{bat}, \quad \forall t, \forall \omega \quad (4.87)$$

$$0 \leq P_{bat}^\omega(t) \leq x_{bat}/\Delta t, \quad \forall t, \forall \omega \quad (4.88)$$

$$E_{bat,eff}^\omega(t) = SOC_{bat}^\omega(t) - SOC_{bat}^{min}, \quad \forall t, \forall \omega \quad (4.89)$$

- Legacy grid power and ramp bounds: The amount of power provided by the grid should be within a specified range and should not exceed the ramp rates.

$$P_g^{min} \leq P_g^\omega(t) \leq P_g^{max}, \quad \forall t, \forall \omega \quad (4.90)$$

$$-P_g^{dn} \leq \Delta P_g^\omega(t) \leq P_g^{up}, \quad \forall t, \forall \omega \quad (4.91)$$

- Decision variables bounds and type: All the decision variables included in the op-

timization would be restricted to a specific range, this is referred to as the search space. Also all variables are discrete (integers).

$$\begin{aligned}
x_{pv}^{min} &\leq x_{pv} \leq x_{pv}^{max}, & x_{pv} &\in \text{Integers} \\
x_{wt}^{min} &\leq x_{wt} \leq x_{wt}^{max}, & x_{wt} &\in \text{Integers} \\
x_{bat}^{min} &\leq x_{tk} \leq x_{bat}^{max}, & x_{bat} &\in \text{Integers}
\end{aligned} \tag{4.92}$$

A distinct difference here in comparison to the water tank storage scenario is that the desalination capacity expansion is no longer a variable. Since the batteries store electrical energy and therefore, the desalination capacity would have the default value of the existing plant.

4.5.5.2 System Operation Strategy

The generated power from the renewable sources has the priority to serve the loads. The excess power after serving all instantaneous demand is directed towards the BESS.

$$\Delta P_{re}(t) = P_{pv}(t)x_{pv} + P_{wt}(t)x_{wt} - P_{L,e}(t) \tag{4.93}$$

$$P_{bat}(t) = \begin{cases} P_{bat,in}(t) & \text{if } \Delta P_{re}(t) > 0; \text{ (Excess)} \\ P_{bat,out}(t) & \text{if } \Delta P_{re}(t) < 0; \text{ (Shortage)} \end{cases}$$

- If $\Delta P_{re}(t) > 0$, this indicates a power excess and its diverted to the battery banks subject to constraints (4.87) and (4.88).

$$P_{bat,in}(t) = \Delta P_{re}(t)\eta_{bat} \tag{4.94}$$

- If $\Delta P_{re}(t) < 0$ and $E_{bat,eff}(t) \geq \frac{|\Delta P_{re}(t)|\Delta t}{\eta_{bat}}$, this represents a power shortage from the renewable sources to supply the load. However, the available energy in the

batteries can supply the whole deficit.

$$P_{bat,out}(t) = \frac{|\Delta P_{re}(t)|}{\eta_{bat}} \quad (4.95)$$

- If $\Delta P_{re}(t) < 0$ and $E_{bat,eff}(t) < \frac{|\Delta P_{re}(t)|\Delta t}{\eta_{bat}}$, the same situation as the previous one. However, The batteries own their own can not fully supply the deficit from the renewable sources and as such the grid is required to supply some of the total load.

$$P_{bat,out}(t) = \frac{E_{bat,eff}(t)}{\Delta t} \quad (4.96)$$

$$P_g(t) = |\Delta P_{re}(t)| - P_{bat,out}(t)\eta_{bat} \quad (4.97)$$

The level of available energy in the battery energy storage system (BESS) for the next time step is:

$$SOC_{bat}(t+1) = \begin{cases} SOC_{bat}(t) + P_{bat}(t)\Delta t & \text{if } \Delta P_{re}(t) > 0; \\ SOC_{bat}(t) - P_{bat}(t)\Delta t & \text{if } \Delta P_{re}(t) < 0; \end{cases} \quad (4.98)$$

4.6 Inverters Sizing

The inverter sizing process involves the determination of the minimum number of inverters required for a given number of PV modules [79], [105]. The calculation of the minimum n_s^{min} and maximum n_s^{max} series of PV modules connected to a single inverter

depends on the inverter's DC input voltage band:

$$n_s^{min} = \text{round up} \left(\frac{V_{inv}^{min}}{V_{pv,mppt}^{min}} \right) \quad (4.99)$$

$$n_s^{max} = \text{round down} \left(\frac{V_{inv}^{max}}{V_{pv,oc}^{max}} \right) \quad (4.100)$$

Where, V_{inv}^{min} and V_{inv}^{max} are the minimum and maximum input voltages for the inverter respectively (V). $V_{pv,mppt}^{min}$ is the PV minimum voltage at maximum power point (V). $V_{pv,oc}^{max}$ is the PV maximum open circuit voltage (V).

$$n_s = \begin{cases} n_s^{max} & \text{if } n_s P_{pv}^{max} \leq P_{inv}^{max} \\ \text{INT} \left(\frac{P_{inv}^{max}}{n_s P_{pv}^{max}} \right) & \text{if } n_s P_{pv}^{max} > P_{inv}^{max} \end{cases} \quad (4.101)$$

Here, P_{inv}^{max} and P_{pv}^{max} are the maximum inverter and PV power (kW). The vector n_s , represents the possible numbers of PV modules connected in series from the minimum to the maximum value with an increment of one. For example, if the minimum is 3 and the maximum is 7, the vector n_s would be [3, 4, 5, 6, 7].

$$\mathbf{n}_s = [n_s^{min} \dots n_s^{max}] \quad (4.102)$$

The minimum parallel PV modules connected to a single inverter is one. The maxi-

mum value depends on both, the inverter's maximum allowable DC power and current.

$$n_p^{max,1} = \text{round down} \left(\frac{P_{inv}^{max}}{n_s P_{pv}^{max}} \right) \quad (4.103)$$

$$n_p^{max,2} = \text{round down} \left(\frac{I_{inv}^{max}}{I_{pv,sc}^{max}} \right) \quad (4.104)$$

$$n_p^{max} = \min(n_p^{max,1}, n_p^{max,2}) \quad (4.105)$$

I_{inv}^{max} and I_{pv}^{max} are the maximum inverter and PV currents (A). The vector \mathbf{n}_p , represents the possible numbers of PV strings connected in parallel from the minimum to the maximum value as in \mathbf{n}_s

$$\mathbf{n}_p = [1 \ \dots \ n_s^{max}] \quad (4.106)$$

A block of PV modules is connected together as a combination of series and parallel strings to form n_{block} connected to a single inverter.

$$n_{block} = n_s n_p \quad (4.107)$$

$$\mathbf{n}_{block} = [n_{block,1} \ \dots \ n_{block,n_b}] \quad (4.108)$$

Here, n_b is number of elements in \mathbf{n}_s multiply by the number of elements in \mathbf{n}_p . The vectors r_{pv}^1 and r_{pv}^2 contains the first and second remaining PV modules that can not be fitted with the selected n_{block} . The following formulas are used to calculate the number of inverters needed for a particular set of PV modules.

$$r_{pv}^1 = \text{mod}(x_{pv}, n_{block}) \quad (4.109)$$

$$\mathbf{r}_{pv}^1 = [r_{pv,1}^1 \ \dots \ r_{pv,n_b}^1] \quad (4.110)$$

$$r_{pv}^2 = \text{mod}(r_{pv}^1, n_{block}) \quad (4.111)$$

$$\mathbf{r}_{pv}^2 = \begin{bmatrix} r_{pv,11}^2 & \cdots & r_{pv,1n_b}^2 \\ \vdots & \ddots & \vdots \\ r_{pv,n_b1}^2 & \cdots & r_{pv,n_bn_b}^2 \end{bmatrix} \quad (4.112)$$

The number of inverters required is given by:

$$n_{inv} = \frac{x_{pv} - r_{pv}^1}{n_{block,i}} + \frac{r_{pv}^1 - r_{pv}^2}{n_{block,j}} + \frac{r_{pv}^2}{n_{block,k}}, \quad i \neq j \rightarrow k \quad (4.113)$$

$$\mathbf{n}_{inv} = \begin{bmatrix} n_{inv,11} & \cdots & n_{inv,1n_b} \\ \vdots & \ddots & \vdots \\ n_{inv,n_b1} & \cdots & n_{inv,n_bn_b} \end{bmatrix} \quad (4.114)$$

From the inverter's matrix, not all of the elements are suitable answers. For example, an element which is not an integer is not an acceptable solution. Thus, the selection criterion is the minimum integer value of the inverter's matrix.

$$n_{inv}^{sel} = \min(\mathbf{n}_{inv}), \quad n_{inv}^{sel} \in \mathbb{N} \quad (4.115)$$

Finally, the total cost of inverters is given by:

$$Cost_{inv} = C_{inv} n_{inv}^{sel} \quad (4.116)$$

4.7 Economical and Technical Analysis

Different metrics are usually used in the GEP problem to address different aspects of the optimized system [106]. The economical metrics are given as follows:

- Business As Usual cost (BAU_{cost}): represent the system cost as it is with only grid supply.

$$BAU_{cost} = \lambda_g^- E_{tot} \quad (4.117)$$

Where E_{tot} is the total energy required by the load over the life time of the project N_p .

- Cost savings: which is the difference between the Business As Usual cost and the differential cost given by the following equation:

$$Cost\ savings = BAU_{cost} - \Delta Cost \quad (4.118)$$

- Total annualized cost of the system (TAC): this cost represents the total system cost divided equally over the project life time while taken into consideration the time value of money.

$$TAC = Cost_{opt} \times CRF \quad (4.119)$$

$$CRF = \frac{i_{real}(1 + i_{real})^{N_p}}{(1 + i_{real})^{N_p} - 1} \quad (4.120)$$

$$i_{real} = \frac{i - f}{1 + f} \quad (4.121)$$

CRF is the capital recovery factor and i_{real} is the real interest rate.

- Levelized Cost of Energy (LCOE): the minimum cost of energy required to cover all the costs associated with the system which makes the present value of the revenues equal to the present value of the costs over the lifetime of the project.

$$LCOE = \frac{Cost_{opt}}{E_{tot,del}} \quad (4.122)$$

Where, $E_{tot,del}$ is the total amount of energy delivered to the load throughout the life time of the project (TWh).

- Total annualized revenue of the system (TAR): is the system yearly revenue

$$TAR = E_{tot}^{year} \times E_{price} \quad (4.123)$$

E_{tot}^{year} is the total energy supplied in a year (MWh). E_{price} is the price of electricity from the utility paid by the consumers (\$/kWh).

- Total revenue net present value of the system (TR): is the present value of all the revenues collected throughout the project life time.

$$TR = TAR \sum_{n=1}^{N_p} \left(\frac{1+f}{1+i} \right)^n \quad (4.124)$$

- Total annualized revenue of the hybrid system (TAR_{hyd}): is the hybrid system yearly revenue.

$$TAR_{hyd} = E_{re,del}^{year} \times E_{price} \quad (4.125)$$

$E_{re,del}^{year}$ is the energy supplied to the load from the renewable sources.

- Total revenue net present value of the hybrid system (TR_{hyd}): is the present value of the revenues collected from the renewable hybrid system throughout the project life time.

$$TR_{hyd} = TAR_{hyd} \sum_{n=1}^N \left(\frac{1+f}{1+i} \right)^n \quad (4.126)$$

- Total system profit (Prof): is the overall profit gain from the energy system given by:

$$Prof = TR - Cost_{opt} \quad (4.127)$$

- Return on Investment (ROI): which represents the percentage gain from the hybrid renewable system

$$ROI = \frac{TR_{hyrd} - Cost_{hyrd}}{Cost_{hyrd}} \times 100 \quad (4.128)$$

The technical metrics include the following:

- Solar farm rated power ($P_{pv,farm}^{rated}$): which is the rated power that can be achieved by the solar farm

$$P_{pv,farm}^{rated} = P_{pv}^{ref} \times x_{pv} \quad (4.129)$$

- Wind farm rated power ($P_{wt,farm}^{rated}$): which is the rated power that can be achieved by the wind farm

$$P_{wt,farm}^{rated} = P_{wt}^{rated} \times x_{wt} \quad (4.130)$$

- Nominal renewable fraction (RF_{nom}): this metric represents the ratio of total energy produced by the renewable sources including dumped energy $E_{re,tot}^{year}$ to the total energy produced by the whole system E_{tot}^{year} .

$$RF_{nom} = \frac{E_{re,tot}^{year}}{E_{tot}^{year}} \times 100 \quad (4.131)$$

- True renewable fraction (RF_{true}): this metric represents the ratio of total energy produced by the renewable sources and delivered to the loads excluding dumped energy to the total energy produced by the whole system.

$$RF_{true} = \frac{E_{re,del}^{year}}{E_{tot}^{year}} \times 100 \quad (4.132)$$

- solar farm capacity factor (CF_{pv}): the ratio of the actual output of the solar farm over a year $E_{pv,farm}^{year}$ to the theoretical output that would be produced if the solar farm was

operating without interruption at its rated capacity during the same period of time

$E_{pv,farm}^{rated}$.

$$CF_{pv} = \frac{E_{pv,farm}^{year}}{E_{pv,farm}^{rated}} \quad (4.133)$$

- Wind farm capacity factor (CF_{wt}): the ratio of the actual output of the wind farm over a year $E_{wt,farm}^{year}$ to the theoretical output that would be produced if the wind farm was operating without interruption at its rated capacity during the same period of time $E_{wt,farm}^{rated}$.

$$CF_{wt} = \frac{E_{wt,farm}^{year}}{E_{wt,farm}^{rated}} \quad (4.134)$$

- Renewable energy sources utilization factor (UF): the ratio of renewable energy utilized to total renewable energy produced $E_{re,tot}^{year}$.

$$UF = \frac{E_{re,del}^{year}}{E_{re,tot}^{year}} \quad (4.135)$$

4.8 Renewable Energy Sources Footprint

4.8.1 Solar Farm Physical Layout

The main assumption made for the physical layout is that the available installation area is rectangular in shape and the PV modules are facing south. The PV modules are arranged within the premises of the installation area in multiple rows [79]. Each row is comprised of multiple lines of PVs. The maximum number of horizontal units in a row $N_{pv,horz}^{max}$ is given by:

$$N_{pv,horz}^{max} = \text{round down} \left(\frac{L_{pv}}{l_{pv}} \right) \quad (4.136)$$

Where, L_{pv} is the length of the solar farm. and l_{pv} is the length of an individual PV panel.

$$N_{pv,horz} = \begin{cases} N_{pv,horz}^{max} & \text{if } x_{pv}/N_{pv,line} \geq N_{pv,horz}^{max} \\ \text{round up}(x_{pv}/N_{pv,line}) & \text{Otherwise} \end{cases} \quad (4.137)$$

$$N_{pv,gup} = N_{pv,horz} N_{pv,line} \quad (4.138)$$

$$N_{gup} = \text{round up}\left(\frac{x_{pv}}{N_{pv,gup}}\right) \quad (4.139)$$

$$n_{pv,last} = \text{mod}(x_{pv}, N_{pv,gup}) \quad (4.140)$$

$N_{pv,line}$ is the number of horizontal lines of PVs. $N_{pv,gup}$ is the number of PV modules in each group. $n_{pv,last}$ is the number of PVs left after dividing all x_{pv} in $N_{pv,gup}$.

The sizing of the last group has two cases as follows:

- If $n_{pv,last} > N_{pv,horz}^{max}$, in this situation the last group has to be sized in the same manner as the other groups. This is shown in the following equations.

$$n_{pv,horz} = N_{pv,horz}^{max} \quad (4.141)$$

$$n_{pv,line} = \text{round up}\left(\frac{n_{pv,last}}{n_{pv,horz}}\right) \quad (4.142)$$

$n_{pv,horz}$ is the number of horizontal PVs in the last row. $n_{pv,line}$ is the number of horizontal lines of PVs in the last group.

- If $n_{pv,last} \leq N_{pv,horz}^{max}$, in this situation the last group is just one row of PVs

$$n_{pv,horz} = n_{pv,last} \quad (4.143)$$

$$n_{pv,line} = 1 \quad (4.144)$$

The width $W_{pv,gup}^T$ and height $H_{pv,gup}^T$ of the tilted PV panel in a group is given by:

$$W_{pv,gup}^T = w_{pv}^T N_{pv,line} \quad (4.145)$$

$$w_{pv}^T = w_{pv} \cos(\beta) \quad (4.146)$$

$$H_{pv,gup}^T = h_{pv}^T N_{pv,line} \quad (4.147)$$

$$h_{pv}^T = w_{pv} \sin(\beta) \quad (4.148)$$

w_{pv}^T and h_{pv}^T are the width and height of a single line of PVs respectively. The width of the last group $W_{pv,last}^T$ is:

$$W_{pv,last}^T = w_{pv}^T n_{pv,line} \quad (4.149)$$

To account for the shading effect of one group over the other, a minimum distance between the adjacent groups d is established which can be calculated as follows:

$$d = \left(\frac{H_{pv,gup}^T}{\tan(\theta_\alpha)} \right) \cos(\theta_\psi) \quad (4.150)$$

Finally, the length $D_{pv,length}$, width $D_{pv,width}$ and subsequently the area A_{pv} of the solar farm can be calculated as follows:

$$D_{pv,length} = N_{pv,horz} l_{pv} \quad (4.151)$$

$$D_{pv,width} = (W_{pv,gup}^T + d)(N_{pv,gup} - 1) + W_{pv,last}^T \quad (4.152)$$

$$A_{pv} = D_{pv,length} D_{pv,width} \quad (4.153)$$

The solar farm layout is shown in figure 4.7.

4.8.2 Wind Farm Physical Layout

The physical layout for the wind turbines placement also follows the same assumption made with the PV solar farm, in which the wind farm is located and placed in a rectangular shaped area. The following equations allows for the calculation of the required length $D_{wt,length}$ and width $D_{wt,width}$ of the field [5], [107]. The maximum number of horizontal wind turbines $N_{wt,horz}^{max}$ is given by:

$$N_{wt,horz}^{max} = \text{round up} \left(\frac{L_{wt} - 2\Delta l}{4 r_{dia}} \right) \quad (4.154)$$

$$\Delta l = 2 r_{dia} \quad (4.155)$$

Here, Δl is the offset distance from the boundaries of the wind farm. r_{dia} is the WT rotor diameter. From the above calculation two outcomes are possible

- If $x_{wt} > N_{wt,horz}^{max}$, the wind turbine need to be distributed into a number of rows.

$$N_{wt,horz} = N_{wt,horz}^{max} \quad (4.156)$$

$$N_{wt,rows} = \text{round up} \left(\frac{x_{wt}}{N_{wt,horz}^{max}} \right) \quad (4.157)$$

$$n_{wt,last} = \text{mod}(x_{wt}, N_{wt,horz}) \quad (4.158)$$

$$D_{wt,length} = 4 r_{dia}(N_{wt,horz} - 1) + 2\Delta l \quad (4.159)$$

$$D_{wt,width} = 10 r_{dia}(N_{wt,rows} - 1) + 2\Delta l \quad (4.160)$$

- If $x_{wt} \leq N_{wt,horz}^{max}$, the wind turbine can be aligned in a single row

$$N_{wt,horz} = x_{wt} \quad (4.161)$$

$$N_{wt,rows} = 1 \quad (4.162)$$

$$n_{wt,last} = 0 \quad (4.163)$$

$$D_{wt,length} = 4 r_{dia}(N_{wt,horz} - 1) + 2\Delta l \quad (4.164)$$

$$D_{wt,width} = 2\Delta l \quad (4.165)$$

$N_{wt,horz}$ is the number of WT in a horizontal line. $N_{wt,rows}$ is the number of WT rows in the wind farm. $n_{wt,last}$ is the number of WT in the last row.

Now that all the required dimensions are calculated, the wind farm area can be easily found as follows:

$$A_{wt} = D_{wt,length}D_{wt,width} \quad (4.166)$$

The wind farm layout is shown in figure 4.8.

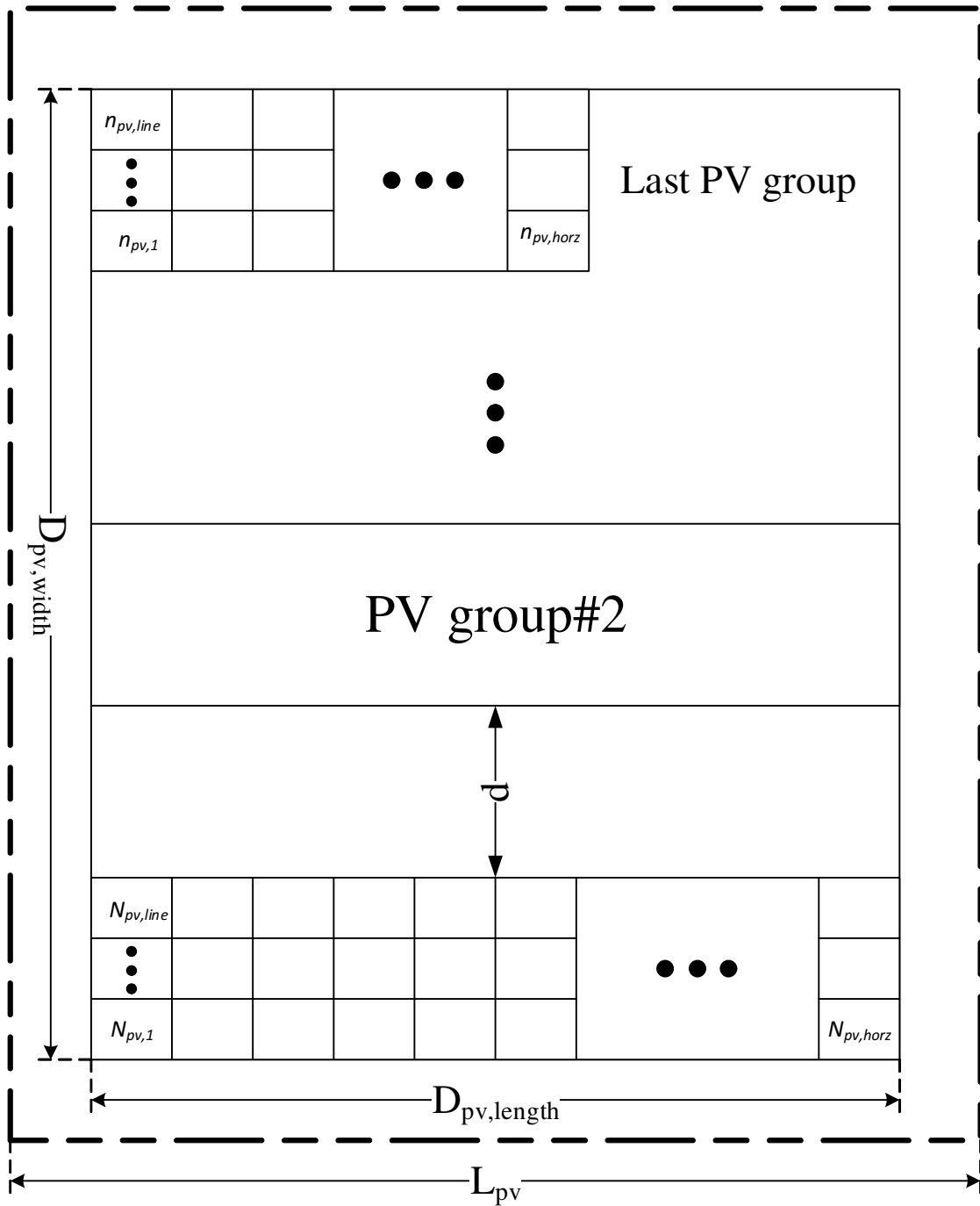


Figure 4.7: Solar farm physical layout

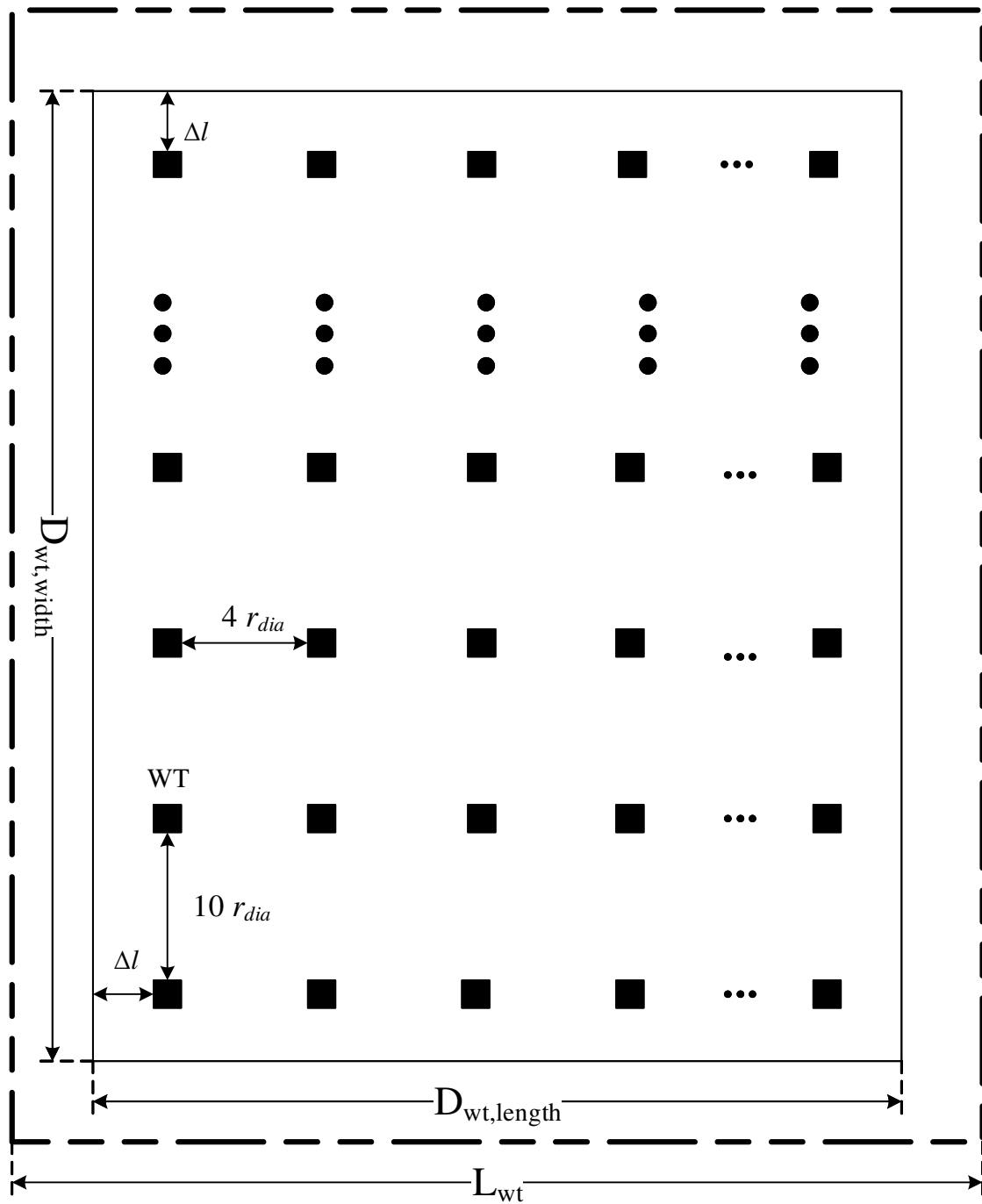


Figure 4.8: Wind farm physical layout

5. IMPLEMENTED OPTIMIZATION TECHNIQUES

5.1 Optimization Methodologies

Theoretical and practical optimization problems are usually formulated to search for an *optimal* configuration based on a set of *decision variables* while maintaining certain *constraints*. A typical optimization problem can be represented as follows [108]:

$$\begin{aligned} \min_x \quad & f_i(x), \quad i = 1, \dots, I. \\ \text{s.t.} \quad & h_j(x) \leq b_j, \quad j = 1, \dots, J. \\ & g_l(x) = c_l, \quad l = 1, \dots, L. \end{aligned}$$

Here, f_i is the objective function to be minimized/maximized, h_j and g_l are the inequality and equality constraints of the problem respectively. i, j, l are the number of objective functions, inequality, and equality constraints respectively. The set of decision variables is represented by x .

The solution methodology for any optimization problem depends on several factors, such as the type of objective function as well as the constraints (linear, nonlinear), whether the decision variables are *continuous* or *discrete*.

The GEP problem is formulated as an optimization problem, where the objective function can be divided into different criteria including, economic, environmental and reliability criteria. economic criteria is usually related to minimizing the total system cost [109–119], cost of energy, [72], [120–122], or cost of fuel [123]. A multi-objective formulation of GEP is also common in the literature. Typically incorporating environmental aspects of the problem in the objective functions, which is concerned with the minimization of hazards gases such as carbon dioxide (CO₂), sulfur dioxide (SO₂) as well as nitrogen oxides (NO_x) emissions [73], [80], [123–126]. Reliability can also be represented as an ob-

jective function characterized by minimizing, the Loss of Load Probability (LOLP), Loss of Load Expectation (LOLE) or Expected Unversed Energy (EUE), [72], [73], [127–131].

The constraints involved with GEP problem are the investment and operational constraints. Where investment constraint is usually related to problem budget and operational constraints are in general, the power balance, generators power limit, generators ramp up/down limits, storage limitation and in some studies, reliability constraints are included.

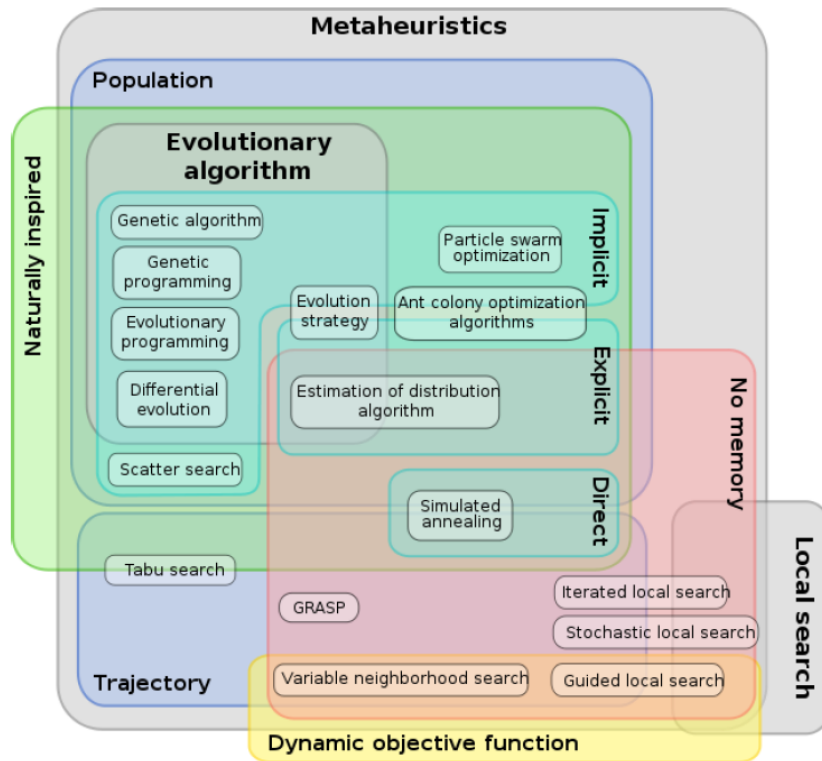


Figure 5.1: Classification of meta-heuristic algorithms. Reprinted from [132]

High dimensional search space optimization problems are tedious to solve using exact optimization algorithms as the search space expand exponentially with the size of the problem. Thus, an exhaustive search is impractical in massive optimization problems such

as the GEP problem. Greedy based algorithms which are considered to be an approximate optimization method has the problem of having too many assumptions by which it could affect the credibility of the solutions obtained [132].

The literature is overwhelmed with various methods for solving the GEP problem. Meta-heuristic methods are a generalization of the problem dependent heuristic methods and require fewer modifications. The definition of the words *meta* and *heuristic* which are Greek means "higher level" and "to find" respectively.

Beheshti *et al.* in [132], reported the definition of meta-heuristic as follows, "an iterative generation process which guides a subordinate heuristic by combining intelligently different concepts for exploring and exploiting the search space, learning strategies are used to structure information to find efficiently near-optimal solutions."

The meta-heuristic methods have the advantage of being a straightforward easy to modify methods. They can handle large and complex problems that include linear and nonlinear constraints and also can reach near-optimal solutions as well as solving multi-objective optimization problems [123], [133], [134].

Meta-heuristic can be classified as *trajectory methods* or *population-based methods*. Trajectory methods are concerned with only a single solution as the search process takes place, and the process outcome is as well a single optimized solution. This approach includes simulated annealing (SA), tabu search (TS), hill climbing (HC) and many others.

Population-based meta-heuristics, on the other hand, utilizes a whole population of solutions within a finite number of iterations, and this population evolves towards the optimal solution as the iterations progress. The output is also a population of solutions. Examples of this type of algorithms include evolutionary algorithms (EA), genetic algorithm (GA), particle swarm optimization (PSO), ant colony optimization (ACO), artificial bee colony optimization (ABCO), and many other [7].

5.2 Constraint Handling

Some methodologies have been proposed in the literature to handle constraints in heuristic-based optimization. On a broader sense, the methodologies are divided into two categories; applying a penalty factor to the objective value when a constraint is violated and the second category is to have a repairing mechanism to adjust the optimized solution and make it feasible [135].

The penalty functions can be established in numerous ways which include static, dynamic, and adaptive penalty functions. The most common approach is the static penalty function where every constraint violation is treated in the same manner regardless of the level of violation or the current iteration of the optimization algorithm. It has the advantage of being simple to implement as any constraint violation would have a significant penalty associated with it.

The dynamic penalty functions are considered to be an upgrade to static approach, where the index of the current iteration is utilized in calculating the violation penalty. Typically at earlier stages of the optimization algorithm, the penalizing factor is low to allow for the exploration of the boundaries of the search space. As the iterations get closer to the final predetermined value, the penalizing factor is adjusted accordingly with higher values.

The adaptive penalty functions are based on the dynamic approach. In addition to utilizing the current iteration in calculating the penalties, the statistics of the population are also used to calculate the overall penalty factor [136].

As previously mentioned repairing an individual solution to make it feasible is an approach for handling constraints. For example, if an individual solution is beyond its boundaries, the repairing mechanism will limit that solution to its boundaries by enforcing a minimum or maximum limitation.

The adopted method in this dissertation is a basic penalty function due its simplicity and ease of implementation. The calculation of the penalty factors are given by the following function:

$$PF = \Gamma^{(i/I)}(g(x) - g^{max}(x))^2 \quad (5.1)$$

Where, PF is the penalty factor, Γ is the penalty coefficient, i, I are the current and maximum iterations respectively. $g(x), g^{max}(x)$ are the constraint and maximum allowable violation respectively.

5.3 Genetic Algorithm (GA)

Genetic Algorithm is a widely known type of evolutionary algorithm. Holland mainly developed it as a means of studying adaptive behavior [84], [135]. This technique is a stochastic global search method based on the principles of natural genetics and natural selection. More Philosophically, GAs are based on Darwin's theory of survival of the fittest. The basic elements of natural genetics include reproduction, crossover, and mutation which are used to construct the GA's search procedure [137]. A string of genes forms a chromosome. Moreover, each gene is a decision variable which can be represented as a binary-coded, real value-coded or integer-coded. A population is formed from several chromosomes.

5.3.1 GA Working Principle

The GA initially starts by randomly generating a predefined number of chromosomes which constitutions a population. Then an objective function is calculated for each chromosome which is referred to as a fitness function. For the production of the next generation, a selection methodology is used to find the most suitable parents to produce offsprings. Depending on the predefined crossover percentage, some parents are selected. The crossover operator has different ways to be realized. The two selected parents are

crossed to produce offspring called (children). The next step is to apply the mutation operator, by randomly selecting a chromosome from the current population and perform the selected mutation operator. An enhancement over the typical simple GA to avoid local minimum solutions is considered here. A local search is adopted where each decision variable (gene) of the elite solution is subjected to a mutation operation, and if the resulting solution is better regarding fitness, it will replace the original best solution. This complete operation is repeated for a fixed number of iterations and the flowchart in figure 5.3 demonstrate the steps to implement GA.

5.3.2 Fitness Function

The fitness of each string s in iteration i with an objective function $Q(x)$ is given by:

$$f_s(i) = \frac{1}{1 + Q(x)} \quad (5.2)$$

A normalization approach for the fitness value is done to avoid premature convergence.

$$\hat{f}_s(i) = \frac{f_s(i) - f^{min}(i)}{f^{max}(i) - f^{min}(i)} \quad (5.3)$$

Where \hat{f}_s^i is the normalized fitness function of string s in iteration i . $f^{min,i}$ and $f^{max,i}$ are the minimum and maximum fitness values respectively in iteration i .

5.3.3 Selection Operators

The selection of reproduction operator is responsible for selecting good chromosomes (strings) based on their fitness value as parents that will breed children in the crossover operation. Depending on how the selection operator is set up it will provide a mating pool. There are many ways reported in the literature to realize this operator. In this dissertation, three different realizations are used [132], [137]:

- *Roulette wheel*: The main idea here is that parents are selected based on their fitness where each string has a probability proportional to its fitness this means that chromosomes with better fitness have more chance to be selected. A ranking selection mechanism is utilized to avoid outstanding individuals taking over the entire population very quickly,

$$p_s(i) = e^{-\gamma \left(\frac{f^{min}(i)}{f_s(i)} \right)} \quad (5.4)$$

$$P_s(i) = \frac{p_s(i)}{\sum_{s=1}^S p_s(i)} \quad (5.5)$$

Where, $P_s(i)$ is the selection percentage for each string s in iteration i . γ is a pre-defined selection pressure. the total number of strings is S . Figure 5.2 demonstrate this selection technique.

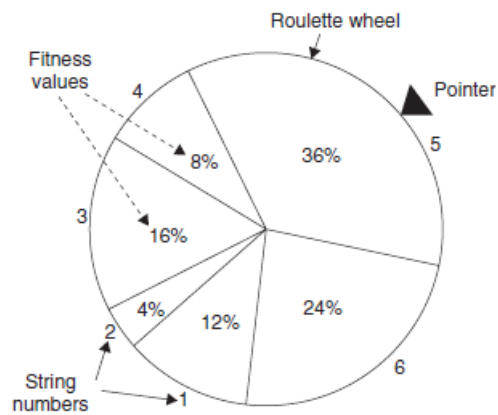


Figure 5.2: Roulette-wheel selection scheme. Reprinted with permission from [137]

- *Tournament selection*: In this selection methodology some strings are randomly selected from the population, and the string with the best fitness value among them

is chosen as a parent. The same operation is repeated to select the other parent. It is conceptually simple and fast to implement and apply.

- *Random selection*: Here a purely random selection process is implemented to select two parents from the population without any knowledge of their fitness.

5.3.4 Crossover Operators

Once parents are selected, the next step is to generate new strings (offsprings) [84]. The purpose of the crossover operator is to create new strings by exchanging information among parents' strings which will exploit the solution (search) space. As in the selection operator, different ways to realize the crossover operator is available. The parents to be crossed are represented by:

$$X^1 = [x_1^1, x_2^1, \dots, x_K^1]$$

$$X^2 = [x_1^2, x_2^2, \dots, x_K^2]$$

The following are the crossover operators implemented [138]:

- *Swap crossover*: In this method a simple swap between the two parents is done to produce offsprings (children). The offsprings are generated by randomly choosing a position k for the swapping to occur.

$$C^1 = [x_1^1, x_2^1, \dots, x_k^1, x_{k+1}^2, \dots, x_K^2] \quad (5.6)$$

$$C^2 = [x_1^2, x_2^2, \dots, x_k^2, x_{k+1}^1, \dots, x_K^1] \quad (5.7)$$

- *Single arithmetic crossover*: Here an individual is randomly selected and an arith-

metric calculation is performed.

$$C^1 = [x_1^1, x_2^1, \dots, \alpha x_k^2 + (1 - \alpha)x_k^1, x_{k+1}^1, \dots, x_K^1] \quad (5.8)$$

$$C^2 = [x_1^2, x_2^2, \dots, \alpha x_k^1 + (1 - \alpha)x_k^2, x_{k+1}^2, \dots, x_K^2] \quad (5.9)$$

$$\alpha \in [0, 1] \quad (5.10)$$

- *Simple arithmetic crossover*: This method is an extend version of the previous one.

And it can be represented as follows.

$$C^1 = [x_1^1, x_2^1, \dots, \alpha x_k^2 + (1 - \alpha)x_k^1, \dots, \alpha x_m^2 + (1 - \alpha)x_m^1] \quad (5.11)$$

$$C^2 = [x_1^2, x_2^2, \dots, \alpha x_k^1 + (1 - \alpha)x_k^2, \dots, \alpha x_m^1 + (1 - \alpha)x_m^2] \quad (5.12)$$

$$\alpha \in [0, 1] \quad (5.13)$$

- *Whole arithmetic crossover*: This methodology performs over all parents' individuals.

$$C^1 = [c_1^1, c_2^1, \dots, c_K^1] \quad (5.14)$$

$$C^2 = [c_1^2, c_2^2, \dots, c_K^2] \quad (5.15)$$

$$c_k^1 = \alpha x_k^1 + (1 - \alpha)x_K^2 \quad (5.16)$$

$$c_k^2 = \alpha x_k^2 + (1 - \alpha)x_K^1 \quad (5.17)$$

$$\alpha \in [0, 1] \quad (5.18)$$

5.3.5 Mutation Operators

The mutation operator is GA's mechanism for solution space exploration and it provides a means to escape local minimums. Many approaches have been proposed in the literature. The process starts by selecting a string from the population to be mutated and

generate a new string.

$$X = [x_1, x_2, \dots, x_K]$$

- *Random mutation*: This is one of the simplest implementations of a mutation operator by randomly choosing an individual from the selected string and change its value according to the range of that individual.

$$x_k \in [x_k^{min}, x_k^{max}] \quad (5.19)$$

- *Normally distributed mutation*: A random number is generated to find which individuals within the selected string will undergo the mutation operator.

$$X^{mutated} = [x_1^{mutated}, x_2^{mutated}, \dots, x_K^{mutated}] \quad (5.20)$$

$$x_k^{mutated} = x_k + \xi\epsilon, \quad \epsilon \sim N(0, 1) \quad (5.21)$$

$$\xi = 0.1(x_k^{max} - x_k^{min}) \quad (5.22)$$

- *Non-uniform mutation*: This approach takes into account the current generation by which in early iterations the mutation range is large and gets smaller as the generations approach the maximum value.

$$x_k^{mutated} = x_k + \tau(x_k^{max} - x_k^{min})(1 - y^{(1-T)^g}) \quad (5.23)$$

$$T = \frac{i}{I} \quad (5.24)$$

In the above equation, τ is a random number of either (-1,1), y is a uniformly distributed random number. The variable i and I are the current iteration (generation) and the total number of iterations respectively. While g is a parameter which deter-

mines the degree of dependency on the number of iterations.

5.3.6 Non-Domination Sorting Genetic Algorithm (NSGA-II)

The GA algorithm is extended to solve multi-objective problems. A Pareto frontier is developed to display the optimal set of solutions without assigning weights to them. In addition to the operators above, the algorithm utilizes a non-domination as well as a crowding distance operators [134]. The method is extensively explained in [139]. An individual is said to dominate another if the objective functions of it are no worse than the other and at least in one of its objective functions, it is better than the other. The individuals are sorted based on non-domination into different levels called fronts. The non-dominant set in the current population of solutions represents the first front and the second front being dominated by the individuals in the first front only and so on. A rank value is assigned to the individuals in each front. Where individuals in the first front are given a rank of one and individuals in the second front are assigned a rank of two and so on. To preserve the diversity of the solutions a crowding distance measure is implemented to calculate how close an individual is to its neighbors. Large average crowding distance will result in a better diversity of the population. The flowchart in figure 5.4 demonstrate the steps to implement NSGA-II.

5.4 Mutation Based Particle Swarm Optimization (MBPSO)

Particle swarm optimization (PSO), is established based on the behavior of a swarm such as a flock of birds. The algorithm is referred to as behaviorally inspired algorithms as opposed to the genetic algorithms, which are called evolution-based procedures. Each particle in a swarm behaves in a distributed manner using its intelligence and the collective or group intelligence of the swarm. Thus, if one particle discovers a good path, the entire swarm will also be able to follow the good path instantly even if their location is far away in the swarm. Kennedy and Eberhart originally proposed the PSO algorithm in 1995 [137], [140].

5.4.1 Working Principle

The PSO algorithm starts by randomly generating different particles. Each particle has a position and a velocity associated with it. First, the velocity of each particle is calculated followed by the calculation of its position. Each particle has its memory of the best position it ever reached regarding the objective function value. Another memory is reserved for the best position ever reached by any particle which is referred to as the global best solution. The algorithm is repeated for a predefined number of iterations. The flowchart in figure 5.5 demonstrate the steps to implement MBPSO.

5.4.2 Velocity Operator

The velocity of each particle is calculated for every iteration as follows

$$V_j(i) = wV_j(i-1) + c_1r_1(P_j^b - X_j(i-1)) \quad (5.25)$$

$$+ c_2r_2(G^b - X_j(i-1)) \quad \forall j \in J \quad (5.26)$$

$$w = \left(\frac{(w_2 - w_1)i}{I} \right) - w_2 \quad (5.27)$$

$$c_1 = \left(\frac{(c_1^f - c_1^0)i}{I} \right) + c_1^0 \quad (5.28)$$

$$c_2 = \left(\frac{(c_2^f - c_2^0)i}{I} \right) + c_2^0 \quad (5.29)$$

The velocity of particle j in iteration i is represented by $V_j(i)$. The variable w is the inertia weight. The time varying acceleration coefficients are c_1, c_2 and the superscripts $0, f$ denotes initial and final values respectively. r_1 and r_2 are a uniformly distributed random numbers. w_2, w_1 are the maximum and minimum inertia weights. X_j is the position of particle j while P_j^b is the best position ever reached by that particle. Finally G^b is the best position ever found by any particle in the set J .

5.4.3 Position Operator

The position of each particle is updated each iteration as follows:

$$X_j(i) = X_j(i-1) + V_j(i) \quad \forall j \in J \quad (5.30)$$

5.4.4 Mutation Operator

Two mutation operators are adopted in the PSO optimization to enhance its search ability. The mutation operator is only performed on the global best position in each iteration.

- *Gaussian mutation*: this type of mutation includes generating random numbers with a normal distribution which is given by ϵ .

$$x_k^{mutated} = x_k(1 + \frac{1}{2}\epsilon) \quad (5.31)$$

- *Beta mutation*: This type of mutation includes generating random numbers with a beta distribution which is given by β .

$$x_k^{mutated} = x_k(1 + \frac{1}{2}\beta) \quad (5.32)$$

5.4.5 Multi-Objective Particle Swarm Optimization (MOPSO)

The implemented MOPSO is based on the work done in [141]. In addition to the previous PSO operators, a non-dominance operator is also used. The working principle is as follows. The first step is to initialize the particles and their velocities as done in the single objective PSO. A repository vector is generated to store all the non-dominated particles. Followed by a grid construction using the lower and upper bounds of the objective functions evaluated so far. A leader particle is selected based on the roulette wheel operator, and both velocity and particle position is updated. Mutation process is also implemented here to ensure higher exploration of the search space. The dominance operator is then used to update each particle best solution as well as updating the repository vector and the grid and its indices. The flowchart in figure 5.6 demonstrate the steps to implement MOPSO.

5.5 Imperialist Competitive Algorithm (ICA)

The Imperialist Competitive Algorithm (ICA), is a meta-heuristic optimization technique introduced by Atashpaz-Gargari and Lucas. Inspired by socio-political behaviors. The algorithm simulates the social-political process of imperialism and imperialistic competition [142].

5.5.1 Working Principle

The first step of the ICA involves the initiation of individuals referred to as countries. Some of the countries will be imperialists, and the rests will be colonies within the different empires. The next step is to move colonies towards their imperialist which is done by the assimilation operator. A revolution operator accomplishes sudden random changes in the position of some of the colonies which mimic the process of mutation. Within each empire, an exchange of positions between a colony and its imperialist is possible, which is called an intra-empire competition. Also, empires compete against each other as the winner will overtake the fallen empire. The inter-empire operator is responsible for this process. The ICA continues until it reaches the predefined maximum number of iterations. The flowchart in figure 5.7 demonstrate the steps to implement ICA.

5.5.2 Total Cost Operator

The power of an empire is computed based on the power of its imperialist and a fraction of the power of its colonies.

$$TC^k = C_{imp}^k + \varphi \times \text{mean}(C_{col}^k), \quad \varphi \in [0, 1] \quad (5.33)$$

Here, TC^k is the total cost of the k th empire. C_{imp}^k and C_{col}^k are the cost of imperialist and its colonies respectively.

5.5.3 Assimilation Operator

This operator is responsible for colonies movements towards their imperialists.

$$X_j^k(i) = X_j^k(i-1)b\mu + (X^k(i) - X_j^k(i-1)) \quad (5.34)$$

Where, $X_j^k(i)$ is the position of the j th colony under the k th imperialist in iteration i and $X^k(i)$ is the position of the k th empire in iteration i . μ is a uniformly distributed random number and b is the assimilation coefficient.

5.5.4 Revolution Operator

The revolution operator is responsible for exploring the solution space as in the mutation operator of the GA.

$$X_j^k(i) = X_j^k(i-1) - \xi\epsilon, \quad \epsilon \sim N(0, 1) \quad (5.35)$$

$$\xi = 0.1(x_j^{k,max} - x_j^{k,min}) \quad (5.36)$$

5.5.5 Intra-Empire Competition Operator

After the revolution operator has been performed, some colonies within an empire might have a better cost value than its imperialist. The intra-empire operator is responsible for identifying such conditions in which the colonies that are found to have better cost value will overtake their imperialist.

(5.37)

5.5.6 Inter-Empire Competition Operator

The ICA also takes into consideration the competition of empires against each other. The weakest empire is the one with the worst total cost value. The weakest colony in

the weakest empire will be given to another empire. The empire receiving this colony is determined by how powerful other imperialists are, based on their total cost. A roulette wheel operator is used to determine which empire is going to get the fallen colony. The weakest empire that does not have any colonies within it will be eliminated.

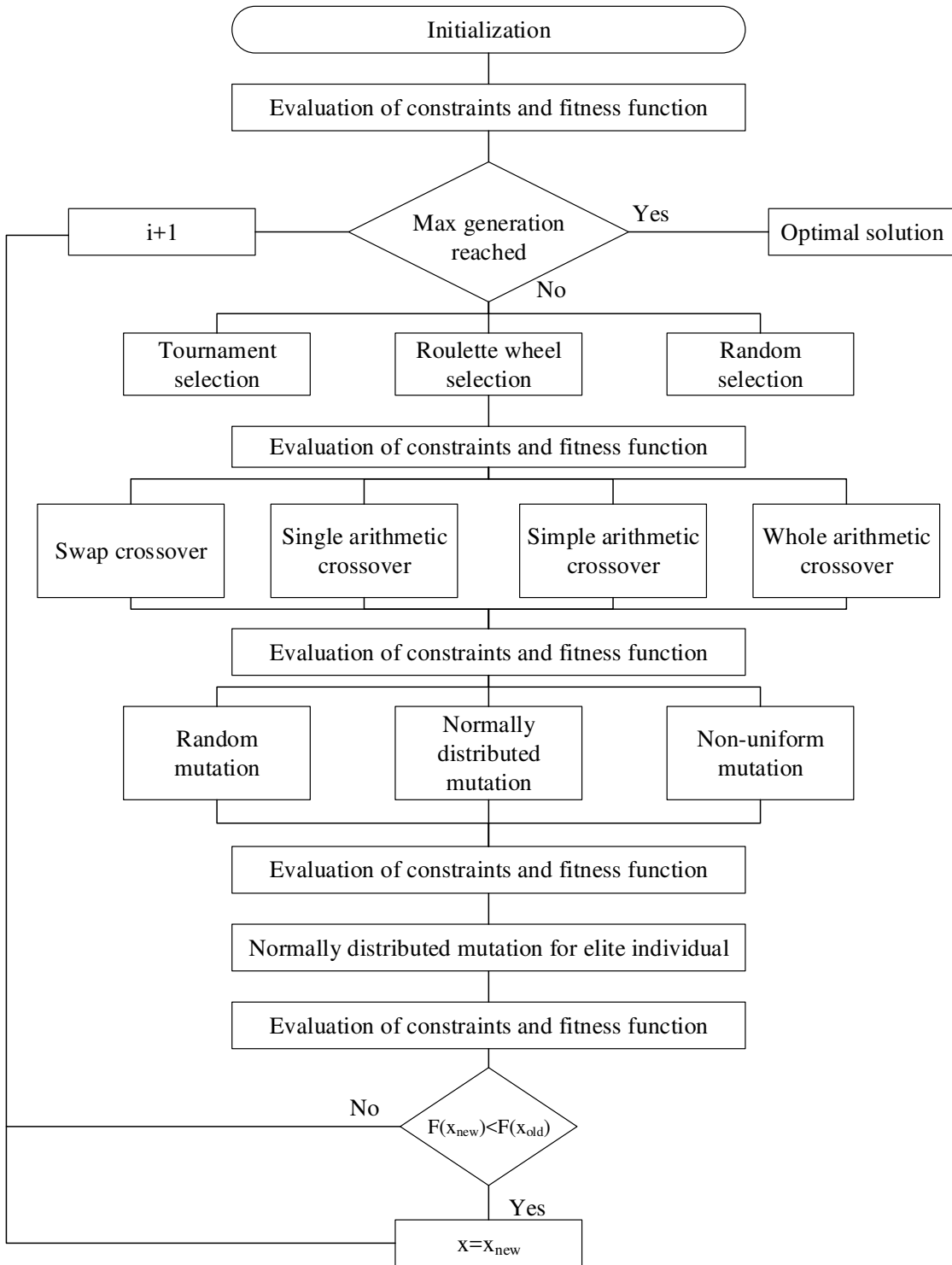


Figure 5.3: Genetic Algorithm (GA) flow chart

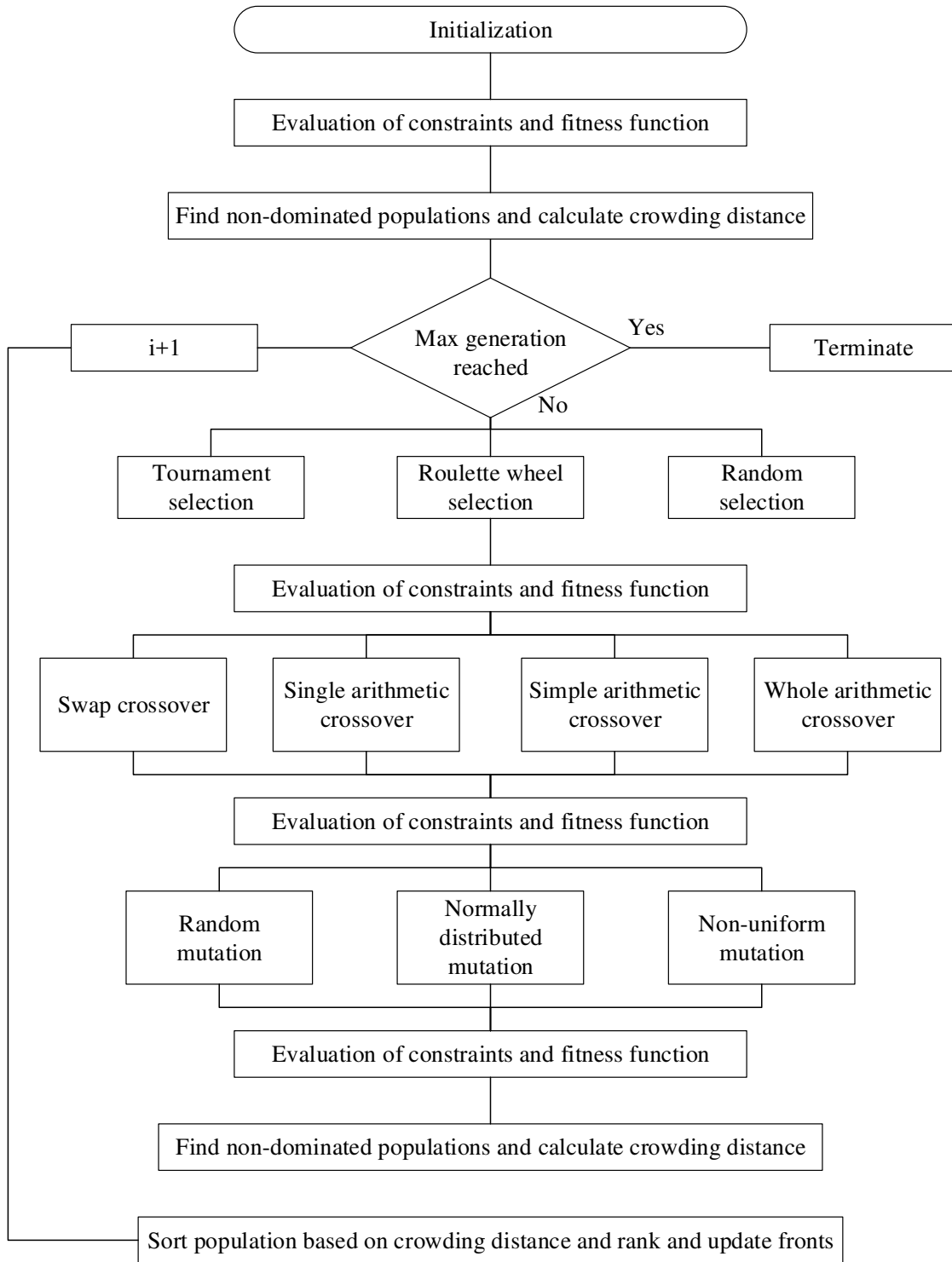


Figure 5.4: Non-dominated Sorting Genetic Algorithm (NSGA II) flow chart

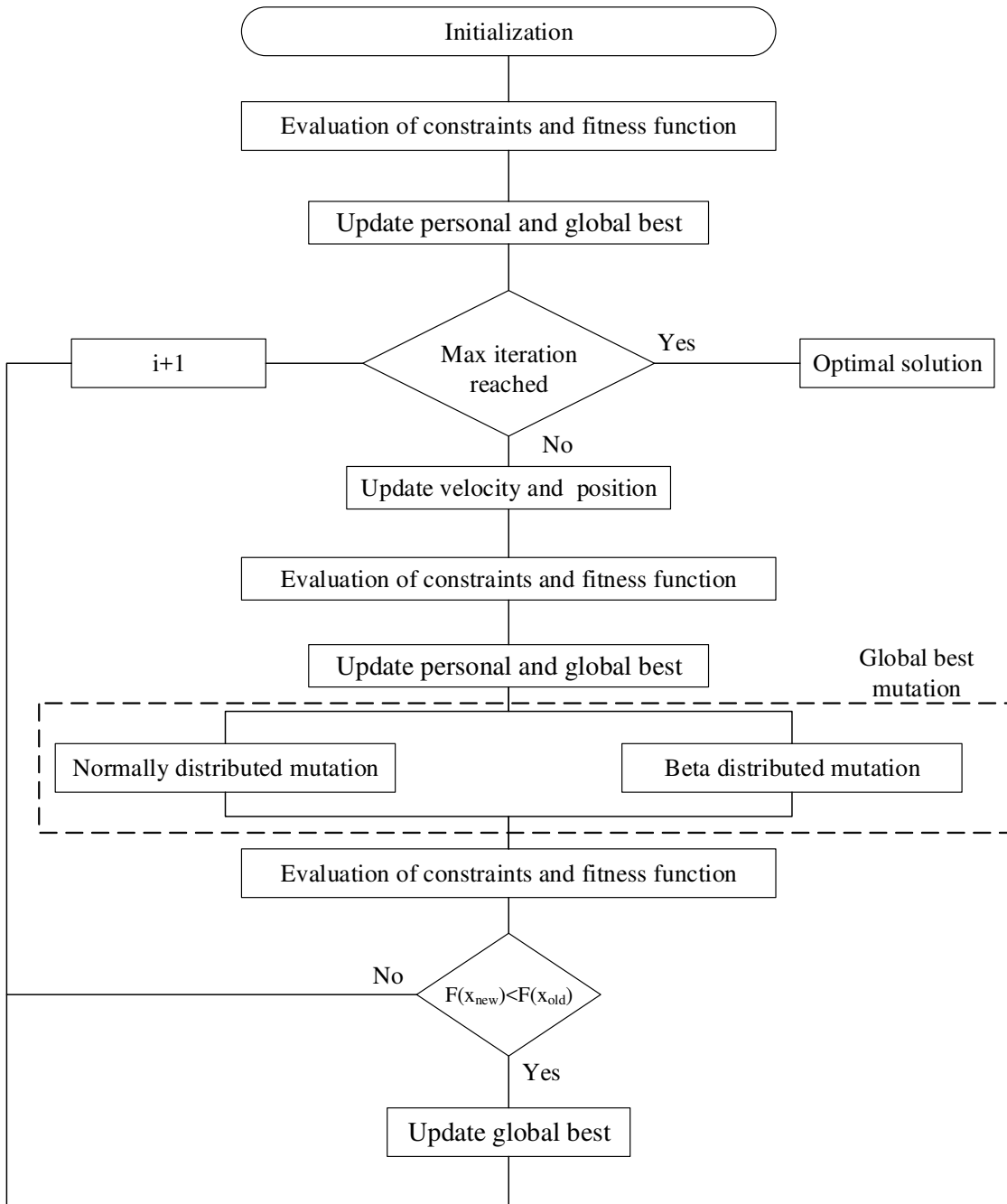


Figure 5.5: Mutation based Particle Swarm Optimization (MPSO) flow chart

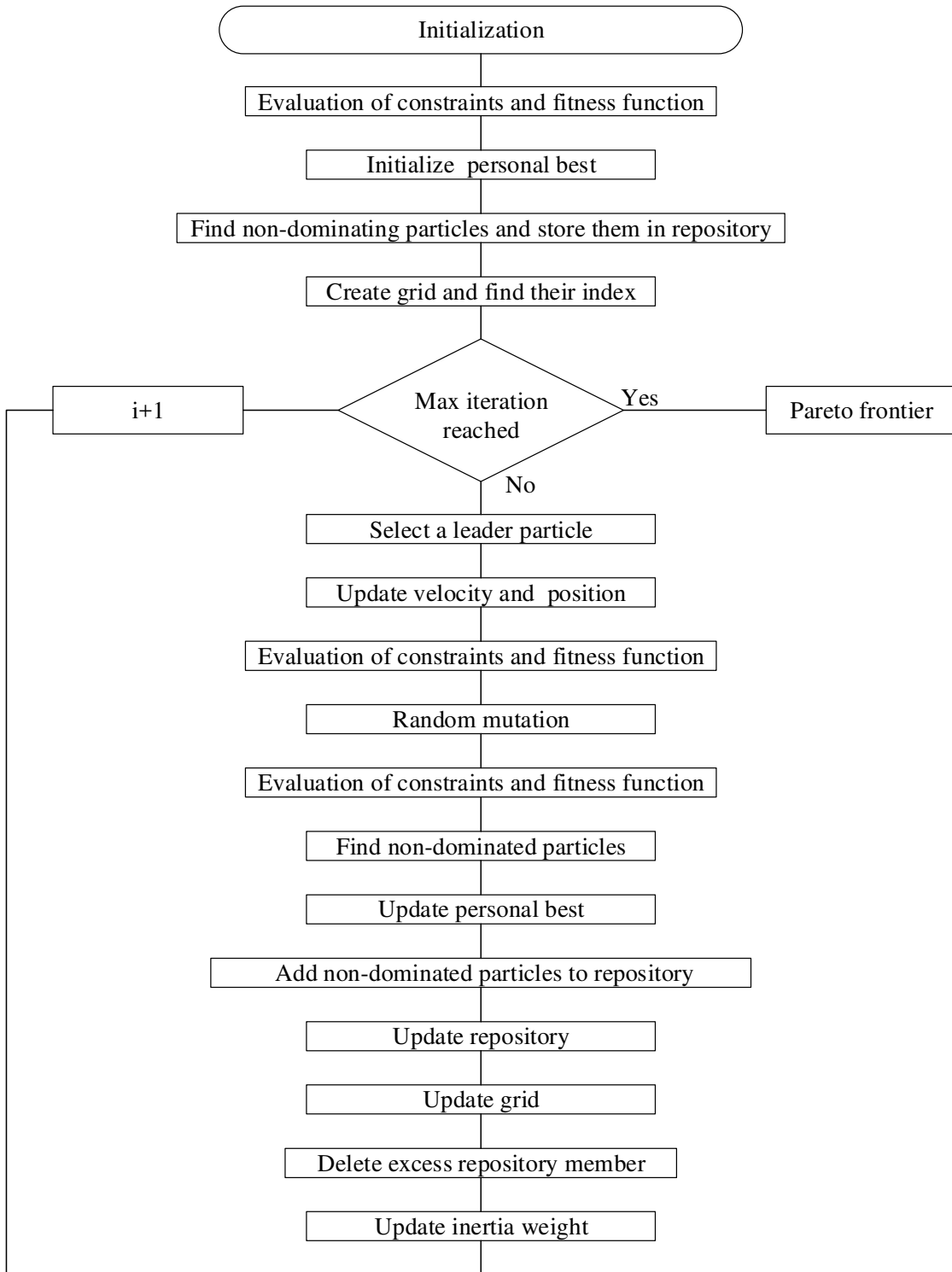


Figure 5.6: Multi-Objective Particle Swarm Optimization (MOPSO) flow chart

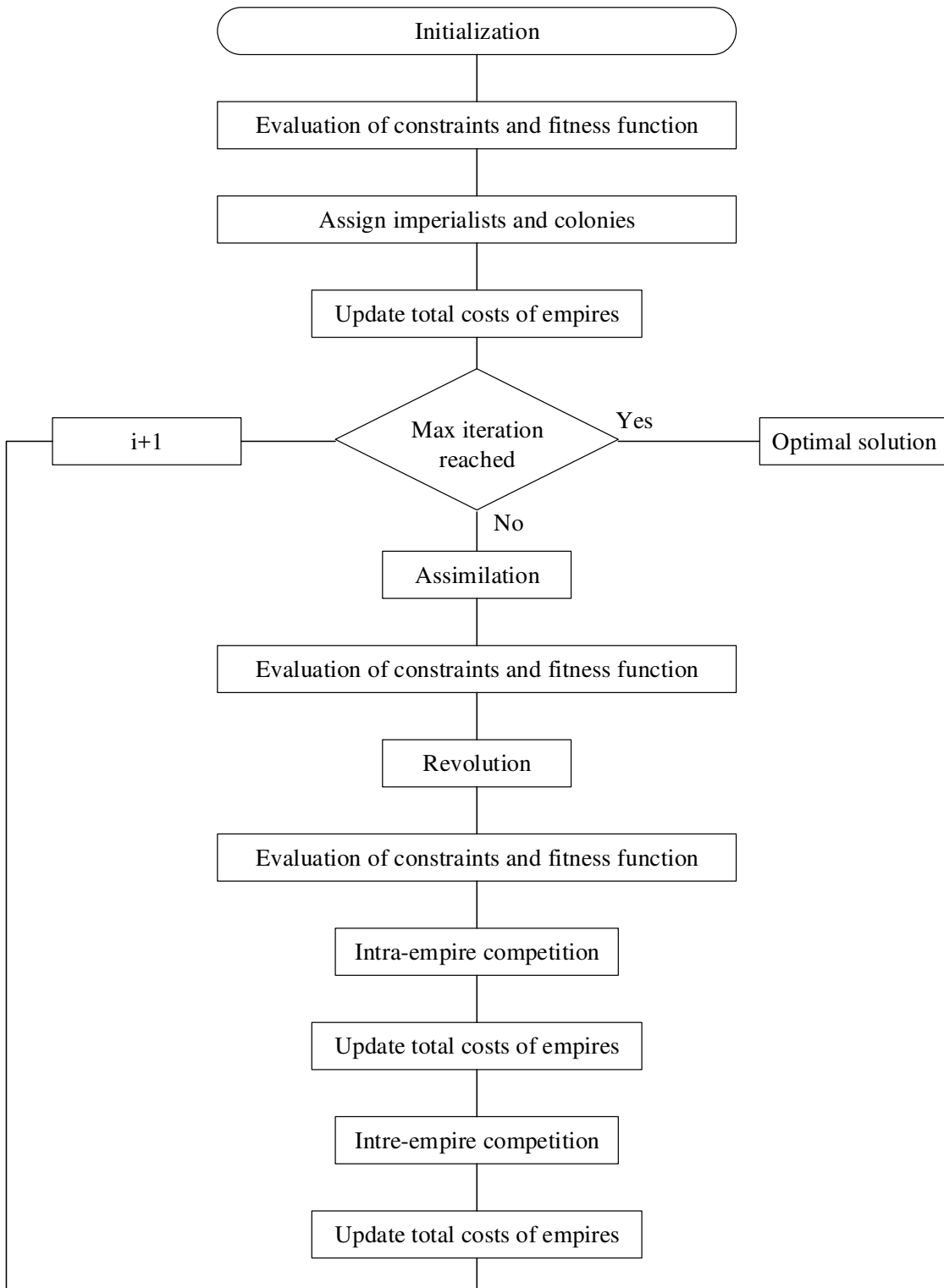


Figure 5.7: Imperialist Competitive Algorithm (ICA) flow chart

6. RESULTS AND SENSITIVITY ANALYSIS

6.1 Candidate Cities and Data Required

The test case for the proposed GEP is the Kingdom of Saudi Arabia. Yanbu city was selected based on its resource availability which is given in the following table.

Table 6.1: Data of candidate city

City	GHI daily average (kWh/m ²)	Average wind speed (m/s)	Average temperature (°C)	Load energy (TWh)	Average load demand (MW)	Peak load demand (MW)
Yanbu	6.17	6.61	28.22	2.823	322.81	547.88

Table 6.2: Load data

	Conventional (TWh/yr)	Desalination plant (Million m ³ /yr)	Industrial plant (Thousand tons/yr)
Load	2.32	39.1	500

The initial parameters for all the optimization algorithms are summarized below where N_{pop} , p_c , p_m and p_{rev} are the number of population, the crossover, mutation and revolution percentages respectively.

Table 6.3: GA parameters

	N_{pop}	I	p_c	p_m
GA	100	100	70%	30%

Table 6.4: MPSO parameters

	N_{pop}	I	p_m	c_1^i/c_1^f	c_2^i/c_2^f	w_1/w_2
PSO	100	100	10%	2/0.25	0.5/2	0.9/0.4

Table 6.5: ICA parameters

	N_{pop}	I	N_{emp}	b	p_{rev}	φ
ICA	100	100	20	2.1	30%	0.2

6.2 System Components Costs and Associated Technical Data

The cost of each component of the system is given in the following tables. Also their technical parameters are shown below.

Table 6.6: Cost parameters of the hybrid system

Component	C^{cap} (\$/kW)	$C^{o\&m}$ (\$/kW-yr)	N (Years)
PV	2014	13	20
WTG	1605	51	20
BESS	300	3	10
Inverters	80	10	10

Table 6.7: Desalination plant associated costs

Component	C^{cap} (\$/m ³)
Water tank	50
Desalination capacity	900

Table 6.8: Legacy grid associated costs

Component	$C_g^{o\&m}$ (\$/MWh-yr)	c_{oil} (\$/bbl)	π_{oil} (\$/bbl)
Legacy grid	24	9	50

Table 6.9: Technical and economical data

N_p (Years)	i (%)	f (%)	κ (kWh/m ³)	δ (kWh/ton)
25	2	2.1	5	620

Table 6.10: Technical parameters of the solar panel

Parameters	Values
P_{mpp}^{ref} (W)	200
$NOCT$ (°C)	48.1
V_{mpp}, V_{oc} (V)	40, 47.8
I_{mpp}, I_{sc} (A)	5, 5.4
$\alpha_{V_{mpp}}, \alpha_{V_{oc}}$ (%/°C)	-0.389, -0.287
$\alpha_{I_{mpp}}, \alpha_{I_{sc}}$ (%/°C)	-0.039, 0.041
η_{mpp}, d_{pv} (%)	16.1, 90
l_{pv}, w_{pv} (m)	1.24, 1
A_{pv} (m ²)	1.24

Table 6.11: Technical parameters of the wind turbine generator

Parameters	Values
P_{rated} (kW)	1000
h_{hub} (m)	70
v_{ci}, v_r, v_{co} (m/s)	3, 12.5, 25
C_p, σ	0.45, 0.194
$\eta_{gb}, \eta_{gen}, \eta_{conv}$ (%)	85, 90, 97
r_{dia} (m)	61.4

Table 6.12: Technical parameters of the inverters

Parameters	Values
P^{max} (kW)	7
V_{mpp}^{min} (V)	270
V_{dc}^{max} (V)	600
I_{dc}^{max} (A)	30
η_{inv} (%)	97

Table 6.13: Technical parameters of the battery energy storage system

Parameters	Values
DOD (%)	80
η_{bat} (%)	95
FOR	0.05

Table 6.14: Technical parameters of the legacy grid

Parameters	Values
HC (mmBTU/bbl)	5.751
HR (BTU/kWh)	10814
ϕ (Ton CO ₂ /MWh)	0.754

6.3 Test Cases for Different System Configurations

6.3.1 Desalination Plant Powered by Renewables

This type of configuration represents the basic system where the source side is a stand-alone hybrid renewable energy source. The load consists of only the water desalination plant. A comparison of the different optimization algorithms is presented in figure 6.1 and the optimal values are shown in table 6.15.

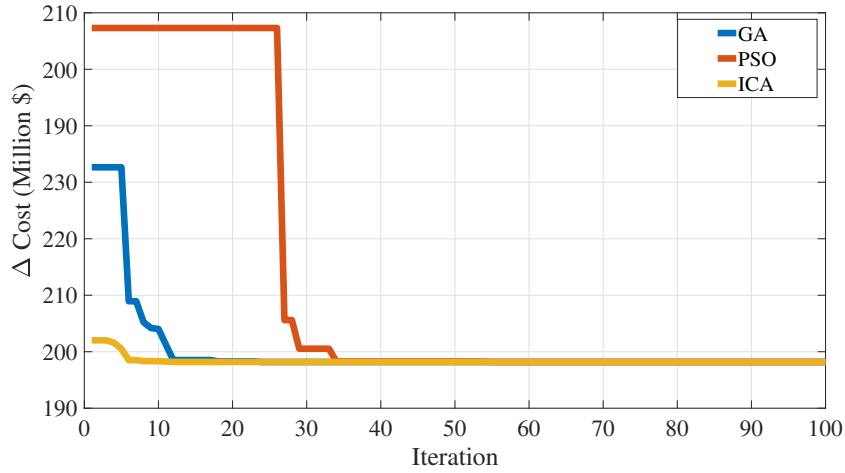


Figure 6.1: Performance of the optimization algorithms of system configuration one with the water storage tank

Table 6.15: Results of system configuration one with the water storage tank

$\Delta Cost$ (Millions \$)	x_{pv} (Units)	x_{wt} (Units)	x_{tk} (m ³)	x_d (m ³ /h)
194.1	531756	0.0	978629	17357

Table 6.16: Technical and economical metrics of system configuration one with the water storage tank

BAU_{cost} (Millions \$)	$Cost\ savings$ (Millions \$)	$Prated_{pv,farm}$ (MW)	$Prated_{wt,farm}$ (MW)	RF_{nom} (%)	RF_{true} (%)	UF (%)
199.4	5.3	106.4	0.0	100	100	100

6.3.2 Desalination Plant Powered by Renewables and Legacy Grid

Here the previous system is used, and a grid-connected hybrid renewable energy source is implemented. The source side includes the legacy grid and the hybrid renewable energy sources. The load side has only the water desalination plant. A comparison of the different optimization algorithms is presented in figure 6.2 and the optimal values are shown in table 6.17

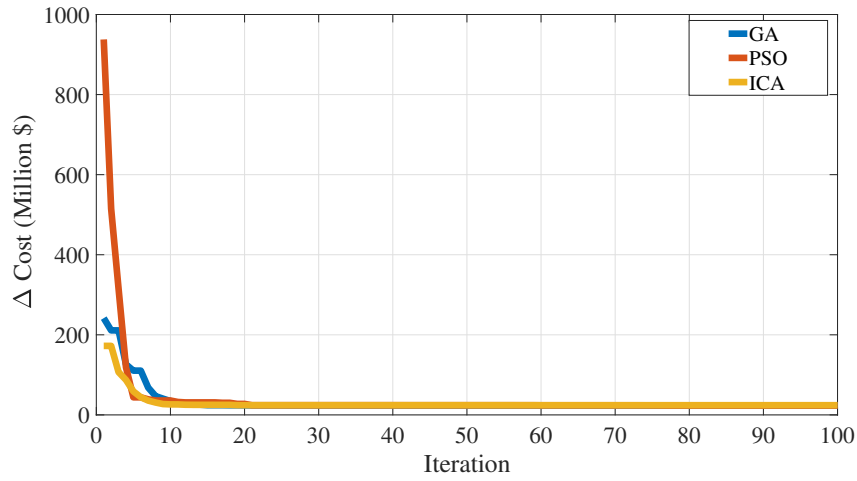


Figure 6.2: Performance of the optimization algorithms of system configuration two with the water storage tank

Table 6.17: Results of system configuration two with the water storage tank

$\Delta Cost$ (Millions \$)	x_{pv} (Units)	x_{wt} (Units)	x_{tk} (m ³)	x_d (m ³ /h)
23.5	241596	35	54848	7690

Table 6.18: Technical and economical metrics of system configuration two with the water storage tank

BAU_{cost} (Millions \$)	$Cost\ savings$ (Millions \$)	$P_{pv,farm}^{rated}$ (MW)	$P_{wt,farm}^{rated}$ (MW)	RF_{nom} (%)	RF_{true} (%)	UF (%)
199.4	175.9	48.3	35	86.61	76.08	87.84

6.3.3 Conventional Load and Desalination Plant Powered by Renewables and Legacy Grid

A conventional load (i.e., residential load) is incorporated in this system configuration. The source side includes the legacy grid and the hybrid renewable energy sources. The load side is comprised of the conventional load as well as the water desalination plant. A comparison of the different optimization algorithms is presented in figure 6.3 and the optimal values are shown in table 6.19

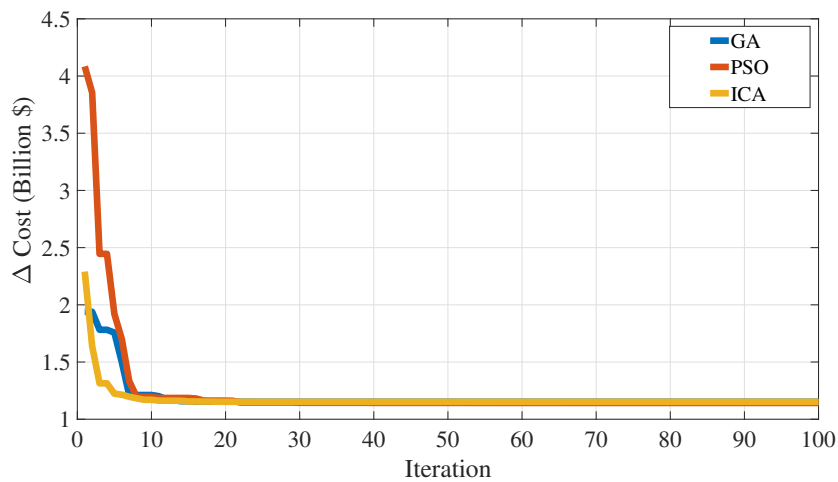


Figure 6.3: Performance of the optimization algorithms of system configuration three with the water storage tank

Table 6.19: Results of system configuration three with the water storage tank

$\Delta Cost$ (Billions \$)	x_{pv} (Units)	x_{wt} (Units)	x_{tk} (m ³)	x_d (m ³ /h)
1.15	1689555	321	36145	6999

Table 6.20: Technical and economical metrics of system configuration three with the water storage tank

BAU_{cost} (Billions \$)	$Cost\ savings$ (Billions \$)	$P_{pv,farm}^{rated}$ (MW)	$P_{wt,farm}^{rated}$ (MW)	RF_{nom} (%)	RF_{true} (%)	UF (%)
2.56	1.41	337.91	321	54.06	45.47	84.10

6.3.4 Conventional Load, Desalination Plant and Industrial Factories Powered by Renewables and Legacy Grid

This is the complete system model. A grid connected hybrid renewable energy sources on the supply side. The load in addition to the conventional and water desalination plant has an industrial load as well. A comparison of the different optimization algorithms for the configuration with a water storage is presented in figure 6.4 and the optimal values are shown in table 6.21. Similarly, A comparison of the different optimization optimization for the configuration with BESS is presented in figure 6.5 and the optimal values are shown in table 6.23. The multi-objective Pareto frontier is shown in figures 6.6 and 6.7.

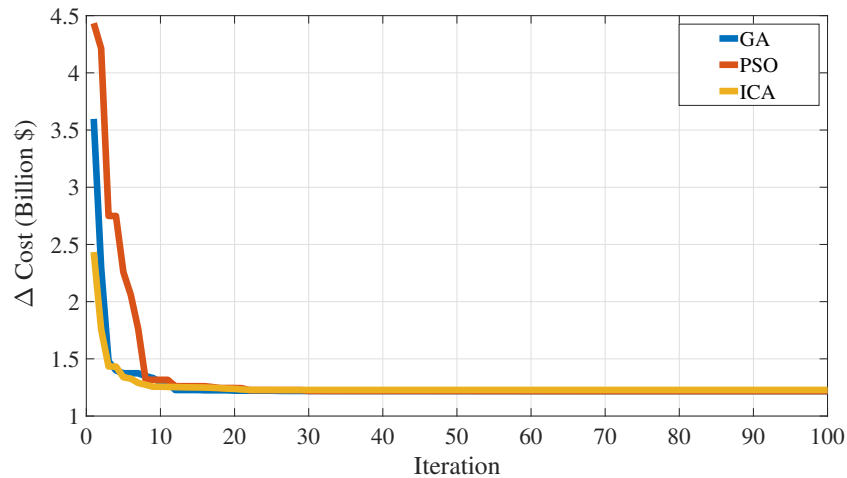


Figure 6.4: Performance of the optimization algorithms of system configuration four with the water storage tank

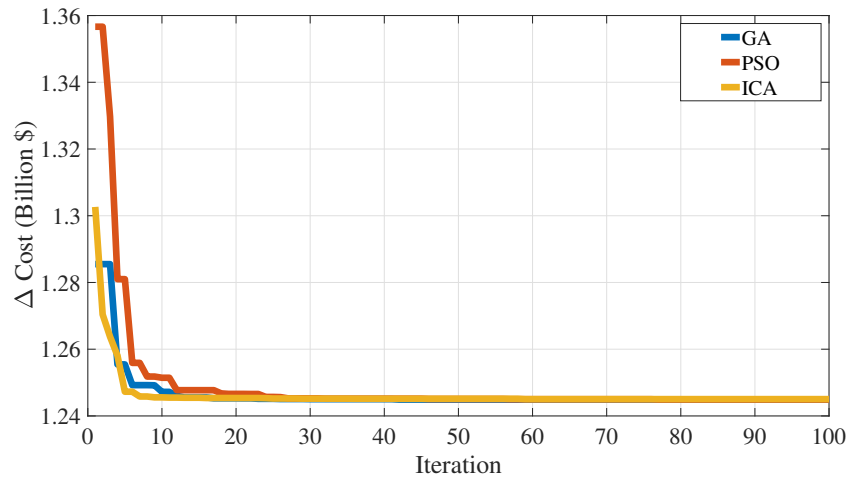


Figure 6.5: Performance of the optimization algorithms of system configuration four with the battery energy storage system

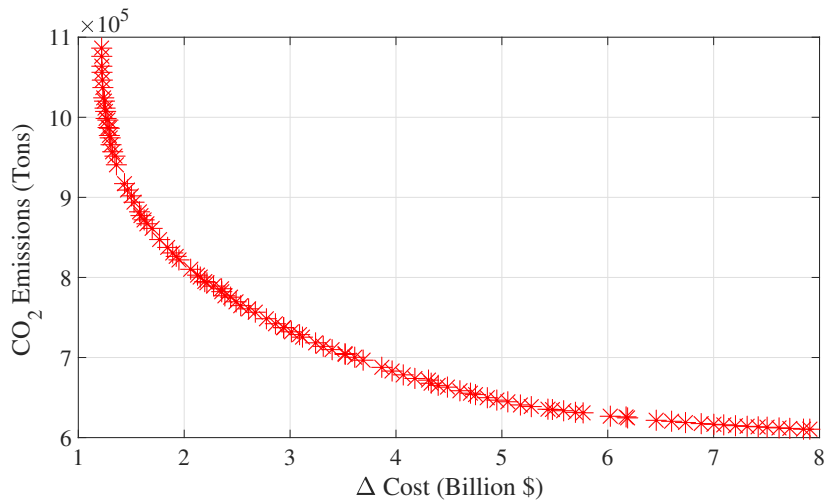


Figure 6.6: Pareto frontier of system configuration four with the water storage tank

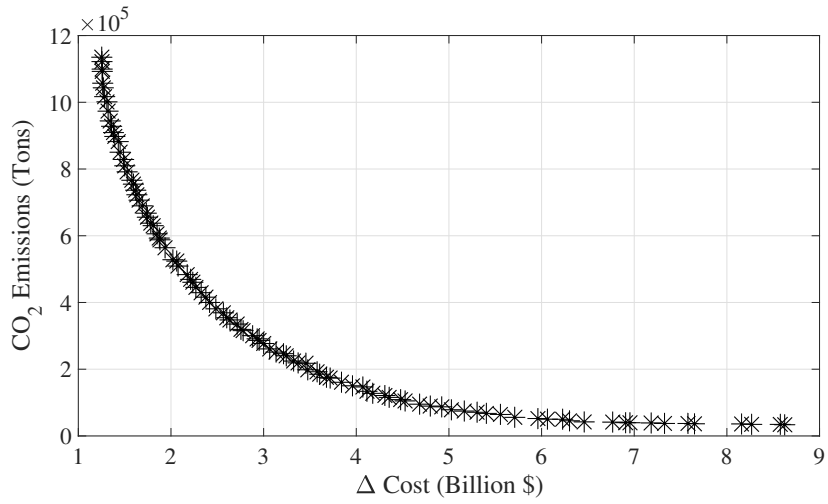


Figure 6.7: Pareto frontier of system configuration four with the battery energy storage system

Table 6.21: Results of system configuration four with the water storage tank

$\Delta Cost$ (Billions \$)	$Emissions$ (Million tons CO ₂)	x_{pv} (Units)	x_{wt} (Units)	x_{tk} (m ³)	x_d (m ³ /h)	n_{inv}^{sel} (Units)
1.22	1.08	2100578	365	185257	10994	63655

Table 6.22: Technical and economical metrics of system configuration four with the water storage tank

BAU_{cost} (Billions \$)	$Cost_{savings}$ (Billions \$)	$Cost_{inv}$ (Millions \$)	$P_{rated}_{pv,farm}$ (MW)	$P_{rated}_{wt,farm}$ (MW)	RF_{nom} (%)	RF_{true} (%)	UF (%)
2.88	1.66	189.16	420.11	365	57.06	49.02	85.91

Table 6.23: Results of system configuration four with the battery energy storage system

$\Delta Cost$ (Millions \$)	$Emissions$ (Million tons CO ₂)	x_{pv} (Units)	x_{wt} (Units)	x_{bat} (MWh)
1.24	1.12	1924635	371	96

Table 6.24: Technical and economical metrics of system configuration four with the battery energy storage system

BAU_{cost} (Billions \$)	$Cost\ savings$ (Billions \$)	$Prated_{pv,farm}$ (MW)	$Prated_{wt,farm}$ (MW)	RF_{nom} (%)	RF_{true} (%)	UF (%)
2.88	1.64	384.93	371	55.26	47.45	86.04

6.4 Sensitivity Studies

Since the system configuration with the water storage had the least cost solution, it was used to perform the rest of the studies that follow. A rigorous sensitivity/scenario analysis should accompany any planning problem. The sensitivity analysis would identify important and sensitive variables that will require careful consideration and certainty. In this section, a number of sensitivity studies are carried out to visualize the problem's behavior under different conditions where 100% represent the base case with no variation.

6.4.1 Oil Prices

One of the main variables and the key driver for this planning study is the price of oil in the global market which constitutes the opportunity cost. A different variation of the oil price is assumed, and its impact on the differential cost is shown in figure 6.8.

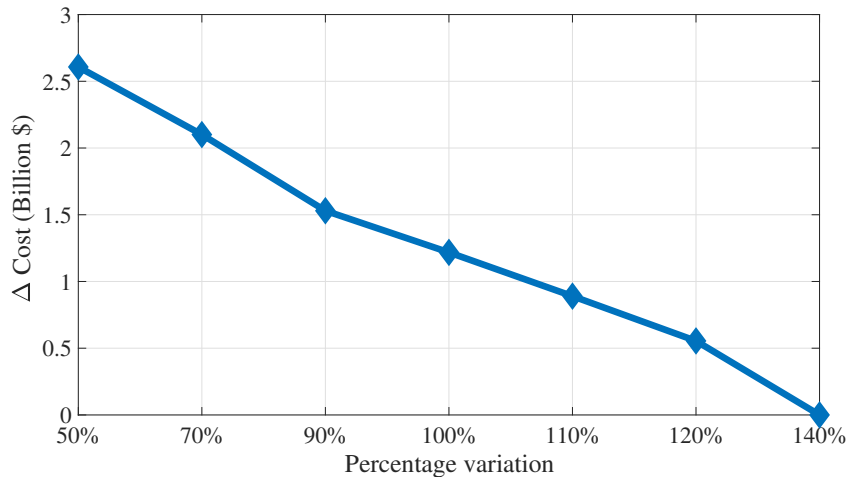


Figure 6.8: Variation of differential cost with global oil prices

6.4.2 System Components Cost

The system component cost sensitivity analysis include the variation of the capital costs of the PVs, WTGs, water storage tank and the desalination expansion. The figures 6.9 and 6.10 demonstrate the sensitivity with the differential cost.

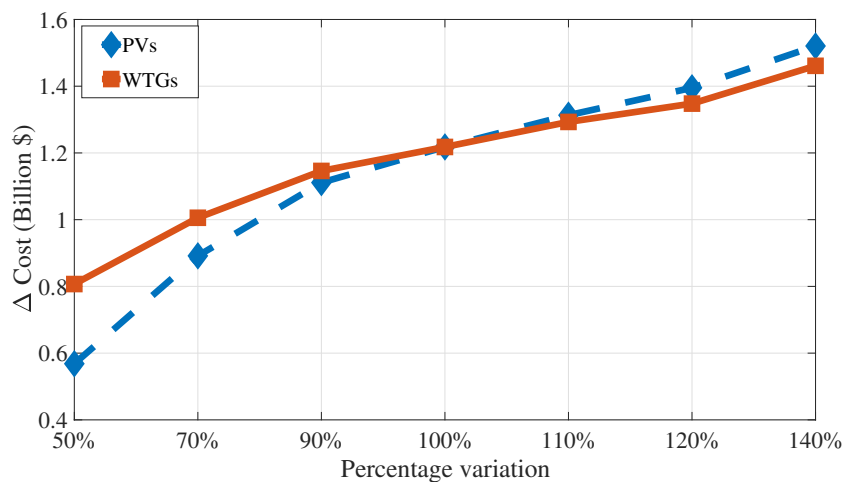


Figure 6.9: Variation of differential cost with PVs and WTGs capital cost

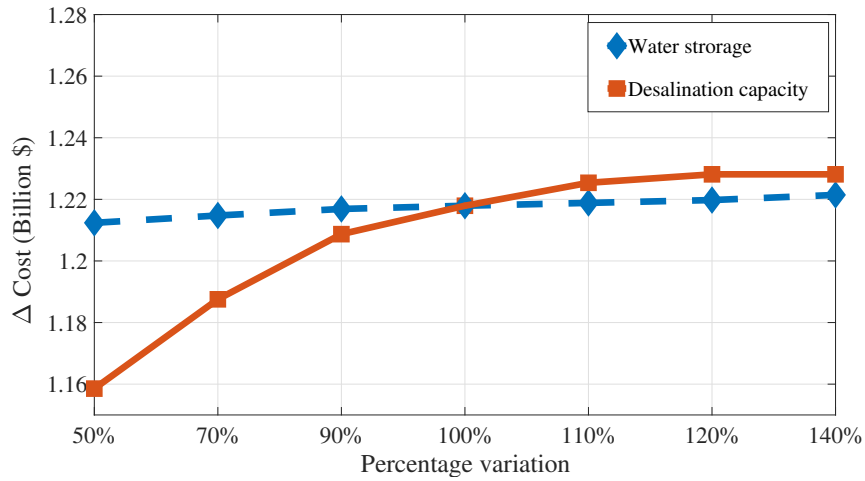


Figure 6.10: Variation of differential cost with water storage and desalination expansion capital cost

The influence of capital cost variation of the PVs and WTGs towards the differential cost share a similar behavior with higher impact attributed to the capital cost of PVs given that the system is penetrated with more PVs than WTGs in terms of units and energy production. The capital cost of the desalination capacity expansion also had an impact on the differential cost close to a linear relation in the variation range from 50-100% and its impact saturated beyond that range. A slight impact of the variation of water storage capital cost is observed on the differential cost given the initial low cost per unit volume of the storage (i.e., 50 \$/m³).

6.4.3 Solar Radiation and Wind Speed Variability

Renewable resource availability is also a critical variable that requires careful consideration which is included in the sensitivity analysis. The study demonstrates the variation of the differential cost as the renewable resources are higher or lower than expected.

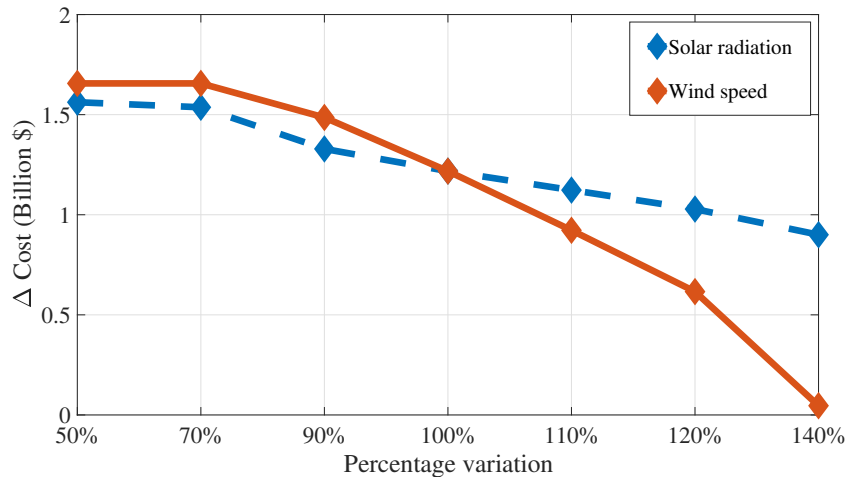


Figure 6.11: Variation of differential cost with solar radiation and wind speed

An interesting point to note here is when the wind speed is higher than the nominal value by 40%. As indicated in the figure 6.11 the differential cost is almost zero which means that the cost of the hybrid system and grid supply for the load over the project lifetime can be offset by the revenues collected from the displaced barrels of oil which otherwise would be used as grid fuel to supply the load.

6.4.4 Water Load Percentage to Total Load

In this section the impact of the water load $P_{desal,w}$ on the differential cost is analyzed and shown in figure 6.12. As previously mentioned the water load is similar to the conventional load P_{con} . However, the availability of water storage helps leverage the excess renewable energy and utilize it to produce desalinated water for times of low renewable availability. The water load in the base case configuration represents about 7% of total load. The study is performed by increasing the percentage of water load to the total load.

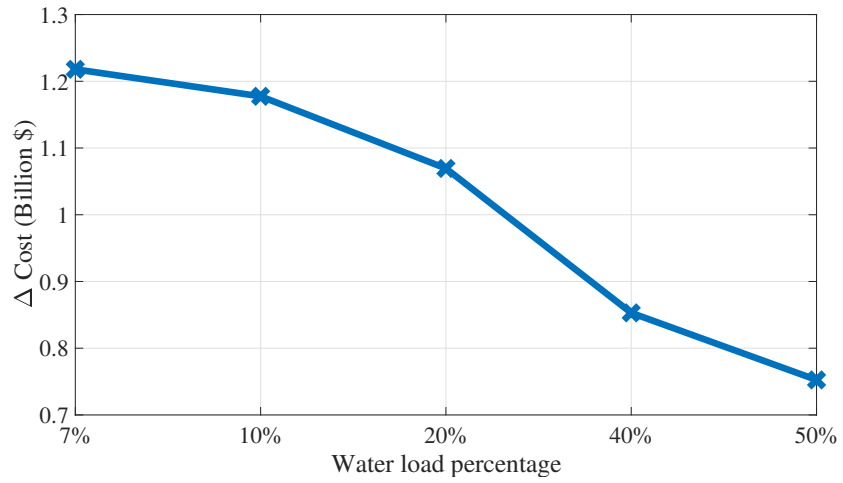


Figure 6.12: Impact of water to total load percentage on the differential cost

From the above figure it is clear that as the water load percentage increases given that it has a low cost storage element will provide a lower differential cost.

7. CONCLUSIONS AND FUTURE WORK

7.1 Conclusions

As the electric power generation planning is moving to incorporate more renewable sources, it is evident that a new and a better way of planning is required, one which is flexible and distributed. This dissertation provides a novel approach towards integrating renewable sources within the SG framework and by adopting DSM techniques without the need for conventional battery storage systems. The availability of different types of loads depending on the way they need to be served paved the way to the concept of value storage. The results show that even a country that is a net exporter of oil would financially benefit from shifting to a more sustainable energy structure. It follows that under many different scenarios of resource availability, a renewable power source penetration of the grid would be economical and environmentally beneficial. While the primary focus for DSM application in the literature was in the residential side of the load, this dissertation took an alternative route by exploring industrial loads that can provide flexibility for the electrical energy sector and divided the loads into different categories based on the ability to shift their demand.

This dissertation has explored different topics in regarding integration of renewable energy sources with the existing legacy grid which includes:

- Modeling renewable energy resources which include solar radiation and wind speed. Starting by the calculation of all the important sun and surface angles required. Different models of solar radiation striking a tilted surface were introduced. With this preliminary variables, the power output from the PVs and WTGs were calculated based on different models commonly found in the literature.

- A vital component of this dissertation is the load modeling. In which three categories of loads were introduced and categorized based on their servability. Which includes non-deferrable, semi-deferrable and fully-deferrable loads. This classification was possible with the help of storage elements and DSM techniques, namely, load shifting.
- With the given load models different configurations of power systems were explored. A GEP problem was formulated as an optimization problem with different objective functions including minimizing differential system cost as well as reducing CO₂ emissions.
- Due to the lack of data availability the uncertainty handling for the stochastic variables needed a more rigorous approach. A forecast error following a normal distribution was assumed for both the solar radiation and the wind speed. A Monte Carlo simulation was implemented to capture the stochastic behavior and their impact on the system.
- Different heuristic optimization algorithms were studied. Among the many algorithms available in the literature, the Genetic Algorithms (GA), Particle Swarm Optimization (PSO) and the Imperialist Competitive Algorithm (ICA) were selected for this dissertation. The first two algorithms are widely known and implemented in many disciplines including optimization studies for power systems. The third algorithm the (ICA), is a relatively new concept in the area of heuristic optimization and there are not many studies utilizing this algorithm in the power system planning field.
- The inverter sizing for the solar farm was also performed in this dissertation as they could have relatively high capital and operation costs which can affect the solution of

the optimization problem. Most renewable sources planning studies in the literature would ignore the cost of this component and implicitly incorporate its cost with the PVs. Here the sizing and subsequently the cost of inverters are explicitly included in the constructed optimization algorithm.

- Physical layout of the solar and wind farms are also part of the implemented software tool. The total required area for the renewable resources is calculated given the number of PVs and WTGs. This area can be used in the optimization algorithm where land area is constrained within a specific range.
- As previously mentioned, the lack of sufficient data would require an extensive sensitivity analysis which is done for many candidate variables in which their impact on the objective functions was quantified and analyzed to understand their role in the planning problem better.

7.2 Further Study

Given the cost reduction of PVs, WTGs, and energy storage systems, also the technological advancement of renewable source the future of electricity generation is shifting towards a more sustainable system. Several directions can be taken to further this dissertation which is summarized below:

- The availability of more forecast metrological data including solar radiation, wind speed as well as temperature, would increase the accuracy and validity of the results where probability distribution for the uncertain variable can be used to model these variables to have a better representation of the stochastic behavior.
- Reliability of the system components is usually incorporated in long-term power system planning. Forced outages are assumed for the conventional generators and the renewable sources. A multi-objective optimization problem can be formulated

to address both the system cost and reliability of the system. System reliability is usually quantified as the Loss of Load Expectation (LOLP) or the expected Energy not Served (ENS) metrics.

- Other renewable sources can be investigated beyond the typical hybrid PV-WTG system. An ideal candidate would be the CSP technology, as the Kingdom of Saudi Arabia enjoys an enormous availability of solar radiation. This technology has a distinctive characteristic in a sense that a thermal storage system can be incorporated into the CSP plant which would virtually allow for dispatchability of power. More rigorous studies and investigations are needed to analyze the impact of such technology.
- As the electric power sector is undergoing a deregulation phase, the implications of this transition economically and technically are significant and require careful assessment and analyzing its impact on the power system planning and operation as different independent power producers (IPP) would compete to sell their electricity. Also with the rapid increase of electric vehicles, their impact on the grid would be substantial, which opens up a considerable amount of complexity and uncertainty in the system and requires more detailed models and computation needs.
- The power system operation can be a part of the planning study where optimal power flow is performed to ensure the optimal operation of the purposed power system while adhering to operational constraints including voltage and line limits as well as minimizing system losses.
- The multi-area aspect of power system planning is an interesting approach to resolving the issues and barrier for adopting a high percentage of renewable energy sources. As the variability of the renewable resource can be mitigated given the spa-

tial and temporal differences between areas. However, this adds a completely new level of complexity.

REFERENCES

- [1] S. Krauter, *Solar Electric Power Generation - Photovoltaic Energy Systems: Modeling of Optical and Thermal Performance, Electrical Yield, Energy Balance, Effect on Reduction of Greenhouse Gas Emissions*. New York, NY: Springer Berlin Heidelberg, 2007.
- [2] A. McEvoy, T. Markvart, L. Castañer, T. Markvart, and L. Castaner, *Practical handbook of photovoltaics: fundamentals and applications*. New York, NY: Elsevier, 2003.
- [3] S. Kalogirou, *Solar Energy Engineering: Processes and Systems*. Elsevier Science, 2013.
- [4] M. Sathyajith, *Wind Energy: Fundamentals, Resource Analysis and Economics*. Netherlands: Springer Berlin Heidelberg, 2006.
- [5] E. Hau and H. von Renouard, *Wind Turbines: Fundamentals, Technologies, Application, Economics*. London, UK: Springer Berlin Heidelberg, 2013.
- [6] D. A. Baharoon, H. A. Rahman, W. Z. W. Omar, and S. O. Fadhl, “Historical development of concentrating solar power technologies to generate clean electricity efficiently – a review,” *Renewable and Sustainable Energy Reviews*, vol. 41, pp. 996–1027, 2015.
- [7] R. Baños, F. Manzano-Agugliaro, F. G. Montoya, C. Gil, A. Alcayde, and J. Gómez, “Optimization methods applied to renewable and sustainable energy: A review,” *Renewable and Sustainable Energy Reviews*, vol. 15, no. 4, pp. 1753–1766, 2011.
- [8] H. M. Taleb, “Barriers hindering the utilisation of geothermal resources in Saudi Arabia,” *Energy for Sustainable Development*, vol. 13, no. 3, pp. 183–188, 2009.

- [9] A. Chauhan and R. P. Saini, "A review on integrated renewable energy system based power generation for stand-alone applications: Configurations, storage options, sizing methodologies and control," *Renewable and Sustainable Energy Reviews*, vol. 38, pp. 99–120, 2014.
- [10] F. Rahman, S. Rehman, and M. A. Abdul-Majeed, "Overview of energy storage systems for storing electricity from renewable energy sources in saudi arabia," *Renewable and Sustainable Energy Reviews*, vol. 16, no. 1, pp. 274–283, 2012.
- [11] T. Kousksou, P. Bruel, A. Jamil, T. El Rhafiki, and Y. Zeraouli, "Energy storage: Applications and challenges," *Solar Energy Materials and Solar Cells*, vol. 120, pp. 59–80, 2014.
- [12] M. H. Nehrir, C. Wang, K. Strunz, H. Aki, R. Ramakumar, J. Bing, Z. Miao, and Z. Salameh, "A review of hybrid renewable/alternative energy systems for electric power generation: Configurations, control, and applications," *IEEE Transactions on Sustainable Energy*, vol. 2, no. 4, pp. 392–403, 2011.
- [13] J. L. Sawin, "Renewables 2017 global status report," report, Renewable Energy Policy Network, 2017. [Online]. Available: <http://www.ren21.net/gsr-2017/>.
- [14] NERC, "Accommodating high levels of variable generation," report, 2009. [Online]. Available: https://www.nerc.com/docs/pc/ivgtf/IVGTF_Outline_Report_040708.pdf.
- [15] L. Bird, M. Milligan, and D. Lew, "Integrating variable renewable energy: challenges and solutions," report, 2013. [Online]. Available: <https://www.nrel.gov/docs/fy13osti/60451.pdf>.
- [16] A. Gastli and J. S. M. Armendáriz, "Challenges facing grid integration of renewable energy in the gcc region," *Gulf Research Centre, GRC Gulf Papers*, pp. 4–15, 2013.

- [17] “General Authority for Statistics - Statistical Yearbook of 2016.” Web, August 2017. [Online]. Available: <https://www.stats.gov.sa/en/193>.
- [18] General Authority for Statistics, “Oil exports,” report, 2016. [Online]. Available: <https://www.stats.gov.sa/en/node/10127>.
- [19] “The World Fact Book.” Web, August 2017. [Online]. Available: <https://www.cia.gov/library/publications/the-world-factbook/geos/sa.html>.
- [20] Saudi Aramco, “Saudi aramco annual review 2016,” report, 2016. [Online]. Available: <http://www.saudiaramco.com/content/dam/Publications/annual-review/2016/English-PDFs/2016-AnnualReview-full-EN.pdf>.
- [21] Saudi Electricity Company, “Annual report 2016,” report, 2016. [Online]. Available: <https://www.se.com.sa/en-us/Pages/AnnualReports.aspx>.
- [22] E. Authority and C. Regulatory, “Activities and achievements of the authority in 2014,” report, 2014. [Online]. Available: <http://www.ecra.gov.sa/en-us/MediaCenter/doclib2/Pages/SubCategoryList.aspx?categoryID=4>.
- [23] Saudi Electricity Company, “Annual report 2014,” report, 2014. [Online]. Available: <https://www.se.com.sa/en-us/Pages/AnnualReports.aspx>.
- [24] “Historical Data-Electricity and Cogeneration Regulatory Authority.” Web, August 2017. [Online]. Available: <http://www.ecra.gov.sa/en-us/DataAndStatistics/NationalRecord/HistoricalData/pages/Home.aspx>.
- [25] “Desalination by the Numbers.” Web, August 2017. [Online]. Available: <http://idadesal.org/desalination-101/desalination-by-the-numbers/>.
- [26] Saline Water Conversion Corporation, “Annual report,” report, 2014. [Online]. Available: <http://www.swcc.gov.sa/english/MediaCenter/SWCCPublications/Pages/default.aspx>.

- [27] T. Mezher, H. Fath, Z. Abbas, and A. Khaled, "Techno-economic assessment and environmental impacts of desalination technologies," *Desalination*, vol. 266, no. 1–3, pp. 263–273, 2011.
- [28] B. Valdez Salas and M. Schorr Wiener, "Desalination, trends and technologies," *Desalination and Water Treatment*, vol. 42, no. 1-3, pp. 347–348, 2012.
- [29] A. Al-Karaghoul and L. L. Kazmerski, "Energy consumption and water production cost of conventional and renewable-energy-powered desalination processes," *Renewable and Sustainable Energy Reviews*, vol. 24, pp. 343–356, 2013.
- [30] M. A. Eltawil, Z. Zhengming, and L. Yuan, "A review of renewable energy technologies integrated with desalination systems," *Renewable and Sustainable Energy Reviews*, vol. 13, no. 9, pp. 2245–2262, 2009.
- [31] S. M. H. Saleh Hussein Alawaji, "Role of solar energy research in transferring of technology to saudi arabia," *Energy Sources*, vol. 21, no. 10, pp. 923–934, 1999.
- [32] A. Hepbasli and Z. Alsuhaibani, "A key review on present status and future directions of solar energy studies and applications in saudi arabia," *Renewable and Sustainable Energy Reviews*, vol. 15, no. 9, pp. 5021–5050, 2011.
- [33] H. Steeb, W. Seeger, and H. Aba Oud, "Hysolar: an overview on the german-saudi arabian programme on solar hydrogen," *International Journal of Hydrogen Energy*, vol. 19, no. 8, pp. 683–686, 1994.
- [34] S. H. Alawaji, "Evaluation of solar energy research and its applications in saudi arabia — 20 years of experience," *Renewable and Sustainable Energy Reviews*, vol. 5, no. 1, pp. 59–77, 2001.
- [35] C. M. A. Yip, U. B. Gunturu, and G. L. Stenchikov, "Wind resource characterization in the arabian peninsula," *Applied Energy*, vol. 164, pp. 826–836, 2016.

- [36] S. Sharples and H. Radhi, "Assessing the technical and economic performance of building integrated photovoltaics and their value to the gcc society," *Renewable Energy*, vol. 55, pp. 150–159, 2013.
- [37] L. M. Al-Hadhrami, "Performance evaluation of small wind turbines for off grid applications in saudi arabia," *Energy Conversion and Management*, vol. 81, pp. 19–29, 2014.
- [38] S. Rehman, M. A. Bader, and S. A. Al-Moallem, "Cost of solar energy generated using pv panels," *Renewable and Sustainable Energy Reviews*, vol. 11, no. 8, pp. 1843–1857, 2007.
- [39] A. M. Al-Nasser, "Performance and economics of a solar thermal power generation plant in jubail, saudi arabia: Parabolic trough collector," in *2010 IEEE International Energy Conference*, pp. 752–757.
- [40] M. J. Adinoyi and S. A. M. Said, "Effect of dust accumulation on the power outputs of solar photovoltaic modules," *Renewable Energy*, vol. 60, pp. 633–636, 2013.
- [41] T. Sarver, A. Al-Qaraghuli, and L. L. Kazmerski, "A comprehensive review of the impact of dust on the use of solar energy: History, investigations, results, literature, and mitigation approaches," *Renewable and Sustainable Energy Reviews*, vol. 22, pp. 698–733, 2013.
- [42] H. El Khashab and M. Al Ghamedi, "Comparison between hybrid renewable energy systems in saudi arabia," *Journal of Electrical Systems and Information Technology*, vol. 2, no. 1, pp. 111–119, 2015.
- [43] M. A. Elhadidy and S. M. Shaahid, "Parametric study of hybrid (wind + solar + diesel) power generating systems," *Renewable Energy*, vol. 21, no. 2, pp. 129–139, 2000.

- [44] S. Rehman, T. O. Halawani, and M. Mohandes, "Wind power cost assessment at twenty locations in the kingdom of saudi arabia," *Renewable Energy*, vol. 28, no. 4, pp. 573–583, 2003.
- [45] H. Al Garni, A. Kassem, A. Awasthi, D. Komljenovic, and K. Al-Haddad, "A multicriteria decision making approach for evaluating renewable power generation sources in saudi arabia," *Sustainable Energy Technologies and Assessments*, vol. 16, pp. 137–150, 2016.
- [46] A. M. Eltamaly, M. A. Mohamed, and A. I. Alolah, "A novel smart grid theory for optimal sizing of hybrid renewable energy systems," *Solar Energy*, vol. 124, pp. 26–38, 2016.
- [47] "Energy Sustainability for Future Generations-King Abdullah City for Atomic and Renewable Energy." Web, August 2017. [Online]. Available: <https://www.kacare.gov.sa/en/FutureEnergy/Pages/vision.aspx>.
- [48] Electricity and Cogeneration Regulatory Authority, "Bringing demand-side management to the kingdom of saudi arabia," report, 2011. [Online]. Available: <http://www.ecra.gov.sa/en-us/ECRAStudies/Pages/stdy3.aspx>.
- [49] E. Zell, S. Gasim, S. Wilcox, S. Katamoura, T. Stoffel, H. Shibli, J. Engel-Cox, and M. A. Subie, "Assessment of solar radiation resources in saudi arabia," *Solar Energy*, vol. 119, pp. 422–438, 2015.
- [50] Z. Aljarboua, "The national energy strategy for saudi arabia," *World Academy of Science, Engineering and Technology*, vol. 57, pp. 501–510, 2009.
- [51] S. M. Shaahid, L. M. Al-Hadhrami, and M. K. Rahman, "Economic feasibility of development of wind power plants in coastal locations of saudi arabia – a review," *Renewable and Sustainable Energy Reviews*, vol. 19, pp. 589–597, 2013.

- [52] N. M. Al-Abbadi, "Wind energy resource assessment for five locations in Saudi Arabia," *Renewable Energy*, vol. 30, no. 10, pp. 1489–1499, 2005.
- [53] A. M. Radhwan, "Wind energy applications in remote areas of Saudi Arabia," *International Journal of Ambient Energy*, vol. 15, no. 3, pp. 123–130, 1994.
- [54] Council of Economic and Development Affairs, "Vision 2030," report, 2016. [Online]. Available: <http://vision2030.gov.sa/en>.
- [55] Council of Economic and Development Affairs, "National transformation program 2020," report, 2016. [Online]. Available: <http://vision2030.gov.sa/en/ntp>.
- [56] M. L. Tuballa and M. L. Abundo, "A review of the development of smart grid technologies," *Renewable and Sustainable Energy Reviews*, vol. 59, pp. 710–725, 2016.
- [57] X. Fang, S. Misra, G. Xue, and D. Yang, "Smart grid—the new and improved power grid: A survey," *IEEE Communications Surveys & Tutorials*, vol. 14, no. 4, pp. 944–980, 2012.
- [58] G. Strbac, "Demand side management: Benefits and challenges," *Energy Policy*, vol. 36, no. 12, pp. 4419–4426, 2008.
- [59] D. Myers, *Solar Radiation: Practical Modeling for Renewable Energy Applications*. Boca Raton, FL: CRC Press, 2016.
- [60] J. J. Michalsky, "The astronomical almanac's algorithm for approximate solar position (1950–2050)," *Solar Energy*, vol. 40, no. 3, pp. 227–235, 1988.
- [61] P. Gilman, "Sam photovoltaic model technical reference," report, National Renewable Energy Laboratory (NREL), 2015. [Online]. Available: <https://www.nrel.gov/docs/fy15osti/64102.pdf>.
- [62] F. Vignola, J. Michalsky, and T. Stoffel, *Solar and Infrared Radiation Measurements*. Boca Raton, FL: Taylor & Francis, 2012.

- [63] J. Duffie and W. Beckman, *Solar Engineering of Thermal Processes*. Hoboken, NJ: Wiley, 2013.
- [64] D. G. Erbs, S. A. Klein, and J. A. Duffie, "Estimation of the diffuse radiation fraction for hourly, daily and monthly-average global radiation," *Solar Energy*, vol. 28, no. 4, pp. 293–302, 1982.
- [65] B. Y. Liu and R. C. Jordan, "The long-term average performance of flat-plate solar-energy collectors: with design data for the us, its outlying possessions and canada," *Solar Energy*, vol. 7, no. 2, pp. 53–74, 1963.
- [66] T. Khatib, A. Mohamed, and K. Sopian, "A review of solar energy modeling techniques," *Renewable and Sustainable Energy Reviews*, vol. 16, no. 5, pp. 2864–2869, 2012.
- [67] M. Benghanem, "Optimization of tilt angle for solar panel: Case study for madinah, saudi arabia," *Applied Energy*, vol. 88, no. 4, pp. 1427–1433, 2011.
- [68] A. Q. Jakhrani, A.-K. Othman, A. R. Rigit, S. R. Samo, and S. Kamboh, "Estimation of incident solar radiation on tilted surface by different empirical models," *International Journal of Scientific and Research Publications*, vol. 2, no. 12, pp. 1–6, 2012.
- [69] R. Perez, R. Seals, P. Ineichen, R. Stewart, and D. Menicucci, "A new simplified version of the perez diffuse irradiance model for tilted surfaces," *Solar Energy*, vol. 39, no. 3, pp. 221–231, 1987.
- [70] M. G. Villalva, J. R. Gazoli, and E. R. Filho, "Comprehensive approach to modeling and simulation of photovoltaic arrays," *IEEE Transactions on Power Electronics*, vol. 24, no. 5, pp. 1198–1208, 2009.

- [71] R. Messenger and A. Abtahi, *Photovoltaic Systems Engineering, Third Edition*. Boca Raton, FL: CRC Press, 2010.
- [72] R. Chedid, H. Akiki, and S. Rahman, "A decision support technique for the design of hybrid solar-wind power systems," *IEEE Transactions on Energy Conversion*, vol. 13, no. 1, pp. 76–83, 1998.
- [73] L. Wang and C. Singh, "Multicriteria design of hybrid power generation systems based on a modified particle swarm optimization algorithm," *IEEE Transactions on Energy Conversion*, vol. 24, no. 1, pp. 163–172, 2009.
- [74] Y. A. Katsigiannis, P. S. Georgilakis, and E. S. Karapidakis, "Hybrid simulated annealing-tabu search method for optimal sizing of autonomous power systems with renewables," *IEEE Transactions on Sustainable Energy*, vol. 3, no. 3, pp. 330–338, 2012.
- [75] M. Thomson and D. G. Infield, "Impact of widespread photovoltaics generation on distribution systems," *IET Renewable Power Generation*, vol. 1, no. 1, pp. 33–40, 2007.
- [76] Y. Yanhong, P. Wei, and Q. Zhiping, "Optimal sizing of renewable energy and chp hybrid energy microgrid system," in *IEEE PES Innovative Smart Grid Technologies*, pp. 1–5.
- [77] D. L. King, J. A. Kratochvil, and W. E. Boyson, "Temperature coefficients for pv modules and arrays: measurement methods, difficulties, and results," in *Photovoltaic Specialists Conference, 1997., Conference Record of the Twenty-Sixth IEEE*, pp. 1183–1186.
- [78] Y. M. Atwa, E. F. El-Saadany, M. M. A. Salama, R. Seethapathy, M. Assam, and S. Conti, "Adequacy evaluation of distribution system including wind/solar dg dur-

- ing different modes of operation,” *IEEE Transactions on Power Systems*, vol. 26, no. 4, pp. 1945–1952, 2011.
- [79] A. Kornelakis and E. Koutroulis, “Methodology for the design optimisation and the economic analysis of grid-connected photovoltaic systems,” *IET Renewable Power Generation*, vol. 3, no. 4, pp. 476–492, 2009.
- [80] M. Alsayed, M. Cacciato, G. Scarcella, and G. Scelba, “Multicriteria optimal sizing of photovoltaic-wind turbine grid connected systems,” *IEEE Transactions on Energy Conversion*, vol. 28, no. 2, pp. 370–379, 2013.
- [81] Y. M. Atwa, E. F. El-Saadany, M. M. A. Salama, and R. Seethapathy, “Optimal renewable resources mix for distribution system energy loss minimization,” *IEEE Transactions on Power Systems*, vol. 25, no. 1, pp. 360–370, 2010.
- [82] Y. M. Atwa and E. F. El-Saadany, “Probabilistic approach for optimal allocation of wind-based distributed generation in distribution systems,” *IET Renewable Power Generation*, vol. 5, no. 1, pp. 79–88, 2011.
- [83] W. Li, *Reliability Assessment of Electric Power Systems Using Monte Carlo Methods*. New York, NY: Springer US, 1994.
- [84] H. Seifi and M. S. Sepasian, *Electric power system planning: issues, algorithms and solutions*. New York, NY: Springer Science & Business Media, 2011.
- [85] C. Wadhwa, *Generation, Distribution and Utilization of Electrical Energy*. New Delhi, India: Wiley Eastern, 1989.
- [86] J. Aghaei and M.-I. Alizadeh, “Demand response in smart electricity grids equipped with renewable energy sources: A review,” *Renewable and Sustainable Energy Reviews*, vol. 18, pp. 64–72, 2013.

- [87] P. Siano, "Demand response and smart grids—a survey," *Renewable and Sustainable Energy Reviews*, vol. 30, pp. 461–478, 2014.
- [88] M. M. Eissa, "Demand side management program evaluation based on industrial and commercial field data," *Energy Policy*, vol. 39, no. 10, pp. 5961–5969, 2011.
- [89] International Renewable Energy Agency, "Smart grids and renewables—a guide for effective deployment," report, 2013. [Online]. Available: <http://www.irena.org/Publications/Publications.aspx?mnu=cat\&PriMenuID=36\&CatID=141\&type=all>.
- [90] L. Gelazanskas and K. A. A. Gamage, "Demand side management in smart grid: A review and proposals for future direction," *Sustainable Cities and Society*, vol. 11, pp. 22–30, 2014.
- [91] S. Saini, "Conservation v. generation," *Refocus*, vol. 5, no. 3, pp. 52–54, 2004.
- [92] J. Ekanayake, N. Jenkins, K. Liyanage, J. Wu, and A. Yokoyama, *Smart Grid: Technology and Applications*. New Delhi, India: Wiley, 2012.
- [93] J. Momoh, *Smart Grid: Fundamentals of Design and Analysis*. Hoboken, NJ: Wiley, 2012.
- [94] T. Logenthiran, D. Srinivasan, and T. Z. Shun, "Demand side management in smart grid using heuristic optimization," *IEEE Transactions on Smart Grid*, vol. 3, no. 3, pp. 1244–1252, 2012.
- [95] P. Palensky and D. Dietrich, "Demand side management: Demand response, intelligent energy systems, and smart loads," *IEEE Transactions on Industrial Informatics*, vol. 7, no. 3, pp. 381–388, 2011.
- [96] C. W. Gellings, "The concept of demand-side management for electric utilities," *Proceedings of the IEEE*, vol. 73, no. 10, pp. 1468–1470, 1985.

- [97] K. Nolde and M. Morari, “Electrical load tracking scheduling of a steel plant,” *Computers & Chemical Engineering*, vol. 34, no. 11, pp. 1899–1903, 2010.
- [98] P. Jong-Bae, P. Young-Moon, W. Jong-Ryul, and K. Y. Lee, “An improved genetic algorithm for generation expansion planning,” *IEEE Transactions on Power Systems*, vol. 15, no. 3, pp. 916–922, 2000.
- [99] J. L. C. Meza, M. B. Yildirim, and A. S. M. Masud, “A model for the multiperiod multiobjective power generation expansion problem,” *IEEE Transactions on Power Systems*, vol. 22, no. 2, pp. 871–878, 2007.
- [100] V. Oree, S. Z. Sayed Hassen, and P. J. Fleming, “Generation expansion planning optimisation with renewable energy integration: A review,” *Renewable and Sustainable Energy Reviews*, vol. 69, pp. 790–803, 2017.
- [101] F. Bouffard and F. D. Galiana, “Stochastic security for operations planning with significant wind power generation,” in *2008 IEEE Power and Energy Society General Meeting - Conversion and Delivery of Electrical Energy in the 21st Century*, pp. 1–11.
- [102] G. Giannakoudis, A. I. Papadopoulos, P. Seferlis, and S. Voutetakis, “Optimum design and operation under uncertainty of power systems using renewable energy sources and hydrogen storage,” *International Journal of Hydrogen Energy*, vol. 35, no. 3, pp. 872–891, 2010.
- [103] Y. Xu, Q. Hu, and F. Li, “Probabilistic model of payment cost minimization considering wind power and its uncertainty,” *IEEE Transactions on Sustainable Energy*, vol. 4, no. 3, pp. 716–724, 2013.
- [104] U. Akram, M. Khalid, and S. Shafiq, “Optimal sizing of a wind/solar/battery hybrid grid-connected microgrid system,” *IET Renewable Power Generation*, vol. 12,

- no. 1, pp. 72–80, 2018.
- [105] T. Kerekes, E. Koutroulis, S. D. x00E, ra, R. Teodorescu, and M. Katsanevakis, “An optimization method for designing large pv plants,” *IEEE Journal of Photovoltaics*, vol. 3, no. 2, pp. 814–822, 2013.
- [106] T. Khatib, I. A. Ibrahim, and A. Mohamed, “A review on sizing methodologies of photovoltaic array and storage battery in a standalone photovoltaic system,” *Energy Conversion and Management*, vol. 120, pp. 430–448, 2016.
- [107] J. Meyers and C. Meneveau, “Optimal turbine spacing in fully developed wind farm boundary layers,” *Wind Energy*, vol. 15, no. 2, pp. 305–317, 2012.
- [108] S. Boyd and L. Vandenberghe, *Convex Optimization*. Cambridge, UK: Cambridge University Press, 2004.
- [109] S. Singh and S. C. Kaushik, “Optimal sizing of grid integrated hybrid pv-biomass energy system using artificial bee colony algorithm,” *IET Renewable Power Generation*, vol. 10, no. 5, pp. 642–650, 2016.
- [110] S. M. Hakimi and S. M. Moghaddas-Tafreshi, “Optimal sizing of a stand-alone hybrid power system via particle swarm optimization for kahnouj area in south-east of iran,” *Renewable Energy*, vol. 34, no. 7, pp. 1855–1862, 2009.
- [111] A. Khare and S. Rangnekar, “Optimal sizing of a grid integrated solar photovoltaic system,” *IET Renewable Power Generation*, vol. 8, no. 1, pp. 67–75, 2014.
- [112] A. Hassan, M. Saadawi, M. Kandil, and M. Saeed, “Modified particle swarm optimisation technique for optimal design of small renewable energy system supplying a specific load at mansoura university,” *IET Renewable Power Generation*, vol. 9, no. 5, pp. 474–483, 2015.

- [113] H. T. Firmo and L. F. L. Legey, "Generation expansion planning: an iterative genetic algorithm approach," *IEEE Transactions on Power Systems*, vol. 17, no. 3, pp. 901–906, 2002.
- [114] T. Senjyu, D. Hayashi, N. Urasaki, and T. Funabashi, "Optimum configuration for renewable generating systems in residence using genetic algorithm," *IEEE Transactions on Energy Conversion*, vol. 21, no. 2, pp. 459–466, 2006.
- [115] H. Yang, Z. Wei, and L. Chengzhi, "Optimal design and techno-economic analysis of a hybrid solar-wind power generation system," *Applied Energy*, vol. 86, no. 2, pp. 163–169, 2009.
- [116] A. Gonzalez, J.-R. Riba, A. Rius, and R. Puig, "Optimal sizing of a hybrid grid-connected photovoltaic and wind power system," *Applied Energy*, vol. 154, pp. 752–762, 2015.
- [117] G. Merei, C. Berger, and D. U. Sauer, "Optimization of an off-grid hybrid pv-wind-diesel system with different battery technologies using genetic algorithm," *Solar Energy*, vol. 97, pp. 460–473, 2013.
- [118] E. Hajipour, M. Bozorg, and M. Fotuhi-Firuzabad, "Stochastic capacity expansion planning of remote microgrids with wind farms and energy storage," *IEEE Transactions on Sustainable Energy*, vol. 6, no. 2, pp. 491–498, 2015.
- [119] R. Atia and N. Yamada, "Sizing and analysis of renewable energy and battery systems in residential microgrids," *IEEE Transactions on Smart Grid*, vol. 7, no. 3, pp. 1204–1213, 2016.
- [120] R. Chedid and S. Rahman, "Unit sizing and control of hybrid wind-solar power systems," *IEEE Transactions on Energy Conversion*, vol. 12, no. 1, pp. 79–85, 1997.

- [121] M. Kolhe, “Techno-economic optimum sizing of a stand-alone solar photovoltaic system,” *IEEE Transactions on Energy Conversion*, vol. 24, no. 2, pp. 511–519, 2009.
- [122] E. I. Vrettos and S. A. Papathanassiou, “Operating policy and optimal sizing of a high penetration res-bess system for small isolated grids,” *IEEE Transactions on Energy Conversion*, vol. 26, no. 3, pp. 744–756, 2011.
- [123] L. Wang and C. Singh, “Environmental/economic power dispatch using a fuzzified multi-objective particle swarm optimization algorithm,” *Electric Power Systems Research*, vol. 77, no. 12, pp. 1654–1664, 2007.
- [124] Y. A. Katsigiannis, P. S. Georgilakis, and E. S. Karapidakis, “Multiobjective genetic algorithm solution to the optimum economic and environmental performance problem of small autonomous hybrid power systems with renewables,” *IET Renewable Power Generation*, vol. 4, no. 5, pp. 404–419, 2010.
- [125] C. Unsihuay-Vila, J. W. Marangon-Lima, A. C. Zambroni de Souza, and I. J. Perez-Arriaga, “Multistage expansion planning of generation and interconnections with sustainable energy development criteria: A multiobjective model,” *International Journal of Electrical Power & Energy Systems*, vol. 33, no. 2, pp. 258–270, 2011.
- [126] P. K. Roy and S. Bhui, “Multi-objective quasi-oppositional teaching learning based optimization for economic emission load dispatch problem,” *International Journal of Electrical Power & Energy Systems*, vol. 53, pp. 937–948, 2013.
- [127] N. Samaan and C. Singh, “Adequacy assessment of power system generation using a modified simple genetic algorithm,” *IEEE Transactions on Power Systems*, vol. 17, no. 4, pp. 974–981, 2002.

- [128] S. Diaf, D. Diaf, M. Belhamel, M. Haddadi, and A. Louche, "A methodology for optimal sizing of autonomous hybrid pv/wind system," *Energy Policy*, vol. 35, no. 11, pp. 5708–5718, 2007.
- [129] H. Yang, W. Zhou, L. Lu, and Z. Fang, "Optimal sizing method for stand-alone hybrid solar-wind system with lpsp technology by using genetic algorithm," *Solar Energy*, vol. 82, no. 4, pp. 354–367, 2008.
- [130] A. Kashefi Kaviani, G. H. Riahy, and S. M. Kouhsari, "Optimal design of a reliable hydrogen-based stand-alone wind/pv generating system, considering component outages," *Renewable Energy*, vol. 34, no. 11, pp. 2380–2390, 2009.
- [131] J. Aghaei, M. Akbari, A. Roosta, M. Gitizadeh, and T. Niknam, "Integrated renewable-conventional generation expansion planning using multiobjective framework," *IET Generation, Transmission & Distribution*, vol. 6, no. 8, pp. 773–784, 2012.
- [132] Z. Beheshti and S. M. H. Shamsuddin, "A review of population-based meta-heuristic algorithms," *Int. J. Adv. Soft Comput. Appl.*, vol. 5, no. 1, pp. 1–35, 2013.
- [133] R. Hemmati, R. A. Hooshmand, and A. Khodabakhshian, "Comprehensive review of generation and transmission expansion planning," *IET Generation, Transmission & Distribution*, vol. 7, no. 9, pp. 955–964, 2013.
- [134] M. B. Shadmand and R. S. Balog, "Multi-objective optimization and design of photovoltaic-wind hybrid system for community smart dc microgrid," *IEEE Transactions on Smart Grid*, vol. 5, no. 5, pp. 2635–2643, 2014.
- [135] A. Eiben and J. Smith, *Introduction to Evolutionary Computing*. Netherlands: Springer Berlin Heidelberg, 2015.

- [136] z. Yeniay, "Penalty function methods for constrained optimization with genetic algorithms," *Mathematical and Computational Applications*, vol. 10, no. 1, p. 45, 2005.
- [137] S. Rao, *Engineering Optimization: Theory and Practice*. Hoboken, NJ: Wiley, 2009.
- [138] F. Herrera, M. Lozano, and J. Verdegay, "Tackling real-coded genetic algorithms: Operators and tools for behavioural analysis," *Artificial Intelligence Review*, vol. 12, no. 4, pp. 265–319, 1998.
- [139] K. Deb, A. Pratap, S. Agarwal, and T. Meyarivan, "A fast and elitist multiobjective genetic algorithm: Nsga-ii," *IEEE Transactions on Evolutionary Computation*, vol. 6, no. 2, pp. 182–197, 2002.
- [140] R. Eberhart and J. Kennedy, "A new optimizer using particle swarm theory," in *Micro Machine and Human Science, 1995. MHS '95., Proceedings of the Sixth International Symposium on*, pp. 39–43.
- [141] C. A. C. Coello, G. T. Pulido, and M. S. Lechuga, "Handling multiple objectives with particle swarm optimization," *IEEE Transactions on Evolutionary Computation*, vol. 8, no. 3, pp. 256–279, 2004.
- [142] E. Atashpaz-Gargari and C. Lucas, "Imperialist competitive algorithm: an algorithm for optimization inspired by imperialistic competition," in *Evolutionary computation, 2007. CEC 2007. IEEE Congress on*, pp. 4661–4667, IEEE.